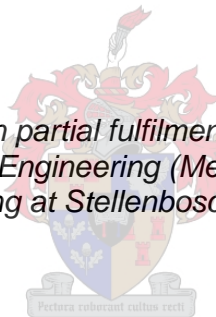


Thermal and hydraulic modelling of an anaerobic digester plant

by
Rynhardt Petrus Vermaak

*Thesis presented in partial fulfilment of the requirements for
the degree of Master of Engineering (Mechanical) in the Faculty of
Engineering at Stellenbosch University*



Supervisor: Mr Robert Thomas Dobson

March 2016

DECLARATION:

By submitting this thesis electronically, I declare that the entirety of the work contained therein is my own, original work, that I am the sole author thereof (save to the extent explicitly otherwise stated), that reproduction and publication thereof by Stellenbosch University will not infringe any third party rights and that I have not previously in its entirety or in part submitted it for obtaining any qualification.

March 2016

ABSTRACT

Thermal and hydraulic modelling of an anaerobic digester plant

R.P. Vermaak

Department of Mechanical and Mechatronic Engineering

Stellenbosch University

Private Bag X1, 7602 Matieland, South Africa

Thesis: MEng (Mech)

March 2016

The use of an anaerobic digestion (AD) process to treat municipal sewage sludge is one of the few options that provides the ability to treat sludge, offers a sustainable option for a carbon-neutral energy source and ability to reclaim wastewater back to potable water. The importance of the anaerobic digestion plant layout is investigated in terms of its process capacity, energy production and electrical energy generation based on thermal numerical modelling.

A design is proposed in the study that is able to treat 986.742 m³/day at 4%TS (81 %) of the available sludge at the wastewater treatment plant, generating 1.293 MW net electrical power and still meet the heat requirements of the anaerobic digestion plant as well as the quality of effluent discharged by the plant. The proposed design is able to treat 53 % more sludge and generate 45.4 % more electrical net power compared to the first conceptual plant layout using a 3/2 two-stage digester configuration.

With the use of hydraulic numerical modelling and experimental work, a mixing system was developed and proposed, that satisfies the biological requirement of micro bacteria inside the digester. The benefits of selecting the proposed mixing system over the mechanical draft tube method include: all the mechanical equipment of the mixing system is located outside the digester, it has no moving parts inside the digester, tedious downtime of clogged rotating equipment is eliminated and a reduction in biogas production rate when the digester is opened and exposed to air for maintenance can be eliminated.

The proposed mixing system consists of five 518 mm draft tubes using a two-phase plug-flow regime formed by five plug-flow generators placed at the bottom of the draft tubes. The mixing system proposed was able to achieve a digester volume turn over time (DVTT) from 0.82 to 1.3 h, at a mixing intensity (G) from 70.58 to 35.88 s⁻¹ requiring a unit power per volume (UP) from 3.41 to 0.88 W/m³.

OPSOMMING

Termiese en hidroliese simulase van 'n anerobiese verteerings werke

R.P. Vermaak

Departement van Meganiese en Megatroniese Ingenieurswese

Universiteit van Stellenbosch

Privaatsak X1, 7602 Matieland, Suid Afrika

Tesis: MIng (Meg)

Maart 2016

Anaërobiese verteer (AV)-prosesse is een van min behandelingsmetodes wat gebruik kan word om munisipale rioolslyk te behandel en bied, 'n volhoubare moontlikheid van 'n koolstofneutrale energiebron, en die vermoë inhou om afvalwater tot drinkbare water te suiwer. Die belangrikheid van die AV-aanlegontwerp is ondersoek aan die hand van werkverrigting in die stabilisering van slyk hoeveelheid sowel as, elektriese en energieproduksie wat gebaseer was op grond van 'n termiese numeriese model.

Die voorgestelde ontwerp van die gevallestudie kon daarin slaag om 986.742 m³/dag teen 4%TS (81 %) van die beskikbare slyk by die afvalwatersuiweringsaanleg te behandel, 1.293 MW netto elektriese krag opwek en steeds aan die hitte vereiste van die aanleg voldoen asook die kwaliteit van wat afgevoer water deur die aanleg. Die voorgestelde ontwerp kon 53 % meet slyk hanteer en kon 45.4 % meer elektriese genereer vergeleke met die eerste voorgestelde ontwerp wat gebruik maak van n 3/2 twee-fase verteerontwerp.

Hidrouliese numeriese modellering en eksperimentele werk is gebruik om 'n mengstelsel ontwikkel en voorgestel wat aan die biologiese vereiste van mikrobakterieë binne-in die toestel voldoen. Die voordele van die gebruik van die voorgestelde mengstelsel bo die van die 'n meganiese afleibuis ontwerp metode sluit die volgende in: al die meganiese toerusting word buite die verteerstelsel gemonteer, dit het geen bewegende dele in die verteerstelsel, die vermorsing van tyd deur rotering toerusting skoon te maak asook die vermindering van die produsering van biogas as gevolg van die oopmaak die verteerstelsel wat die verteerstelsel blootstel aan lug kan vermy word.

Die mengstelsel bestaan uit vyf afleibuis van 518 mm, wat gebruik maak van die tweefase-propvloei form wat deur 'n propvloei-opwekker voortgebring word om die verteertoestel te meng. Die mengstelsel kon 'n verteerstelsel volume omkeertyd van 0.82 tot 1.3 h behaal, teen 'n meng intensiteit (G) van 70.58 tot 35.88 s⁻¹ wat 'n eenheid krag per volume vereis van (UP) 3.41 tot 0.88 W/m³.

ACKNOWLEDGMENTS:

I first want to thank my creator and saviour, for allowing me the privilege to do a master's degree and providing the strength for each day.

I also would like to thank the following;

- Mr R.T. Dobson, for his guidance, assistance and endeavour to help me improve myself
- Dr A.B. Taylor, at Cape Advanced Engineering Ltd., for the funding and time set aside for me to pursue this degree
- All my colleagues at Cape Advanced Engineering Ltd., for their support and understanding
- My parents and the rest of my family, for their prayers, support and love

I will always remember you all, as this was a dream come true.

TABLE OF CONTENTS:

Declaration	ii
Abstract	iii
Opsomming	iv
Acknowledgments	v
List of figures	viii
List of tables	xiii
Nomenclature	xiv
Greek symbols	xv
Subscribes / Superscripts	xv
Abbreviations	xvi
Glossary of Term	xvii
1. Introduction	1
1.1 Background	1
1.2 Motivation	2
1.3 Aim	2
1.4 Objectives	2
1.5 Outline	3
2. Literature review	5
2.1 Introduction to Case Study	5
2.2 Anaerobic digestion	8
2.2.1 Biological process of anaerobic digestion	8
2.2.2 Factors affecting the rate of anaerobic digestion	11
2.3 Confined gas mixing	22
2.3.1 Types of two-phase flow	23
2.3.2 Case studies on two-phase flow-conveying liquids	23
3. Methodology	27
3.1 Anaerobic digestion plant layouts	27
3.1.1 Feedstock for AD plant and disposed method	27
3.1.2 Conceptual layouts for the AD plant	29
3.1.3 Heat, energy and electrical balance on AD plants	33
3.2 Digester mixing system	47
3.2.1 Design criteria and limitations for mixing system	48

3.2.2	Concepts for mixing system	48
3.2.3	Numerical model of draft tube	51
4.	Experimental work	59
4.1	Plug size	59
4.1.1	Effect of geometric construction	60
4.1.2	Effect of hydrostatic pressure	64
4.2	Mass displaced	67
4.2.1	Effect of plug size	67
4.2.2	Effect of hydrostatic pressure	70
5.	Analysis and proposed design	72
5.1	Proposed design layout for AD plant	72
5.1.1	Analysis of conceptual layouts of AD plant	72
5.1.2	Proposed design layout for AD plant	74
5.2	Digester mixing system for proposed AD plant	78
5.2.1	Analysis of concepts for digester mixing system	78
5.2.2	Proposed digester mixing system	80
6.	Discussion and conclusions	89
7.	Recommendations and future work	92
	References	94
	Appendix A: Validation and verification	A-1
A.1	Energy Balance on Plant	A-1
A.2	Digester Mixing System	A-4
	Appendix B: Calibration and error analysis	B-1
B.1	Calibration of rotameter for experimental setup	B-1
B.2	Error analysis on experimental work	B-3
B.2.1	Error analysis on calibration of rotameter	B-3
B.2.2	Error analysis on plug size	B-4
B.2.3	Error analysis on plug frequency	B-5
B.2.4	Error analysis on mass displace	B-6
B.3	Plug formation photo cycle	B-7
	Appendix C: Technical drawing	C-1
	Appendix D: Data sheet	D-1
	Appendix E: Experimental data	E-1

LIST OF FIGURES:

Figure 2.1:	Spillages from manholes in Arebbusch River a) broken man-hole, b) blocked pipe overflowing	6
Figure 2.2:	Gammams plant layout	7
Figure 2.3:	Anaerobic digestion process flow diagram	9
Figure 2.4:	Growth rate of methanogens at different digesting temperature ranges	12
Figure 2.5:	Effect of biogas, CH ₄ yield and VS reduction on SRT of a mesophilic and thermophilic digester	13
Figure 2.6:	Effect of biogas and CH ₄ production on SRT	13
Figure 2.7:	Effect of VS in the influent as a function of HRT and VS destruction in the digester	14
Figure 2.8:	The relationship between CO ₂ and pH as a function of bicarbonate in a single stage digester at 35 °C	15
Figure 2.9:	CSTR reactor configurations: a) single stage, b) two-stage and c) two-phase	16
Figure 1.1:	Heritage diagram of mixing system for an anaerobic digester	18
Figure 1.2:	Mixing methods used for CSTR	19
Figure 2.12:	Damaged horizontal paddle stirrer	22
Figure 2.13:	Blockage of a slurry recirculation pump for a digester mixing system a) before and b) after cleaning	22
Figure 2.14:	Vertical two-phase flow regimes	23
Figure 2.15:	Air lift pump-phase transitions with water mass flow rate as a function of air flow rate	24
Figure 3.1:	Volume of PS drawn from PST's per day over a year	28
Figure 3.2:	Volume flow rate of PS and WAS per day at different TS contents	28
Figure 3.3:	Sludge and SN process flow diagram for AD plant - concept 1	30
Figure 3.4:	Sludge and SN process flow diagram for AD plant - concept 2	31
Figure 3.5:	Sludge and SN process flow diagram for AD plant - concept 3	32
Figure 3.6:	Process flow diagram for the heating the feedstock	34
Figure 3.7:	Discretisation diagram of sumps at AD plant	34
Figure 3.8:	Volume and sump temperatures of concept 3 on 20 March	35
Figure 3.9:	Average heat recovered per day from the effluent in a typical year	35
Figure 3.10:	Average additional heat needed per day for feedstock in a typical year	36
Figure 3.11:	Discretisation diagram of digester	37
Figure 3.12:	Daily averaged heat demand of heated digesters in a typical year	38
Figure 3.13:	Post-digester digestate temperature fluctuations from 20 to 23 June	39

Figure 3.14: Averaged post-digester digestate temperature in a typical year	39
Figure 3.15: Heat losses by type of single heated digester from 22 to 25 September	39
Figure 3.16: Heat losses by section of single-heated digester from 22 to 25 September	40
Figure 3.17: Power available from digesters in the different concepts as a function of TS content	41
Figure 3.18: Electric power generated by concepts at different TS content	42
Figure 3.19: CHP process flow diagram	43
Figure 3.20: Coolant heat recovered from AD plant concepts at different TS content	41
Figure 3.21: Exhaust heat recovered from AD plant concepts at different TS content	41
Figure 3.22: Heat balance of concept 1 at 4 % TS on the solstices and equinoxes	42
Figure 3.23: Average heat balance of concepts at TS contents in typical year	43
Figure 3.24: Averaged overall energy balance of concepts at TS contents in typical year	46
Figure 3.25: Overall electricity balance on AD plants at different TS contents	47
Figure 3.26: Concept 1 – Pressure vessel with automated valve outside digester	48
Figure 3.27: Concept 2 – Gas accumulator with U-tube inside digester	49
Figure 3.28: Concept 3 – Plug-flow generator	50
Figure 3.29: Discretisation diagram of two-phase model of a) geometry and b) momentum balance	52
Figure 3.30: Velocity profile and the mass of liquid displaced over time from a 365 mm draft tube with a plug ratio of $1.2P_e$	54
Figure 3.31: Acceleration profile and mass of liquid displaced over time from of a 365 mm draft tube with a plug ratio of $1.2P_e$	54
Figure 3.32: Velocity profile and the mass displaced over time of five cycles with a plug frequency of 0.048 Hz	55
Figure 3.33: Effect of plug frequency on the average mass flow rate and average mass displaced per cycle	55
Figure 3.34: Sensitivity analysis of mass displaced from mixing system based on geometrical construction	56
Figure 3.35: Sensitivity analysis of averaged mass flow rate of mixing system based on geometrical construction	56
Figure 4.1: Plug-flow generator a) front and b) side section view	59
Figure 4.2: Experimental setup for effect of geometry, pressure and calibration	60

Figure 4.3:	Schematic cycle of a plug-flow generator a) step 1, b) step 2 and c) step 3	62
Figure 4.4:	Volumes of plug generated as a function of air flow rate with an orifice area of $201 \times 10^{-6} \text{ m}^2$	63
Figure 4.5:	Volumes of plug generated as a function of air flow rate with an orifice area of $415 \times 10^{-6} \text{ m}^2$	63
Figure 4.6:	Volumes of plugs generated as a function of air flow rate with an orifice area of $804 \times 10^{-6} \text{ m}^2$	63
Figure 4.7:	Plug frequency as a function of air flow rate with an orifice area of $201 \times 10^{-6} \text{ m}^2$	64
Figure 4.8:	Volumes of plugs at different hydrostatic pressures as a function of air flow rate using plug generator 1.1.1 and an orifice area of $201 \times 10^{-6} \text{ m}^2$	65
Figure 4.9:	Multiple linear regression analysis of mass of plug with R^2 of 0.9098	66
Figure 4.10:	Multiple linear regression analysis of plug frequency with R^2 of 0.9894	66
Figure 4.11:	Experimental setup used to measure liquid mass displaced	67
Figure 4.12:	Liquid mass displaced from the draft tube per plug as a function of air flow rate using plug-flow generator 1.1.1 with its different orifice plates	69
Figure 4.13:	Liquid mass flow rate of mixing system as a function of air flow rate with plug-flow generator 1.1.1 using different orifice plates	69
Figure 4.14:	Liquid mass per plug displaced at different hydrostatic pressures as a function of air flow rate using plug-flow generator 1.1.1 with an orifice area of $415 \times 10^{-6} \text{ m}^2$	70
Figure 4.15:	Liquid mass flow rate displaced at different hydrostatic pressures as a function of air flow rate using plug-flow generator 1.1.1 with an orifice area of $415 \times 10^{-6} \text{ m}^2$	71
Figure 5.1:	Heat balance of concept 3 at 8 % TS contents on 23 September in one-minute intervals	74
Figure 5.2:	Volume and sump temperatures of proposed design layout on 23 September	75
Figure 5.3:	Overall heat balance of the proposed on 23 September in one-minute intervals on 23 September	75
Figure 5.4:	Daily averaged heat addition needed for the proposed design in typical year	76
Figure 5.5:	a) Averaged daily heat and b) energy balance on the proposed design layout in typical year	76
Figure 5.6:	AD plant proposed design layout for the WWTP case study	77

Figure 5.7: Effect of draft tube diameter on the mass and mass flow rate displaced from the top of the digester for a single full-plug cycle at 0.021 Hz and a plug ratio of 1.2P _e	79
Figure 5.8: Effect of plug size on the average mass flow rate and mass displaced per cycle by the a) middle draft tube and b) side draft tube proposed	81
Figure 5.9: Effect of plug frequency on average mass flow rate and mass displaced for the a) middle draft tube with a plug size of 0.818P _e and b) side draft tube a plug size of 0.724P _e	82
Figure 5.10: Number of draft tubes needed for mixing system vs. range of DVTT in which mixing system can operate	82
Figure 5.11: Middle and side draft tube plug frequency versus normalised volumetric gas flow rate	83
Figure 5.12: Number of draft tubes as a function of DVTT and normalised volumetric gas flow rate needed for mixing system	84
Figure 5.13: Liquid ring blower volumetric gas flow rate and power consumption as a function of delivery pressure head	84
Figure 5.14: Unit power and mixing intensity of the proposed mixing system as a function of DVTT	85
Figure 5.15: Process flow diagram of proposed mixing system	87
Figure A.1: Effect of time step on the numerical model of feedstock energy balance	A-1
Figure A.2: Effect of time step on the numerical model of concept 1 post-digesters energy balance on 23 September	A-2
Figure A.3: Liquid mass displaced by draft tube as a function of plug size	A-5
Figure A.4: Predicted friction multiplier as a function of calculated friction multiplier	A-5
Figure A.5: Measured and calculated liquid displaced as a function of normalised volumetric flow rate at different liquid depths	A-6
Figure A.6: Predicted liquid displaced as a function of calculated liquid displaced	A-6
Figure A.7: Effect of time step on the explicit numerical model of the liquid mass displaced through the draft tube and the time duration of the cycle for scale model	A-7
Figure A.8: Effect of time step on the explicit numerical model for the liquid mass displaced through the draft tube and time duration of cycle for the full-scale model	A-8
Figure B.1: Volumetric air flow rate calibration of the rotameter and curve fit	B-2
Figure B.2: Predicted volumetric air flow rate as a function of calculated volumetric air flow rate	B-2

Figure B.3:	Height reading of plug generator 1.1.1 with orifice area of $415 \times 10^{-6} \text{ m}^2$ as a function of normalised volumetric air flow rate	B-3
Figure B.4:	Percentage deviation of recorded height reading from mean at $1.774 \text{ Nm}^3/\text{h}$ reading	B-3
Figure B.5:	Plug frequency of plug generator 1.1.1 with orifice area of $415 \times 10^{-6} \text{ m}^2$ as a function of normalised volumetric air flow rate	B-4
Figure B.6:	Percentage deviation of recorded plug frequency from mean at $0.938 \text{ Nm}^3/\text{h}$ reading	B-4
Figure B.7:	Displaced water per plug of plug generator 1.1.1 with orifice area of $415 \times 10^{-6} \text{ m}^2$ as a function of normalised volumetric air flow rate	B-5
Figure B.8:	Percentage deviation of recorded displaced water per plug from mean at $0.938 \text{ Nm}^3/\text{h}$ reading	B-5
Figure B.9:	Cycle of plug formation by plug generator 1.1.1	B-6
Figure C.1:	Proposed design of plug generators for middle and side draft tubes	C-1
Figure D.1:	Data sheet of selected liquid ring compressor	D-1

LIST OF TABLES:

Table 2.1:	Composition of biogas	8
Table 2.2:	Rate of the hydrolysis process for pure organic compounds and WWTP substrate	10
Table 2.3:	Factors affecting the rate of anaerobic digestion	11
Table 2.4:	Comparison of CSTRs digesting sewage sludge	17
Table 3.1:	Thickened PS and WAS sludge volumes at Gammams WWTP	28
Table 3.2:	Plant operating conditions for concept 1	30
Table 3.3:	Plant operating conditions for concept 2	31
Table 3.4:	Plant operating conditions for concept 3	32
Table 3.5:	Expected plant layout performance of different concepts	32
Table 3.6:	Inlet raw wastewater temperature during the year	33
Table 3.7:	Input values for numerical model of feedstock energy requirements	34
Table 3.8:	Input constants for numerical model of digester energy requirements	37
Table 3.9:	Input parameters for numerical model of digester's energy production	40
Table 3.10:	Parasitic load of the AD plants	45
Table 3.11:	Mixing concept evaluation matrix	51
Table 4.1:	Measured data from the different plug-flow generators	60
Table 5.1:	Input data of selective draft tubes for the proposed design of plug-flow generators at DVTT of 1 h	86
Table 5.2:	Geometrical ratios of proposed plug generators in comparison with plug generator 1.1.1	87
Table E.1:	Mean experimental results of the effect of geometry change	E-1
Table E.2:	Mean experimental results of the effect of hydrostatic pressure	E-3
Table E.3:	Mean experimental results of volume of plug on the mass flow rate	E-4
Table E.4:	Mean experimental results of the effect of hydrostatic pressure on mass flow	E-5

NOMENCLATURE:

AM	Amplitude
A_p	Amplitude of annual air temperature wave, °C
A_x	Cross section area, m ²
A_z	Circumferential area, m ²
CAP	Capacity of CHP, kW
C_f	Friction coefficient
c_p	Specific heat, J/kgK
d	Diameter, m
DVTT	Digester volume turnover time, h
E	Energy, W
\exists	Equation of time, min
FM	Friction multiplier
g	Gravitational acceleration, m/s ²
G	Normalised mixing intensity, s ⁻¹
h	Heat flux, W/m ²
h	Heat transfer coefficient, W/m ² K
HRT	Solid retention time, h
k	Thermal conductivity, W/mK
L	Length, m
L_{st}	Longitude, deg
LVA	Lower heat value, J/kg
\dot{m}	Mass flow rate, kg/s
m	Mass, kg
Nu	Nusselt number
OLR	Organic loading rate, kgVS/d
P	Pressure, Pa
P_e	Plug ratio
P_{mix}	Power used for mixing, W
P_r	Prandtl number
PS	Phase shift of air temperature wave
Q	Energy, J
\dot{Q}	Heat, W
R	Resistance, W/mK ²
R_a	Rayleigh number
R_e	Reynolds number
SR	Submersible ratio
SRT	Solid retention time, h
T	Temperature, °C
t	Time, s
T	Time, s
t_o	Phase shift of air temperature, days
t_s	Solar time, h
TS	Total solids, %
UP	Unit power, W

v	Velocity, m/s
V	Volume, m ³
\dot{V}	Volumetric flow rate, m ³ /s
VS	Volatile solids, %
W	Work done, W
Y	Yield, m ³ /kg
z	Height, m
Z _{At}	Altitude, m
'P	Power, W

GREEK SYMBOLS:

α	Thermal absurdity
β	Solar slope
δ	Declination angle, rad
Δ	Differential
ϵ	Emissivity
η	Efficiency, %
θ	Angle, deg or rad
λ	Friction factor
μ	dynamic viscosity, Pas
ρ	Density, kg/m ³
τ	Shear friction force, N
Φ	Latitude, deg
ω	Hour angle, rad
ϵ	Equation of time, min

SUBSCRIPTS / SUPERSSCRIPTS:

a	Air
acc	Accumulated
alt	Alternator
amb	Ambient
B	Biogas
c	Clearance
cem	Cement
d	Digester
exh	Exhaust
f	Fouling
GHI	Global horizontal irradiation
gr	Ground
h	Convection
HE	Heat exchanger
HP	Hairpins
i	Inlet, i'th value
I	Irradiation
in	Inlet, inward direction

ins	Insulation
k	Concoction
L	Liquid
m	Mean
n	Number
o	Outer
out	Outlet, outward direction
p	Plug
rad	Radiation
Red	Reduction
ref	Reflection
surf	Surface
T	Tube
TS	Total solids
v	Vegetation
VS	Volatile solids
w	Water

ABBREVIATIONS:

AG-MM	Acid Gas - mesophilic, mesophilic digestion
ANOVA	Analysis of variance
ASP	Activated sludge process
CaCO ₃	Bicarbonate
CGA	Cone gas area
CGrA	Cone ground area
CH ₄	Methane
CHP	Combined heat and power
CO ₂	Carbon dioxide
COD	Chemical oxygen demand
CSTR	Continuous stirred reactor
CWA	Cone water area
H ₂	Hydrogen
H ₂ O	Water
LCFA	Long-chain fatty acids
NGWRP	New Goreangab Water Reclamation Plant
NH ₃	Ammonia
OGWRP	Old Goreangab Water Reclamation Plant
PST	Primary settling tank
RAS	Return activated sludge
Re	Recovered
SGrA	Side ground area
SS-M	Single stage - mesophilic digestion
SST	Secondary settling tank
SWA	Side water area
TF	Trickling filtration

TPAD-TM	Temperature phase anaerobic digestion - thermophilic, mesophilic digestion
TS-MM	Two stage – mesophilic, mesophilic digestion
WAS	Waste activated sludge
WWTP	Wastewater treatment plant
SN	Supernatant
VFA	Volatile fatty acids
AD	Anaerobic digestion
PS	Primary sludge

GLOSSARY OF TERMS

Effluent:

Outflowing of water from a reservoir

Supernatant:

The liquid that or is drained above a sediment or precipitate

Hummas tank:

Final settling tanks in the secondary treatment process in a WWTP to separate supernatant from processed sludge before treating or disposing it.

Endocellular bacteria:

Bacteria that is capable to break down organic material either inside or outside cells walls

Hydrogentrophic:

Organisms that is able to metabolize molecular hydrogen as a source of energy

Inoculum:

A small amount of substance containing bacteria is introduced to larger volume to start a new culture.

Activated sludge process:

A biological process that can be using oxidizing carbonaceous or oxidizing nitrogenous matter bacteria to remove nutrients.

Polymers:

Substances that have a high molar mass and are composed out of large number of repeating monomer chains.

Monosaccharides:

Is the simplest form of carbohydrates consisting out of one sugar and are usually colorless, water-soluble, crystalline solids

Lactate:

Is an ester or salt of lactic acid.

Monomers:

Substances that have a low molar mass and are composed out of only a few elements

Sludge thickening:

Increasing the total sold contents of the sludge

1. INTRODUCTION

1.1 Background

Water and energy are critical for the future development and economic growth of the world. These two resources have become some of the most popular topics for research and discussion in order to find an alternative or sustainable source.

Clean water is essential for human life on earth, but it is a finite resource and has become a global concern due to population growth, pollution and climate change. With the increase in demand for clean water supply, more pressure is being placed on municipalities to explore options of reuse or recycling of wastewater treatment plant effluent. In order to reuse or recycle wastewater, the wastewater treatment plants need to ensure that the quality of the water complies with the regulations set out and continuously monitor the effluent discharge.

In most southern African countries, many investigations have indicated that raw or partially treated wastewater and sewage sludge discharged from wastewater treatment plants (WWTP) are among the major pollutants of freshwater sources such as rivers, dams and ground water summarized in Cashman (2014) study. The 'spillages', also referred to as by-pass or partially treated wastewater, have been identified to be due to poor plant operation, lack of maintenance, financial constraints and limited plant capacity (Mema, 2009).

The raw or partially treated wastewater for municipal sewage plants not only threatens freshwater resources, but also contains bacteria, parasites, viruses and heavy metals. These elements that the wastewater contains are toxic to all human and marine life forms. If a human is infected with *E. coli* bacteria, the Hepatitis virus or Polyoma viruses, the symptoms can range from diarrhoea to liver failure and colon cancer and, in some cases, if not treated may be fatal. Therefore, adequate treatment and continuous monitoring of wastewater and especially sewage sludge effluent from WWTP are necessary to prevent health and safety risks to humans and to preserve freshwater resources.

The option of recycling municipal wastewater had already been exploited and implemented by the city of Windhoek (Namibia) in 1968 due to the city's limited water resources. The city started off by recycling 4.8 ML/day from wastewater effluent and reservoir water. Today the city recycles 21 ML/day, 35 % of the city's potable water demand. The city also has a long, successful history of managing its water resources and has been used by various researchers as a model to implement policies on an integrated demand-side water management strategy in water-strict areas (Du Pisani, 2006, Lahnsteiner & Lempert, 2007; Hasheela, 2009).

This study will use the Gammams WWTP in Windhoek as a case study to look at different configurations to treat the sewage sludge at a WWTP with anaerobic digesters (AD) and digester mixing systems to a product that complies with the set-out regulations. This option of using anaerobic digestion to treat sewage sludge delivers high-quality, odour-free digestate that can be sold as fertiliser and stabilised supernatant effluent and provide the option to reclaim the supernatant effluent back to potable water. The additional benefit of using anaerobic digestion is the methane

generated in the reactors by the micro-bacteria and can be used as a CO₂-neutral, renewable fuel for electrical power generation.

1.2 Motivation

By stabilising or treating municipal sewage sludge effectively, the risk of contaminating freshwater resources is reduced, as the majority of the contaminating bacteria and viruses bond to the sludge. The stabilised sludge can also be processed further, which can lead to a financial benefit for the WWTP, as it can be sold as fertiliser.

Stabilising the raw municipal sewage sludge by using an anaerobic plant can also lead to another financial benefit for the WWTP in terms of electricity generated from the biogas produced by the anaerobic digesters. The supernatant wastewater drawn from the digesters can be reused or reclaimed back to potable water if treated further. Therefore, using an anaerobic digester to stabilise municipal sewage sludge not only reduces the health and contamination risks, but also addresses the issue of a sustainable energy and water resource for the future.

The motivation for the second part of this thesis, which focuses on the development of a mixing system with no mechanical parts inside the digester, is due to the recurring maintenance of mechanical mixing systems. The fibrous nature of the sewage sludge causes blockages in rotating equipment, giving rise to a recurring maintenance problem. In order to do the maintenance on a mechanical mixing system, the digester needs to be opened, which sets back the biogas production rate as the digester is exposed to air.

1.3 Aim

The first aim of the thermal modelling of the anaerobic digestion plant in this thesis was to illustrate the benefits and importance that the selection of the plant configuration holds for the plant's electrical production, energy production, processing capacity and effluent quality output.

The second aim of this thesis was the hydraulic modelling and development of a mixing system for a continuously stirred anaerobic digester that will comply with the digester's internal requirements that has no moving parts inside the digester and will be able to operate at an increased solid content of the influent.

1.4 Objectives

The objectives set out for this thesis were as follows:

- Acquire an understanding of how the biological process in an anaerobic digester breaks down raw sludge.
- Identify and understand the different environmental and process operating factors affecting the health and biogas production rate of an anaerobic digester.
- Based on the knowledge gained, configure three different conceptual layouts for an anaerobic digestion plant, each with its own environmental and operating conditions.
- Evaluate the three different conceptual plant layouts with an overall heat, energy and electrical production balance.

- Propose a plant layout design for an anaerobic digestion plant from the results obtained from the overall heat, energy and electrical production balance.
- Identify an effective mixing system for an anaerobic digester.
- Develop a concept design for a mixing system, and build and test a scale model of it.
- Draw up a numerical model that can predict the performance of the concept mixing system.
- Propose a design at full-scale for a digester mixing system.

1.5 Outline

This thesis comprise seven chapters, structured as follows:

Chapter 1 is the introduction to the study, which contains background to the study that explains the need of water treatment. The motivation and importance of this study are also provided, together with the aim, objectives outline and inclusion and exclusion section of the study.

Chapter 2 provides an introduction to the case study used for the thesis. It also includes a literature review on the biological process of anaerobic digestion and the factors affecting anaerobic digestion performance. The third section of the chapter presents a literature review on confined gas mixing methods and the different two-phase gas-liquid flow regimes that can be used in a digester.

In *Chapter 3*, the total available feedstock at the WWTP is covered and three different AD plant configuration layouts are presents. These three AD plant configurations are then evaluated with an overall heat energy and electrical production balance. In addition, the chapter presents the concept design of the mixing system for an anaerobic digester, accompanied by a numerical model of the system.

Chapter 4 details the experimental work conducted for the proposed design of the digester mixing system.

Chapter 5 analyses the results obtained from the different AD plant configurations in Chapter 3 from the point of view of an overall heat energy and electrical production balance, and also analyses the concept from the digester mixing system. On the basis of the findings, the study concludes by proposing a plant layout for the case study and a full-scale mixing system design for a digester.

Chapter 6 presents the discussion and conclusions drawn from this study.

Recommendations and options for future research are presented in *Chapter 7*.

1.6 Inclusion and exclusion

The study will include a background of the case study that this thesis is based on, together with the current infrastructure available to treat raw municipal sludge using anaerobic digestion. In the study three different AD plant configurations will draw up to treat the sludge where the environmental and process factors will be limited to only the main factors. Temperature phase digestion and thermophilic digestion process will be excluded from this study due to complexity and increased sensitivity.

The feedstock of the WWTP case study will be additional thickening to between 4 % and 10 %, but the actual thickened process will be excluded from this study. The effluent and supernatant drained from the AD plant which has to be treated further by secondary and tertiary treatment processes to fertilizer and portable water will also be excluded from this study.

The study will include the energy production of the different AD plant concepts, but the biogas production rates for the different concepts were calculated only including one variable of the digestion process. This variable was obtained from case studies reviewed in the literature survey. The study will also include the modelling of converting the biogas generated by the AD plant concepts to electricity, using a combined heat and power (CHP) internal combustion (IC) unit and recover the available waste heat from these units to satisfy the different AD plant concepts heat requirements.

To determine the heat and energy requirements of the different AD plant concepts the study include a numerical heat and energy balance over concepts taking the following aspects into account: incoming feedstock heat demand, available heat and to be recovered from effluent, incoming solar irradiation on digesters, convection, conduction and radiation losses to atmosphere and ground from digester as well as heat losses due to mass transfer. The shadow effect on the digester as well as the micro bacteria metabolic heat and the exothermic reactions inside the digester will be excluded from numerical heat and energy balance in this study. The verification of the energy model on the digester will also be excluded from this study.

In the second part of the thesis, different mixing systems for a continuous stirred reactor (CSTR) used, commercially and experientially will be examined of which one will be selected. From the selected concept three different concepts will be drawn up, evaluated and one will be selected modeled and tested experientially. The numerical modelling and experimental testing of the selected mixing system will only be in newtonian fluid and not with a non-newtonian fluid at different total solid contents. The numerical modelling of the draft tube of the selected mixing system will be selected from commercially available pipe sized and a step geometry or a taper draft tube geometry to increase the mixing system effectiveness will be excluded from this study.

2. LITERATURE REVIEW

Thornton *et al.* conducted a study on the possible toxic elements in municipal wastewater in 2009 and found that 60 % to 80 % of the possible toxic elements (bacteria and pathogens) are transferred or bonded to the sludge. Therefore, stabilising sewage sludge is very important to minimise the risk of contaminating freshwater resources. Sludge stabilisation can be divided into three main groups, namely biological stabilisation, chemical stabilisation and thermal stabilisation. The biological stabilisation of sludge can be further divided into two subgroups, namely aerobic digestion and anaerobic digestion. This study will focus on sludge stabilisation with the use of anaerobic digestion, as it is one of the few options that enhance the sustainability of alternative energy and water resource consumption.

This chapter will provide an introduction to the case study used, a detailed literature review of the biological degrading process of anaerobic digestion, and the factors affecting the digestion performance and a digester mixing method, based on the literature. The objectives set out for the chapter are:

- To acquire an understanding of how the biological process in an anaerobic digester breaks down the biodegradable fraction of the sludge
- To identify the different parameters affecting the anaerobic digestion process, digester health and biogas production rate
- To review the different mixing systems available and to identify a possible alternative

2.1 Introduction to Case Study

Namibia is one of the most arid countries in the world, as more than 80 % of the country consists of desert or semi-desert. Windhoek, the capital city, has an annual rainfall of approximately 370 mm, while the potential surface evaporation rate is 3 200 mm per annum. Therefore, water in this city is a scarce resource.

The city already had to start exploring alternatives for water in the early 1960s, such as recycling wastewater. In 1968, the first Old Goreangab Water Reclamation Plant (OGWRP) was constructed, with a capacity of 4.8 ML/day, which was used mainly for irrigation. In 2002, the New Goreangab Water Reclamation Plant (NGWRP) followed, with a recycling capacity of 22 ML/day. The NGWRP has the capability to reclaim wastewater to potable water suitable for human consumption. The plant was designed with two inlets; 50 % of its supply was made up by Gammams, together with the small Otjomuize WWTP, and the other 50 % of the water was supplied from the Goreangab reservoir. Due to the deterioration of the Goreangab reservoir, the NGWRP is supplied with 100 % secondary effluent from the Gammams WWTP and the small Otjomuize WWTP (Du Pisani, 2006).

The cause of the deterioration in the water quality of the Goreangab reservoir has been considered by previous studies (Lahnsteiner & Lempert, 2007; Hasheela, 2009) to be the increase in informal settlements in the catchment area and the surface runoff water from the city. However, a new in-depth study by Cashman *et al.* (2014) found that most of the sewage manholes located in the Arebbusch River were either forced/broken open due to excess flow volumes or due to blockages in the sewerage network (see Figure 2.1), and that the main pollutant is domestic sewage effluent.

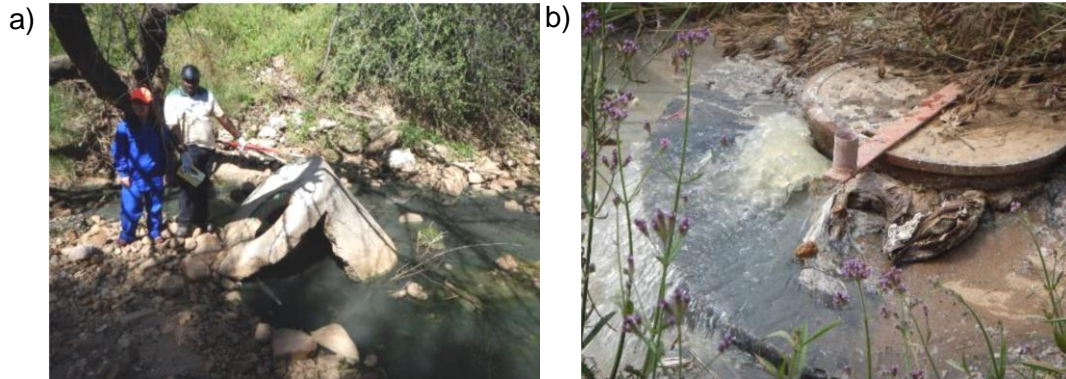


Figure 2.1: Spillages from manholes in Arebbusch River a) broken man-hole, b) blocked pipe overflowing (from Cashman, 2014)

With Gammams being the main domestic sewage WWTP, the bulk of the city's sewage effluent is directed to this plant. The plant had an initial design capacity of 29 ML/day, although the plant was receiving an average flow of 48 ML/day in 2014. The infrastructure of the Gammams WWTP consists of three processes, namely primary treatment processes, secondary treatment processes and tertiary treatment processes.

The primary treatment process comprises mechanical screens, forced vortex grit removal systems, primary settling tanks (PSTs) and anaerobic digesters. The sludge and scum from the PSTs are directed to the anaerobic digesters, with the overflow of the PSTs directed to the secondary treatment process. The treated primary sludge from the anaerobic digesters is sent off to the belt press plant, where the supernatant drawn off from the digester is sent to the secondary treatment process to ultimately be reclaimed as potable water.

At the belt press plant, the treated sludge from the digesters is separated into solids and liquids to lower the moisture content in the sludge. The solids are piled and composted before they are palletised and sold as fertiliser. The liquid part is sent to the secondary treatment process for further treatment to be reclaimed as potable water.

The secondary treatment process comprises trickling/biological filtration (TF) with associated humus tanks, as well as an activated sludge process plant (ASP) with associated secondary settling tanks (SSTs) and waste-activated sludge thickening. The overflow from the PSTs, as well as the supernatant wastewater from the digester and belt press plant, are split 40 % to the TFs and 60 % to the ASP. The effluent of the TFs is sent to the tertiary treatment process, and the underflow effluent of the TFs is sent back to the ASP or to the Otjomuize WWTP, depending on the load on the WWTP.

The activated sludge in the ASP is directed to the SST. A part of the effluent from the SST is directed back to the ASP as return-activated sludge (RAS), and the other part is sent to the activated sludge thickener as waste-activated sludge (WAS). After the WAS has settled in SSTs and then sent to the activated sludge thickener, it has to be thickened additional before treated by the AD plant or is sent to Otjomuize WWTP. The overflow of the SSTs is directed to the tertiary treatment process.

The tertiary treatment process at Gammams comprises a series of maturation ponds. The overflow from the SSTs and the effluent from the TFs spend about three days in these series of ponds before they are discharged to the NGRWRP, Goreangab reservoir and/or OGRWPR, depending on the demand. A descriptive illustration of the Gammams plant can be seen in Figure 2.2.

It can be concluded that the quality of effluent from Gammams, which currently is the main supply for the NGWRP, is very important, as this water is reclaimed back to potable water for the city. This means that the treatment of sewage sludge at Gammams WWTP is vital for the treatment of the toxic elements in the sludge, as the majority is bonded to the sludge, as proven by the study of Thornton et al., in 2009. As the sludge is treated mainly by the anaerobic digester at Gammams, the plant performance plays a vital role in the process of meeting the potable demand of the city.



Figure 2.2: Gammams plant layout (from Google Earth, 2014)

2.2 Anaerobic digestion

Anaerobic digestion is a multi-biological process whereby anaerobic microorganisms break down complex organic substances in the absence of oxygen.

In the anaerobic degradation process, the organic substances are converted into different gases and new cell mass by microorganisms. The mixture of gases produced is called *biogas* and comprises CH₄, CO₂ and some trace gases, such as N₂, H₂, O₂ and H₂S. The composition of the biogas can be seen in Table 2.1.

Table 2.1: Composition of biogas (adapted from Çalli, 2010)

Component of biogas	Volume percentage of biogas (%)
Methane	50 to 80
Carbon dioxide (CO ₂)	20 to 40
Nitrogen (N ₂)	0 to 5
Hydrogen (H ₂)	<1
Oxygen (O ₂)	<0.4
Hydrogen sulphide (H ₂ S)	0.1 to 3

The reasons for this fluctuation in the biogas composition are the quality of influent feedstock, as well as different population numbers of the micro-bacterial organisms in the digesters, which are largely affected by the environment and the operating conditions. To be able to produce biogas from the organic substances, the micro-bacterial community inside the digester needs to degrade these organic substances in a chain of events/reactions.

The following two sections of the literature review focus on the biological process of degrading the organic substances (2.2.1), as well as the factors affecting the rate of digestion (2.2.2).

2.2.1 Biological process of anaerobic digestion

All of the organic substances in the feedstock entering the anaerobic digestion plant can be divided into the following organic compounds: carbohydrates, proteins, lipids and inert material. All of these organic classes of compounds can be broken down to form biogas, except the inert material. Inert material cannot be chemically or biologically digested, and typical examples found at a WWTP are sand, stones and heavy metals.

The breakdown of complex organic substances (carbohydrates, proteins and lipids) by the micro-bacterial community inside the digester can be characterised in four steps, namely hydrolysis, acidogenesis, acetogenesis and methanogenesis (Eliyan, 2007). A schematic flow diagram of the different organic compounds and the four steps of the anaerobic digestion process are illustrated in Figure 2.3. The different groups of micro-bacteria in the digestion process are also included in the figure.

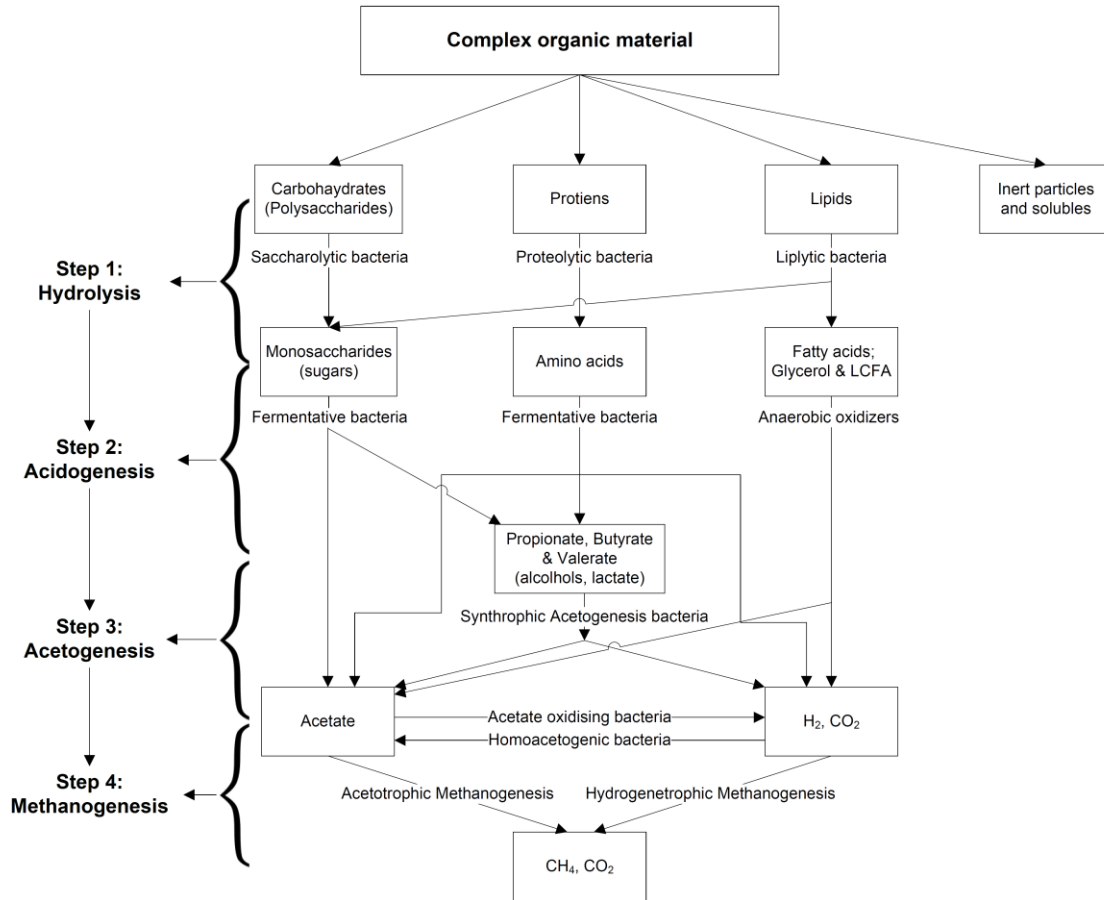


Figure 2.3: Anaerobic digestion process flow diagram, adapted from Batstone *et al.* (2002) and Schön, (2009).

Hydrolysis (Step 1):

In the first step of anaerobic digestion, complex organic material or also known as polymers (carbohydrate, proteins and lipids) has to be broken down into soluble compounds called intermediates. This process is necessary for the rest of the micro bacterial community to feed on, as they are only capable of decomposing soluble compounds (Schön, 2009).

The rate of the hydrolysis process is influenced by the solid concentration of substance, the external dimensions of the substance (size, shape and surface area) and the rate of the enzyme production by the hydrolytic bacteria. The rate of the hydrolysis is also influenced by the environmental factors like pH and temperature. These two environmental factors will be dealt with in more detail in the following section (2.2.2).

In Table 2.2 below, the rate of the hydrolysis process for pure organic substances and mixed organic substances in WWTP's sludge are listed. The table indicates that the carbohydrates are the easiest to digest and the more complex substances like primary sludge take much longer.

Table 2.2: Rate of the hydrolysis process for pure organic compounds and WWTP substrate, adapted from Vavilin et al., (2008) and Moo-Young, (2011)

Substrate/compounds	Hydrolysis rate (/day)	Temperature (°C)
Carbohydrates	2.4 to 4.1	32
Proteins	0.2 to 0.8	32
Lipids	0.3 to 0.7	32
Primary sludge (PS)	0.99	35
Waste activated sludge (WAS)	0.17 to 0.6	35

Acidogenesis (Step 2):

In the acidogenesis step of anaerobic digestion, the soluble intermediates (monosaccharides, amino acids, glycerol and LCFA) are degraded further by endocellular bacterial enzymes.

The acidogenesis process of anaerobic digestion is the most vigorous stage and, in general, the fastest stage during the digestion process. However, if the H₂ formed by the fermentative bacteria and anaerobic oxidiser bacteria cannot be consumed by the methanogens at the same rate as they are produced, the digestion process slows down. The reason for the slower digestion process can be explained as follows: the increase in the H₂ partial pressure leads to an increase in simple volatile fatty acid, alcohol and lactate formation. In the case of an accumulation of simple volatile fatty acids and alcohols, the digester can still continue operation, but the degradation process will be prolonged, as acetogenesis bacteria have a slower growth rate than acidogenesis bacteria.

In the case of a high accumulation of glycerol and LCFA, the digester can become toxic and bring methane formation to a halt (Schön, 2009). Therefore it is very important to be able to control the environmental and process operating conditions so that the partial pressure of H₂ (less than 1 x10⁻⁴ atm) is kept to a minimum (Moo-Young, 2011). The partial pressure of H₂ is mainly affected by the pH of the solution and the digester's loading rate (these factors will be explained in section 2.2.2).

Acetogenesis (Step 3):

The third step in anaerobic digestion is when the soluble intermediates (organic acids and alcohols) are degraded further to monomers. The organic acids and alcohols formed in acidogenesis are degraded by endocellular acetogenesis bacteria that colonise over the soluble intermediates. The third stage in anaerobic digestion is one of the more complex stages and is one of the stages that are very sensitive to environmental fluctuations and the organic load rate at which the digester is fed (Schön, 2009).

Methanogenesis (Step 4):

In the last step of anaerobic digestion, the monomers (acetate, H₂ and CO₂) that were formed by the previous degradation steps are converted into CH₄ and CO₂ by the endocellular bacteria. In a study conducted by Boe (2006), it was found that the hydrogenotrophic methanogenesis bacteria were less sensitive to environmental changes compared to acetotrophic methanogenesis bacteria. The study concluded that it is of fundamental importance that the H₂ partial pressure is kept lower than 1 x10⁻⁴ atmospheres by hydrogenotrophic methanogenesis bacteria in order to prevent the accumulation of simple volatile fatty acids, alcohols and lactate (Moo-Young, 2011).

2.2.2 Factors affecting the rate of anaerobic digestion

In order to increase the rate of anaerobic digestion and gas production by the digester, it is now known, from the section above (2.2.1), that

- The different types of micro-bacterial communities need to live in equilibrium with each other to ensure that the digester is healthy
- The environmental and process operating conditions at which the digester is operated affect the different types of micro-bacterial stages inside the digester

To be able to create a favourable internal environment inside a digester, the effect of the environmental and process operating factors on the degradation process needs to be investigated. There are many different factors affecting the digestion process in an anaerobic digester. Some of the main environmental and process operating factors identified by researchers are listed in Table 2.3. From these main environmental and process operating factors, only the key parameters that affect the plant design will be dealt with in this study.

Table 2.3: Factors affecting the rate of anaerobic digestion (Augusto de Lemos Chernicharo, 2007).

Environmental factors	Process operating factors
• Operating temperature	• Type of digesters
• Retention time	• Type of feedstock
• Organic loading rate	• Digester configuration
• pH	• Mixing
• Nutrient supply	• Feeding frequency
• Metals	
• Volatile fatty acids	
• Oxygen concentration in digester	
• Ammonia	
• Sulphide	

Environmental factors

The environmental factors have been limited to the following as it is the main factors affecting the plant layout;

- Operating temperature
- Retention time
- Organic loading rate
- pH

Operating temperature

In anaerobic digestion, the operating temperature is one of the most important environmental factors as it has a large effect on the micro-bacterial organism's metabolism and enzyme production. The effect of temperature on digesters has been widely studied by a variety of researchers, such as El-Mashad *et al.* (2004), Donoso-Bravo *et al.* (2009), Halalsheh *et al.* (2005) and Young-Chae *et al.* (2004). From the different studies conducted it was found that anaerobic digestion can take place in a wide range of temperatures, 5 to 65 °C. This range at which anaerobic digestion takes place was subdivided into three groups, namely psychrophilic (5-20 °C), mesophilic (20-45 °C) and thermophilic (50-68 °C) digestion (see Figure 2.4).

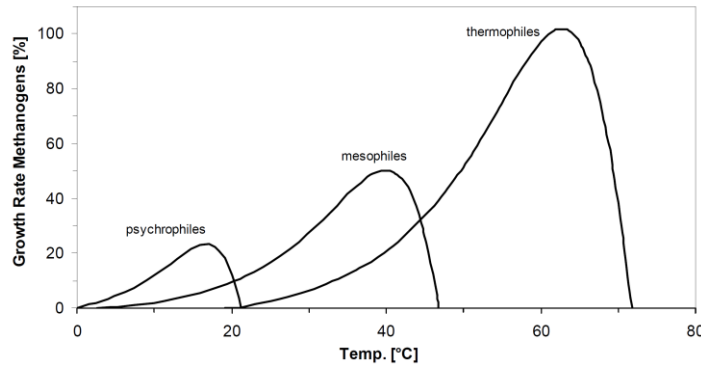


Figure 2.4: Growth rate of methanogens at different digesting temperature ranges (adopted from Moo-Young, 2011)

From the experimental studies it has been observed that an increase of digester temperature leads to an increase in the metabolism of the different groups of micro-bacteria. Above a specific temperature – depending on the temperature operating range of the digester – the micro-bacteria give way to inhibition and their growth rate slows down; this is illustrated in Figure 2.4. With an increase in digester temperature it has also been found that a digester can operate healthily for shorter retention times, which leads to higher gas-production rates. However, as the temperature increases, the micro-bacteria become more sensitive to environmental and process operating factors (Moo-Young, 2011).

Based on the points raised in the above literature review, it is clear that it is beneficial to raise the temperature of the digester. An increase in digestion temperature can lead to an increase in biogas production, and more stable digestion with shorter retention times, but may also lead to an increase in digester sensitivity.

Retention time

The retention time of an anaerobic digester is an important factor to be considered when designing a plant. This factor determines the digester size and affects the biogas production rate, biogas yield as well as the effluent quality of a digester. The retention time can be subdivided into two categories, namely solid retention time and hydraulic retention time.

Solid retention time (SRT) is a measure of the average time period in days that the solids are retained in the digester. This can be calculated using equation 2.1 below:

$$SRT = \frac{V VS_d}{\dot{V}_{out} VS_{out}} \quad (2.1)$$

where V is the volume of the digester in m^3 , VS_d is the concentration of volatile solids in the digester in percentage, \dot{V}_{out} is the effluent exiting flow rate in m^3/day , and VS_{out} is the concentration of volatile solids in the effluent in percentage (Dennis & Burke, 2001).

The solid retention time of an anaerobic digester can be directly related to the volatile solid (VS) reduction and biogas yield, and it relates indirectly to biogas production rate. In 2010, Nges and Liu conducted a study on the effect of the solid retention time of sewage sludge in mesophilic (40 °C) and thermophilic (55 °C) conditions, illustrating the relationship of SRT to VS reduction, biogas yield and biogas production rate. The results of the study are presented in Figure 2.5 and Figure 2.6.

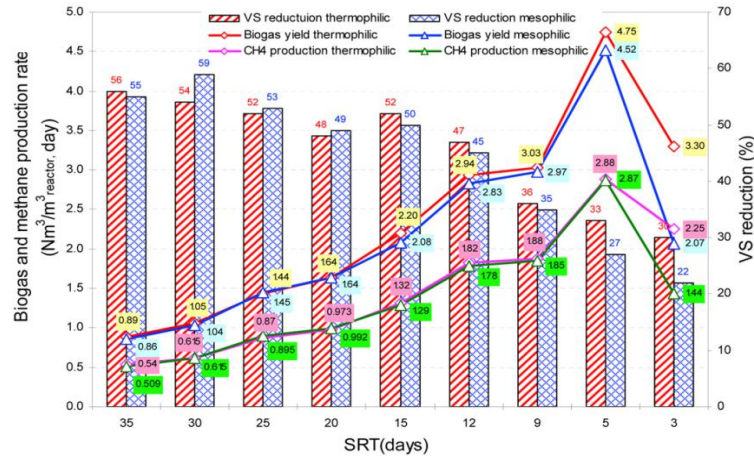


Figure 2.5: Effect of biogas, CH₄ yield and VS reduction on SRT of a mesophilic and thermophilic digester (adopted from Nges & Liu, 2010)

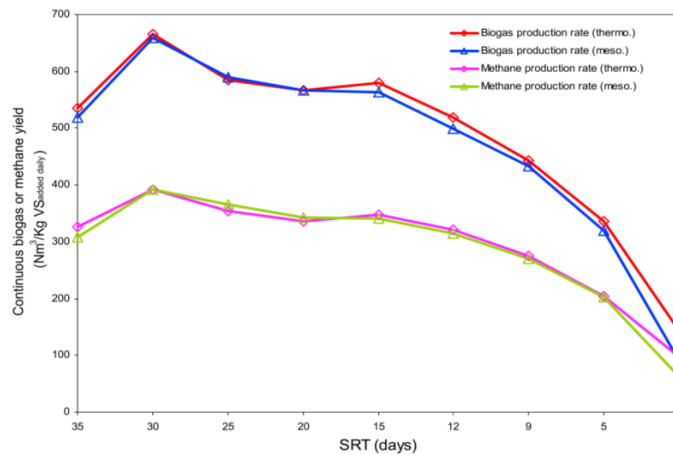


Figure 2.6: Effect of biogas and CH₄ production on SRT (adopted from Nges & Liu, 2010)

The study above indicates that, with an increase in SRT, more VS can be digested and a higher biogas yield can be obtained from the feedstock. In the case where SRT decreases, the VS destroyed was less, but the biogas production rate increased. The study concludes that, if the critical point of a CSTR's SRT is at five days, when the micro-bacterial community growth rate can keep up with the influent rate, it leads to a drop in pH and accumulation of amino and fatty acids inside the digester.

The hydraulic retention time (HRT) is a measure of the average time period in days that the influent remains in the digester, and can be calculated by using equation 2.2.

$$HRT = \frac{V}{\dot{V}_{in}} \quad (2.2)$$

where V is the volume of the digester in m³ and \dot{V}_{in} is the flow rate of the influent entering the digester in m³/day.

In the most conventional CSTR, the HRT is equal to the SRT, but it can be decoupled from the SRT by applying an intermittent mixing scheme or adding a clarifier to the end of the works. Obtaining a SRT-to-HRT ratio of 2 effectively means that the digester can be half the size for the same energy output (Turovskiy & Mathai, 2006).

Organic loading rate

The organic loading rate (OLR) is a measure of the biological conversion capacity of the volatile solids in the feedstock of an anaerobic digester. The OLR is calculated in order to indicate the amount of feedstock that has to be supplied to a digester on a daily basis. It also can be used to quantify how effectively the digester volume is being utilised and is expressed in terms of the mass of volatile solids supplied per day (VS_{in}), in unit of kgVS/d, as a ration of the digester volume (V) in m^3 , as formulated in equation 2.3 below:

$$OLR = \frac{VS_{in}}{V} \quad (2.3)$$

By increasing the OLR at a constant temperature it is possible to increase the metabolism of the micro-bacteria inside the digester. This phenomenon is illustrated in Figure 2.7 with the change in line gradient of feedstock sludge with a concentration VS of 60 % are compared to 85 % VS vs. the VS destruction.

If the OLR is too high, the rate of metabolism of the methanogenic bacteria cannot keep up with that of the acetogenic bacteria and leads to an increase in H_2 partial pressure. In the case that the OLR is low, the digester capacity is under-utilised, but the energy demand of the digester remains the same to keep it at a constant temperature.

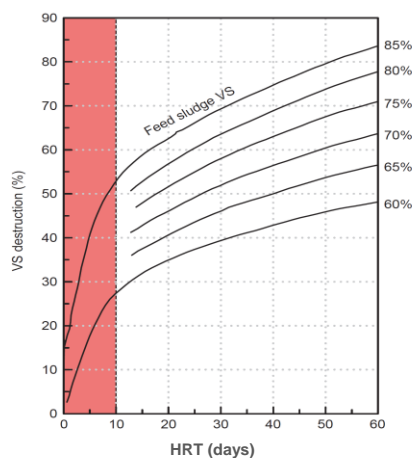


Figure 2.7: Effect of VS in the influent as a function of HRT and VS destruction in the digester (adopted from Moo-Young, 2011)

In general, the OLR for a single mesophilic digester treating sewage sludge can vary between 2 and 9.2 kgVS/ m^3d (Il-Su *et al.*, 2011), but for a two-phase digester configuration also operating at mesophilic conditions, the OLR can be as high as 22 kgVS/ m^3d (Demirer & Chen, 2005).

pH

The pH of the substrate in the digester needs to be monitored closely and adjusted by dosing, if needed, as it is directly related to the growth rate and the metabolism of the microorganisms inside the digester, as discussed. Each group of microorganisms inside the digester has its own optimum pH range, which creates a challenge to satisfy each group. The optimum pH range for the hydrolysis and acetogenic bacteria has been found to be acidic, ranging from 5.2 to 6.3. For the acetogenic and methanogenic groups, on the other hand, the pH range is between 6.8 and 7.2. It is also known from section 2.2.1 that these two groups are very sensitive to pH and pH fluctuation (Moo-Young, 2011).

As a result of the production of VFA in the first and second stages of AD, the pH of the substrate lowers. The lowering of the pH is then countered by the formation of CO_2 and bicarbonate (CaCO_3) by methanogenesis. The counter-reaction of methanogenesis is called the 'buffer' capacity of a digester. In a healthy, stable digester the buffer capacity of the microorganism is able to keep the pH of the substrate between 6.9 and 7.1, with a CaCO_3 concentration of between 1 000 and 2 500 mg/l. This relationship of CO_2 , CaCO_3 and pH is indicated in Figure 2.8 below.

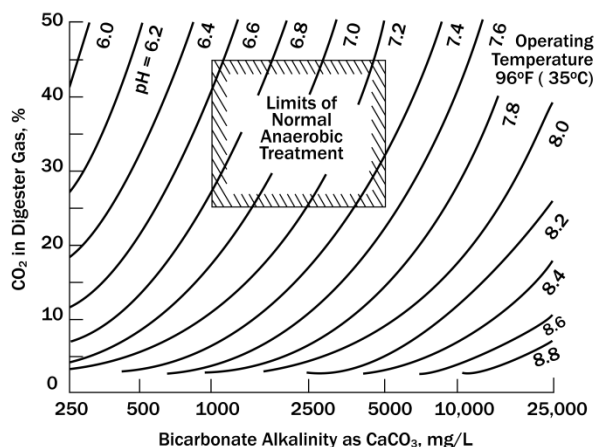


Figure 2.8: The relationship between CO_2 and pH as a function of bicarbonate in a single stage digester at 35 °C (from Turovskiy & Mathai, 2006)

In the case where the VFA accumulates inside a single digester and the pH drops below 6.7, the digester needs to be adjusted by dosing it with sodium bicarbonate for example before it turns toxic. By changing the anaerobic digestion reactor configuration to two-phase, it is possible to operate the pre-digester stably at a pH of 6.2 and the post-digester at a pH of 6.9 to 7.1. The digester configuration will be dealt with in more in detail later.

Process operating factors:

The process operating factors listed in Table 2.3 that affect the rate of AD will be limited to the following in this thesis:

- Digester configuration
- Feeding frequency
- Mixing

The reason for not covering the type of digester and digester feedstock in detail is because these parameters are fixed for the case study and therefore will only be discussed briefly. The reactors available at Gammams WWTP are five semi-egg-shaped digesters with a working volume of 1 600 m³ each. The digester can be fed by pumping the raw sludge in at the bottom or the top. The supernatant effluent from the digesters can be withdrawn from a series of drains at four different levels, where the treated sludge is withdrawn from the bottom of the conical shape of the digester. The digesters are also equipped with an overflow weir box in the case of overflowing, and the biogas take-offs for the digesters are located at the top, leading to the gas storage tank (refer back to Figure 2.2 for plant overview).

The feedstock available at Gammams WWTP is primary sludge from the PSTs and secondary sludge from the SSTs known as waste-activated sludge (WAS). The quality and quantities will be discussed in Chapter 3.

Digester configuration

From the 1960s, researchers started to investigate and develop different configurations of CSTRs. The different CSTR configurations that are available today are single-stage, two-stage and two-phase. These three different digester configurations are illustrated in Figure 2.9. A single-stage reactor is the most basic reactor configuration and consists of a single large tank with a conical shape at the bottom (see Figure 2.9a). The reactor is equipped with a mixing system and exchanger mounted either externally or internally to heat the sludge. A single-stage reactor is also fitted with multiple substrate extraction points, a single sludge take-off at the bottom, gas take-off at the top and one or more supernatant take-off points in the middle. The function of the multiple supernatant take-off points is to drain mainly supernatant at the height it settles (Dennis & Burke, 2001).

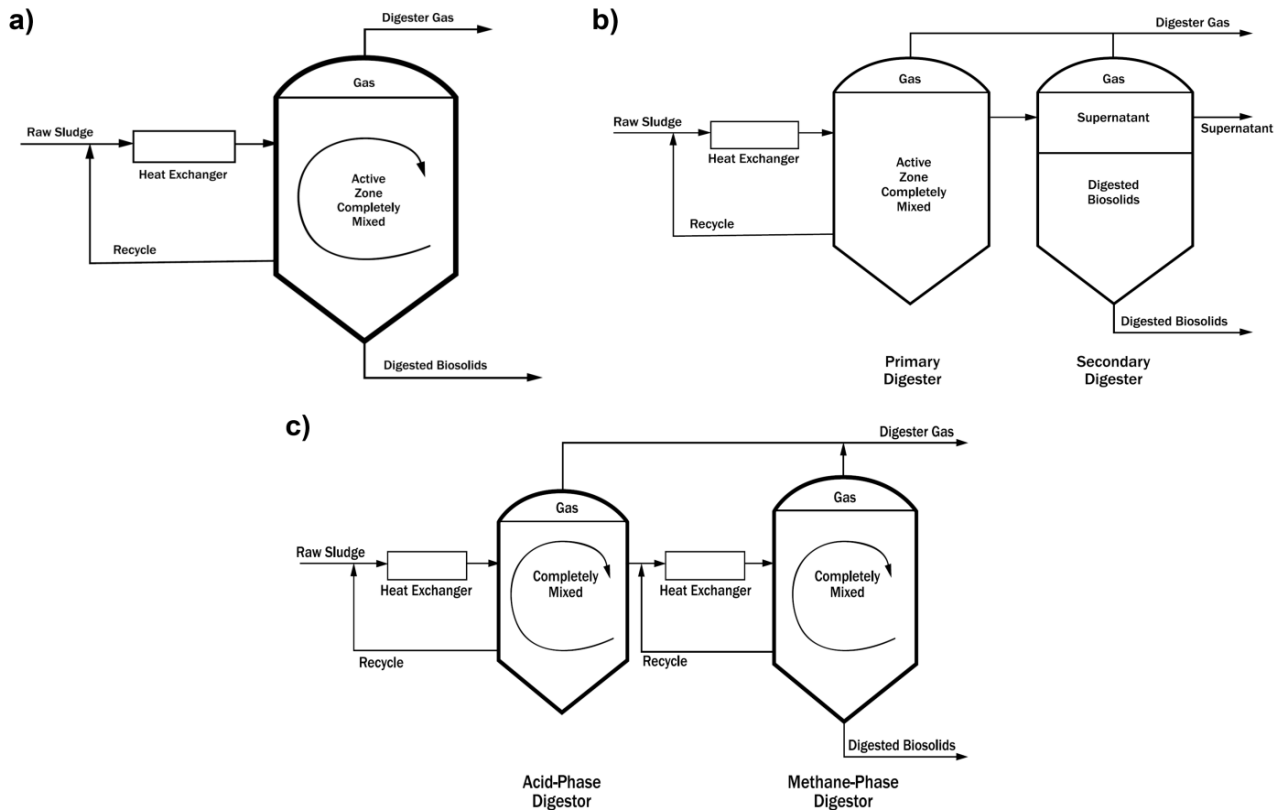


Figure 2.9: CSTR reactor configurations a) single stage, b) two-stage and c) two-phase (from Turovskiy & Mathai, 2006)

The two-stage reactor configuration consists of two or more large tanks, typically the same size with a conical shape at the bottom (see Figure 2.9b). The first and second reactors are referred to as primary and secondary reactors. In this configuration only the primary reactor is mixed and heated. The primary reactor is then connected to the secondary reactor with a single extraction point for sludge as well as a biogas take-off. The second reactor is not mixed or heated. The solids are left to settle and the supernatant is tapped off at the middle. These two-stage digesters can also be configured with different reactor operating temperatures. For example, the primary reactor can be operated at a thermophilic temperature and the second reactor at a mesophilic temperature. This configuration is known as two-stage temperature-phase digestion.

The more recent CSTR configuration is the two-phase arrangement (see Figure 2.9c). This configuration consists of two or more reactors connected in series. The first reactor is known as the acid-phase reactor and the second as the methane-phase reactor. In a typical two-phase reactor configuration, the acid-phase reactor is four to six times smaller than the methane-phase reactor. Both of these reactors are heated and mixed with a conically shaped bottom. The acid-phase reactor only has one extraction point – at the bottom of the reactor – that is connected to the middle of the acid-phase reactor. The methane-phase reactor is in some cases fitted with an additional external heat exchanger placed between the acid-phase reactor and the methane-phase reactor. The function of this additional heat exchanger is for when a temperature-phase digestion configuration is desired (Turovskiy & Mathai, 2006).

The aim of the two-phase reactor configuration is to divide the biological process of the digestion process into the two different reactors. In the acid-phase reactor, the aim is for the hydrolysis and acidogenesis stages to take place, whereas acetogenesis and the methanogen stages take place in the methane-phase reactor.

In the following section, different case studies are included to investigate a comparison between the different digester configurations:

Zhang and Noike (1991), Azbar and Speece (2001), Panichnumsin *et al.* (2010) and Nasr *et al.*, (2012) all conducted comparative studies of the different CSTR configurations and found that the two-phase digester configurations outperformed the other two reactor configurations based on gas production and stable operation under shorter HRT and higher OLRs. Table 2.4 provides a comparative summary of the three different reactor configurations based on a review of the case studies.

Table 2.4: Comparison of CSTRs digesting sewage sludge, (Schafer *et al.*, 2002)

Type of CSTR	Single stage (SS-M)	Two-stage (TS-MM)	Two-stage (TPAD-TM)	Two-phase (AG-MM)
HRT (days)	20 - 38	15 - 32	8 - 35	11 - 22
Max OLR (kgVS/m ³ day)	9.2	16.3	18	22
Avg VS destroyed (%)	65	62	66	59.8
Avg specific biogas production rate (m ³ /kgVS _{des})	0.89	0.94	1.12	1.1
CH ₄ in biogas (%)	54-75	56- 72	58- 68	58- 75

Feeding frequency

Anaerobic digesters can be fed in three different regimes, namely continuous, semi-continuous and batch loading. In a continuous feeding regime, a digester is fed by a continuous inflow, mostly at a constant volume flow rate. In a semi-continuous feeding regime, the digester is fed at set time intervals with equal time spacing in between the intervals. In the case of batch loading, the digester is filled with raw feedstock together with an inoculum to start the digestion process, then left until the organic material is digested and emptied. This feeding regime falls outside the scope of this study and will not be discussed further.

Case studies on semi-continuous feeding are reviewed in the section below:

In 2007, Bombardiere *et al.* studied the performance of a thermophilic digester under different semi-continuous feeding frequencies. The digester was fed once, twice, six times and twelve times per day with chicken litter, keeping the OLR and the HRT constant. The results indicated that the feeding frequency of six times per day outperformed the others based on the biogas production rate. The feeding frequency

of twice per day followed, with 4.4 % lower gas production, then twelve times per day, with 16.1 % lower, and lastly once per day, with a 16.6 % lower biogas production rate compared to the feeding frequency of six times per day. The authors recognised that the results were influenced by thermal shock to the digester due to the influent not being preheated, especially at the feeding frequency of twelve times per day.

In a more recent publication on semi-continuous feeding frequencies by Piao *et al.* (2013), the digester's performance was studied at frequencies of twice per day, once per day and once every second day, based on CH₄ production and the stability of the digesters at a constant HRT and OLR. The results showed that the frequency of twice per day had the highest CH₄ production and was more stable, with lower VFA concentrations in the digester and a stable pH. A feeding frequency of once per day produced 33 % less biogas compared to the first digester, while a frequency of once every two days ended up toxic, with an accumulation of VFA inside the digester and a drop in pH.

Based on the results of these studies and the lessons learned, a decision can be made to select a feeding frequency for the AD plant layout. However, further studies are needed to find the optimum frequency for CSTR digesting sewage sludge.

Mixing

Mixing is an important process operating factor, which is essential to transfer new organic substances to the microorganisms. When mixing a digester substrate, it increases the surface contact area of the organic substances to the microorganisms and acts as a transportation mechanism for the microorganisms inside the digester. Mixing a digester is also essential to create a homogeneous solution to prevent a scum layer forming on top of the substrate level in the digester.

Mixing of a digester can be classified into three different categories namely, method, intensity and intervals. These categories can further be broken down as illustrated in heritage diagram in Figure 2.10 below and will be followed the available mixing methods and sizing a system.

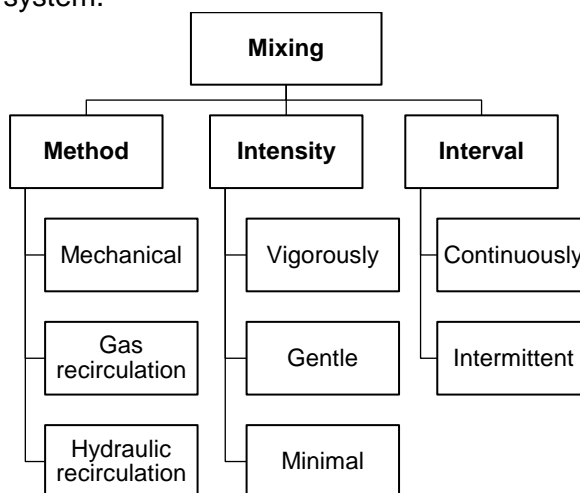


Figure 2.10: Heritage diagram of mixing an anaerobic digester

In order to design a mixing system for an anaerobic reactor, the three categories listed above should be studied carefully, as mixing has a large effect on biogas production rate and the pH inside the digester (Augusto de Lemos Chernicharo, 2007).

The method of mixing a reactor is based mainly on the type and design of the reactor. In this study the focus was on methods used to mix a CSTR experimentally and commercially, which are broken down into three subcategories, namely mechanical, gas recirculation and the hydraulic recirculation mixing method.

In the mechanical mixing method some sort of impeller is used, with or without a cowling, and driven by an electrical motor to stir the digester that is mounted internally or externally on the reactor. In the gas recirculating method, biogas is compressed by a compressor and reintroduced into the digester in a confined or unconfined manner, relying on the differential density to mix the reactor. In hydraulic recirculation, a sludge pump is installed outside the digester, sucking from the bottom and reintroducing it into the reactor by a set of nozzles. An illustration of the different methods used experimentally and commercially are summarised in Figure 2.11 below.

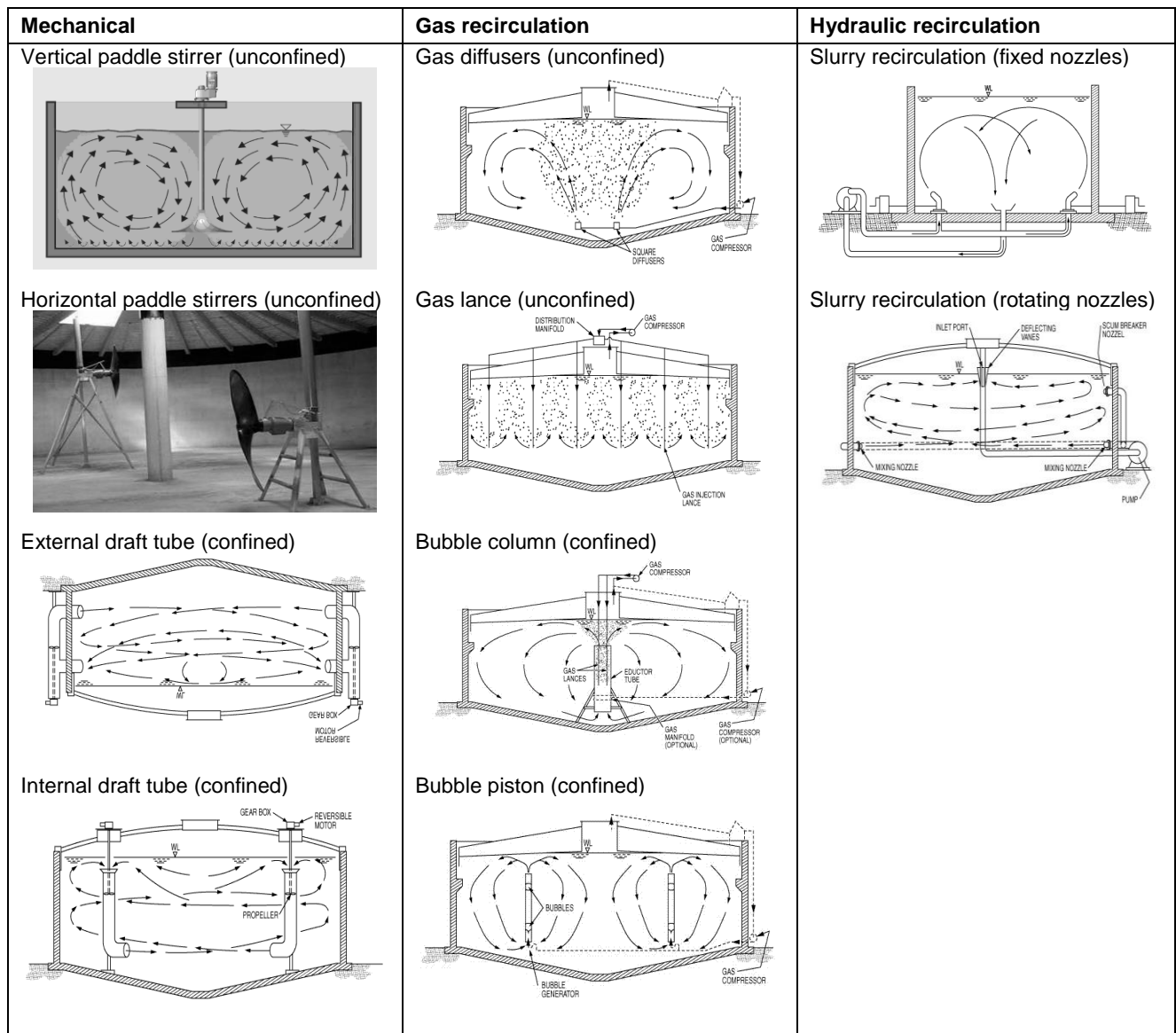


Figure 2.11: Mixing methods used for CSTR (Turovskiy & Mathai, 2006)

When selecting a mixing method from the options provided above for a CSTR a digester, the internal hydraulic fluid flow of the digester has to be considered. The mixing design has to maximise the effective volume in the digester by eliminating the dead zones and obtaining a homogenous solution in the digester.

Several research studies in the past focused on increasing the effective volume of a digester and quantifying the amount of mixing needed for a digester. The parameters that are mainly used to quantify the mixing inside a digester today are: digester volume turnover time (DVTT), averaged velocity inside digester (v_{avg}), unit power (UP) and the normalised mixing intensity (G). According to Turovskiy and Mathai (2006), the desired ranges for these mixing parameters in a CSTR are a DVTT, UP and G in the ranges of 0.8 to 1.2 h, 5.2 to 7.9 W/m³ and 50 to 85 s⁻¹ respectively.

The DVTT is a measure of the anticipated capacity of the mixing system in hours and can be calculated using equation 2.4, where V is the volume of the reactor in m³ and \dot{V} is the mixing flow rate in m³/h.

$$DVTT = \frac{V}{\dot{V}} \quad (2.4)$$

The UP is a power-to-volume ratio in W/m³ that is normally used to compare different mixing methods based on power consumption. It can be calculated using equation 2.5 below, where P_{mix} is the mixing power in W and V is the volume of the reactor in m³.

$$UP = \frac{P_{mix}}{V} \quad (2.5)$$

The G parameter is a normalised mixing intensity inside the reactor in s⁻¹ and can be determined using equation 2.6, where μ is the dynamic viscosity of the sludge in Pas.

$$G = \left(\frac{P_{mix}}{V \mu} \right)^{\frac{1}{2}} \quad (2.6)$$

In more recent years, CFD simulations have been used to optimise the digester effective volume and to compare different mixing methods. One of the more recent studies on CSTR mixing systems, done by Wu (2010a), simulated mechanical draft tube mixing vs. the slurry recirculation mixing method. The study also included direction of pumping with a draft tube and mixing of egg-shaped vs. cylindrical reactor. The results obtained to obtain the same average velocity in the reactor were:

- Pumping upward through the draft tube was 30.7 % more efficient than downwards
- The egg-shape digester turned out to have a power saving of 55 % over the cylindrical digester
- The DVTT, UP and G of the cylindrical reactor were 0.4 h, 6.6 W/m³ and 90 s⁻¹ respectively, whereas those of the egg-shaped digester were 0.85 h, 2.97 W/m³ and 65.5 s⁻¹ at 0 % TS
- The mechanical draft tube had a power saving of 49.7 % with a UP of 2.4 W/m³ and G of 58.89 s⁻¹, compared to the UP of 4.77 W/m³ and G of 83.02 s⁻¹ in the slurry recirculation method

Wu (2010b) continued his research by comparing a bubble column gas diffusers, a mechanical draft tube and the slurry recirculating method in a cylindrical digester using ANSYS Fluent 12.0. The result obtained indicated that, at a TS content of 5.4 % and an average velocity in the reactor of 0.08 m/s, the mechanical draft tube was most efficient (0.52 h, 4.1 W/m³, 71 s⁻¹). It was followed by the bubble column method, with a 29 % increase in UP (5 W/m³, 78.4 s⁻¹) and then by the slurry recirculation method, with a 43 % increase in UP (5.9 W/m³, 85.17 s⁻¹). The gas recirculation

method using the gas diffusers was excluded from the comparison study, as large dead zones occurred due to insufficient mixing.

Many researchers have noted the effect of mixing on the biological enactment of a digester, but the optimum intensity and intervals are a subject of much debate. In the section below, case studies on mixing methods, intensity and intervals will be reviewed:

In 2001, Stroot *et al.* conducted two sets of experiments to study the effect of mixing intensity and intervals on the digester, based on biogas production rate. The results of the experiments showed that intermittent mixing accompanied by a gentle mixing intensity increased the biogas production rate and the digester was able to operate stably under a higher OLR. When a continuous mixing interval was applied with a vigorous intensity, the digester become unstable and ended up toxic. The study concluded that an unstable digester can be stabilised by an intermittent mixing interval and reduced mixing intensity.

Karim *et al.* (2005a) studied the effect of mixing on a digester with sludge at 5 % and 10 % TS content using a mechanical paddle stirrer, gas recirculation, bubble column, hydraulic recirculation and an unmixed digester. The results of the study at 5 % TS content showed that the unmixed digester had the highest biogas production rate. At 10 % TS content, the results indicated that the hydraulic recirculation digester outperformed the other digesters based on biogas production, followed by the biogas-recirculation digesters with 15 % less than the mechanical mixing digesters with 22 % less, and lastly by the unmixed digesters, which produced 29 % less biogas. Based on the experience gained, Karim *et al.* (2005a) proposed the biogas recirculation mixing method for large-scale digesters, as slurry at 10 % TS content is difficult to handle.

Karim *et al.* (2005b) took their research work further to study the effect of the three different mixing methods at 5 %, 10 % and 15 % TS content sludge. It was found that mixing makes a difference in the digester biogas production rate at a TS of 10 % and higher. It also was found that mixing during the start-up of a digester in the first 20 days of mixing is not beneficial for the digester in terms of biogas production rate and pH.

In a more recent study, Kaparaju *et al.*, (2008) studied the effect of different mixing intervals on laboratory-scale digesters based on their biogas production rate using a mechanical paddle stirrer. In the laboratory-scale experiments, the first digester selected had a continuous interval with a gentle intensity, the second an intermittent interval of 10 min mixing followed by 10 min of rest, with a gentle intensity, and the third had an intermittent interval of 2 hours mixed followed by 2 hours of rest period, also at a gentle intensity. The results indicated that intermittent mixing intervals of 2 hours increased the biogas production rate by 12 % and intervals of 10 min increased the rate by 7 % compared to the continuous mixing interval.

Summary of mixing anaerobic digester

From the literature reviewed on mixing, it is evident that mixing is necessary from a biological perspective to obtain stable digestion and to increase the biogas production rate. From a hydraulic perspective it is necessary to mix a digester to maximise the effective volume.

In the studies reviewed in relation to different mixing methods, the mechanical upward pumping in a draft tube was the most effective. The problem with all the mechanical

rotating equipment used for mixing is clogging of the impellers due to the fibres in municipal sludge. In the case of devices such as horizontal paddle stirrer and slurry-recirculation pumps located inside the digester, these fibres lead to recurring maintenance of these devices and tedious downtime. Images of these fibre blockages can be seen in Figure 2.12 and Figure 2.13 below.



Figure 2.12: Damaged horizontal paddle stirrer (from CAE, 2012).



Figure 2.13: Blockage of a slurry-recirculation pump for a digester mixing system: a) before and b) after cleaning (from CAE, 2012).

These figures do not illustrate a mechanical draft tube, but indicate the conditions under which the impeller needs to operate. The additional problem with mechanical mixing systems is that a large shear stress is placed on the microorganisms, as can be seen in the study of Karim *et al.*, (2005b), and the power consumption of mechanical systems increases exponentially as TS increases Wu (2010a).

The second most effective method for mixing a digester after the mechanical draft tube was the gas recirculation bubble column, as proposed by Wu (2010b) and Kaparaju *et al.*, (2008).

From the studies reviewed in relation to the effect of mixing on the biological side, it was illustrated that an intermittent mixing interval of 2 hours at a minimal intensity was the most promising option. The additional benefit of using an intermittent mixing scheme is that solids get time to settle to the bottom and that mainly supernatant can be drained from the middle. This accumulation of solids is also known to lead to an increase in the SRT/HRT ratio inside the digester, and an increase in biogas yield (Turovskiy & Mathai, 2006).

2.3 Confined gas mixing

In the literature review of the mixing methods, the effect of mixing on the biological perspective and hydraulic side was reviewed. Based on the literature reviewed, the confined gas recirculation method was selected to be studied further as an alternative to the mechanical draft tube.

The aim of this section was to find the most effective regime of confined gas recirculation for mixing as indicated by the literature. In order to find this regime, different types of vertical two-phase flow regimes were reviewed.

2.3.1 Types of two-phase flow

The term “two-phase flow” covers a broad range of scenarios. Two-phase flow can include a combination of two or three phases of solids, liquids and gases. Examples of different types of two-phase flows are solid-gas, solid-liquid or gas-liquid. As the focus was to find the most effective regime of confined gas mixing for a digester, only the gas-liquid phase was looked at. The main flow regimes that can be identified for vertical gas-liquid flow are:

- Bubbly flow – Where small spherical bubbles flow approximately uniformly upwards in the tube.
- Slug flow – At an increased gas flow rate, the small spherical bubbles coalesce, resulting in the formation of bullet-shaped bubbles. These bubbles are also known as plugs, Taylor bubbles or slugs.
- Churn flow – With a further increase in the gas flow rate, the plugs break up, which leads to an unstable flow regime. This can be identified also by the liquid near the wall in an oscillating up- and downwards motion.
- Annular flow – If the gas flow rate is increased further, a liquid film forms on the wall, with the gas phase in the centre of the tube. Usually some of the liquid phase is entrained as small drops or mist in the gas core in the centre of the tube.

In Figure 2.14 on the following page, these main two-phase flow regimes can be identified, as well as some of the intermittent flow regimes as a function of water-to-air-flow Reynolds numbers.

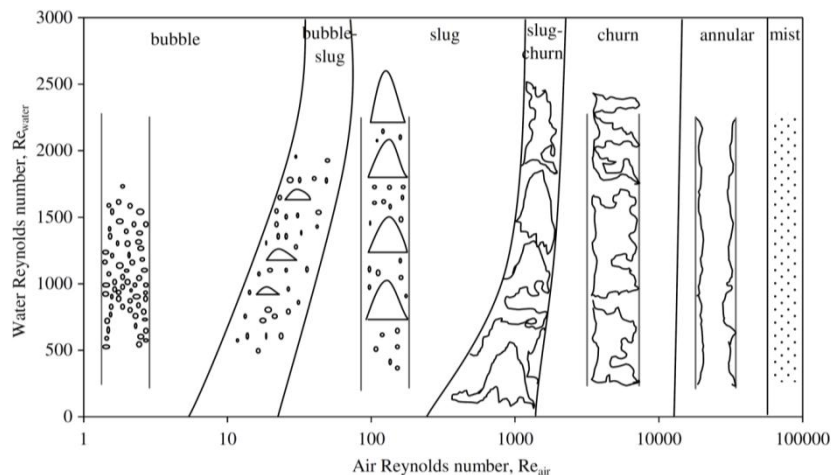


Figure 2.14: Vertical two-phase flow regimes (from Da Hlaing *et al.*, 2007).

2.3.2 Case studies on two-phase flow-conveying liquids

The application of two-phase flow to convey liquids has been used in industry for centuries and is known as an “airlift pump”. Airlift pumps have been used in the following industrial sectors to convey liquids: the petroleum industry, deep-sea mining, the oil field industry, the fishery industry as well as in the biochemical industry for reactor mixing.

The pump characteristics of an airlift pump have recently been studied by Kassab *et al.* (2009). The study was based on a numerical 1D steady state mass momentum balance model assuming isothermal expansion, and was validated against experimental work conducted. The results of the study indicated the following;

- As the SR ratio increases, the efficiency increases at a constant gas flow rate
- The maximum efficiency does not occur at the maximum flow rate
- The maximum efficiency of the pump was found to be in the slug or slug-churn flow regime

The study concluded with the publication of Figure 2.15, which indicates the phase transitions with increasing air flow rate operating at a SR of 0.4, a length of 3.75 m and an internal diameter of 25.4 mm.

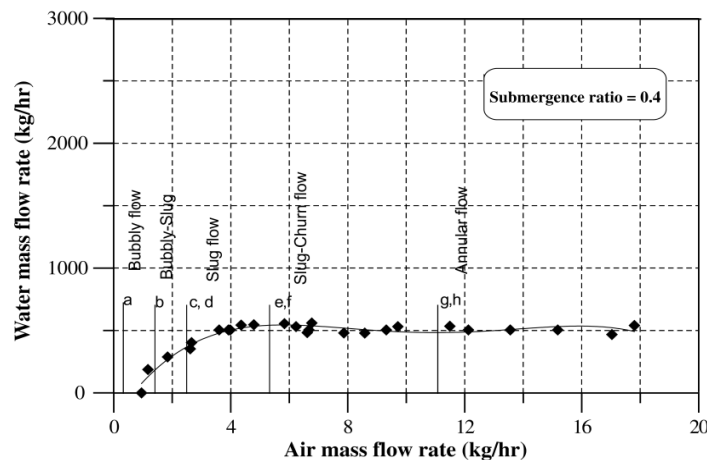


Figure 2.15: Airlift pump-phase transitions with water mass flow rate as a function of air flow rate (from Kassab *et al.* 2009)

Karim *et al.* (2010) looked at improving the performance of an airlift pump using an increasing step geometry upriser. The study was based on a 3D eulerian–eulerian mass momentum balance model, assuming isothermal expansion using the ANSYS Fluent V11 software package. The numerical model was verified by experimental work done by White (2001). The results of the study were as follows:

- The maximum efficiency of the pump was found to be in the plug-flow regime
- An increase in the cross-section area of the upriser due to the step geometry led to an increase in the efficiency of the pump
- It was also found that an optimum step height could be found for a certain aspect ratio of the different diameters of the upriser

Hanafizadeh *et al.* (2010) took the previous study further, using the same numerical model with a tapered upriser, ranging from 0° to 3°, to increase performance. The study was concluded with the following remarks:

- The efficiency of the pump increased as the SR ratio increased at a constant flow rate
- The best efficiency of the pump was found to be in the bubbly-plug regime
- The tapered upriser outperformed the step geometry upriser. The best angle for the tapered upriser was found to be at 3°.

Based on the knowledge gained from two-phase flow and the application of the airlift pump, a concept could be drawn up for a mixing system using the gas recirculation method.

2.4 Conclusion

Anaerobic digestion is one of the few options available that can stabilize raw municipal sludge and address the issue of a sustainable alternative for energy and potable water resource. The case study selected (Windhoek, Namibia) is already reclaiming 22 ML/day of potable water (35 % of the city's demand) from secondary effluent of Gammams WWTP and has the capability to generate electricity from the current plant infrastructure. Sludge stabilization is very important at Gammams to reduce the load on the rest of the WWTP and to minimize the risk of contaminations of fresh resources as up to 80 % of the possible toxic elements bonds to the sludge.

Anaerobic digestion is a complex degradation process, affected by environmental and process operating factors where the organic fraction of the feedstock is decomposed in the absence of air in a chain of events broken up into four main steps. In the first two steps hydrolysis and acidogenesis, bacteria degrade the organic fraction into soluble intermediates and soluble monomers operating at an optimum pH of between 5.2 up to 6.3. The acidogenesis is the most vigorous step in anaerobic digestion, however the bacteria at this stage is sensitive to the environmental pH and the OLR. In the second two steps acetogenesis and methanogenesis, bacteria convert the soluble monomers into biogas operating in an optimum pH solution of between 6.6 up to 7.2. The acetogenesis bacteria are very sensitive to environmental fluctuations whereas the methanogenesis are sensitive to the H₂ partial pressure.

The digestion process is affected by several environmental factors which have been limited to the temperature, retention time, OLR and pH in this study as these are the main factors affecting a plant design layout. Anaerobic digestion can take place at three different temperature ranges namely psychrophilic (5-20 °C), mesophilic (20-45 °C) and thermophilic (50-68 °C) (Moo-Young, 2011). An increase in temperature leads to an increase in the metabolism of the bacteria, but also leads to an increase to sensitivity. The retention time can be subdivided into solid retention time and hydraulic retention time.

Studies conducted to predict biogas production found that there is a directly proportional relation of solid retention time to biogas production and indirectly proportional relation to the biogas yield as shown in Figure 2.5 and Figure 2.6. The decoupling of hydraulic retention time from the SRT leads to increased digester performance and also a reduction in digester size. The OLR is a measure to calculate the amount of feedstock that can be fed to the digester in a day and can also be used compare different digester configuration effectiveness.

The process operating factors affecting the anaerobic digestion process were limited to the digester configuration, feeding frequency and mixing of the digester. The digester configuration of a CSTR can be broken down in to three categories namely single stage, two-stage and two-phase, where the aim of the two phase is to separate the first two steps of the last two steps of anaerobic digestion. Experimental case studies show that the most promising feeding regime is semi continuous at four to six times per day evenly spaced. The last process operating factor that was studied in this report was mixing a CSTR digester.

Mixing of a CSTR digester can be divided in three sub categories namely mixing method, mixing intensity and mixing interval. From experimental and numerical studies it indicated that mechanical daft tube mixing in an upwards direction was the

most effective mixing method. The second most effective mixing method was the bubble column, but from investigating two-phase conveying more in detail it was found that the plug flow regimen is more effective than bubble flow. Experimental work also indicated that minimal mixing on an intermittent interval was the most promising option to select for a CSTR digester.

It can be concluded, based on the literature review an understanding of how the biological process in an anaerobic digester breaks down the biodegradable fraction of the sludge was acquired. An understanding of the different key parameters affecting the anaerobic digestion process, biogas production rate and the plant design was also obtained from the literature survey conducted for this study.

3. METHODOLOGY

The thermal and hydraulic control of an anaerobic digestion plant is important, as it affects the overall AD plant in numerous ways presented in the previous chapter. The effect of the environmental and process factors on the digestion process were studied in the literature review.

Based on the knowledge gained, the first aim in this chapter was to evaluate different conceptual AD plant layouts based on an overall heat, energy and electrical production balance. The second aim in this chapter was to generate a concept for a CSTR mixing system using the gas recirculation method in a confined plug-flow regime and predicting its mass rate using a numerical model.

The objectives set for this chapter are divided into two sections – the AD plant layout and the digester mixing system. The objectives set for the AD plant layout were to:

- Draw up three different conceptual AD plant layouts, considering the available infrastructure at the WWTP and the knowledge gained on the environmental and process factors on the anaerobic digestion process
- Perform a transient overall heat, energy and electrical production balance on the three different conceptual AD plant layouts through a typical year
- Evaluate the results obtained from the overall heat, energy and electrical production balance

In the second section, the digester mixing system, the objectives were to:

- Outline the design criteria and limitations of the mixing system
- Generate and evaluate three different concepts for the mixing system
- Derive a transient numerical model for the selected concept
- Use the numerical model to perform sensitivity analysis on the mixing system geometry

3.1 Anaerobic digestion plant layouts

The selection of the configuration for an AD plant layout not only affects the digesters in terms of energy generated and energy demand, which can be seen in the performance comparison of the high-rate CSTR in Table 2.4, but also the effluent quality.

In order to draw up a conceptual AD plant layout for processing municipal sewage sludge, the following key points need to be considered:

- The quantity, quality and TS content of the sludge that needs to be processed
- The method used for the disposal of the digested sludge at the WWTP
- The required quality of the effluent discharged from the AD plant
- The Inlet sludge temperature
- The climate at the WWTP

3.1.1 Feedstock for AD plant and disposal method

Gammams WWTP, which was used for the case study, receives an average wastewater influent flow of 48 ML/day, as mentioned in section 2.1. The volume of the primary sludge drained from the PSTs is measured at the plant and is presented in Figure 3.1. The deviation in Figure 3.1 is due to the fact that it was a manual process. The total WAS sludge volume was not measured at the plant, but the volume per day

was calculated based on the number of times the WAS sludge sump was filled. The calculated quantity and quality of the thickened WAS sludge is tabulated in Table 3.1.

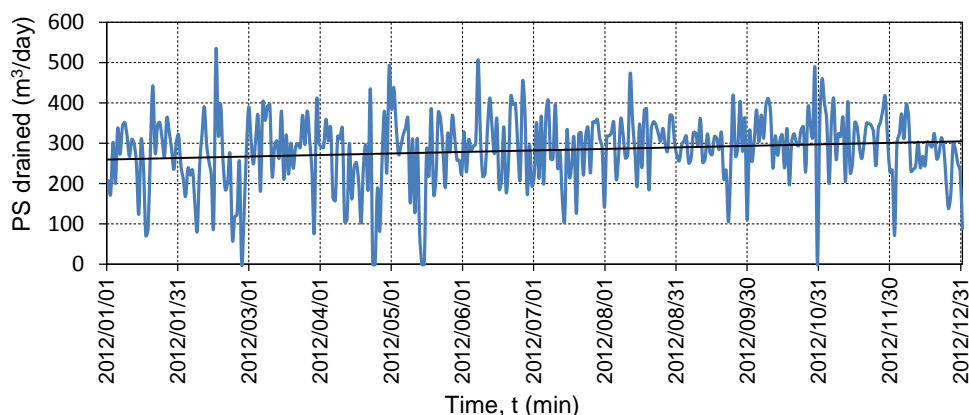


Figure 3.1: Volume of primary sludge drawn from PST's per day over a year

Table 3.1: Thickened PS and WAS sludge volumes at Gammams WWTP

Raw sludge	Volume per day (m ³ /day)	Draw off interval per day	% TS	% VS	pH
PS	283.3	4x	3.23	82.3	6.14
WAS	958.7	Continuously	3.15	81.3	6.33

For the known quantities of sludge available, a comparison study was conducted for this thesis on feeding the proposed concepts with sludge containing 4 %, 6 %, 8 % and 10 % TS . The additional thickening of the PS and the WAS feedstock was not covered in this thesis, as it falls outside the scope of this study.

In this comparison study of feeding the three concept plants with different TS contents the HRT of each individual concept were kept constant from 4 % to 10 % TS. In the study the primary sludge was first considered and the WAS sludge was added if additional capacity was available. The reason for this is that the primary sludge places a higher load on the plant (Thornton et al., 2009). The available sludge volumes provided in Table 3.1 can be reduced to the volumes indicated in Figure 3.2 at the corresponding TS contents. Increasing the TS contents from 2 % to 10 % TS reduces the volume threefold.

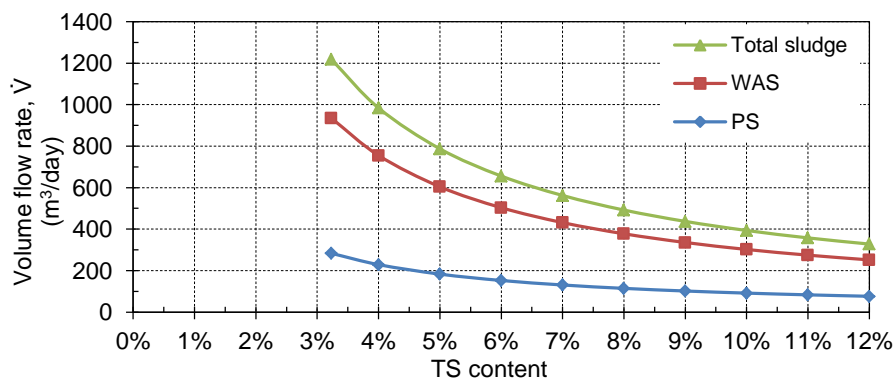


Figure 3.2: Volume flow rate of PS and WAS per day at different TS concent ratios

The treated sludge from the conceptual AD plants will be disposed to a belt press plant, where it will be dewatered further to approximately 25 % TS content. After the

sludge is dewatered it will be piled and treated with an aerobic compost process. Additional elements will be added to the composted sludge before it will be pelletised and sold as fertiliser. The remaining untreated sludge, which cannot be treated by the conceptual AD plant at Gammams due to limited capacity will be pumped to Otjomuize WWTP for treatment.

Using a belt press plant with a compost process for the processed sludge means that the quality of the sludge treated by the AD plant needs to comply with the following regulations set (DWAF, 2009):

- Supply the belt presses plant with B-series quality sludge
- Reduction of 50 % VS needs to be maintained in the AD plant

3.1.2 Conceptual layouts for the AD plant

In selecting a conceptual layout for the AD plant at Gammams works, the current infrastructure first had to be considered. The current AD plant is equipped with five egg-shaped digesters with a working volume of 1 600 m³, one expanding roof gas storage tank with a storage capacity of 1 000 m³ of gas, a pump station, an inlet and outlet sludge sump, and an effluent clarifier for the digesters.

To configure the three different conceptual layouts for Gammams WWTP, the different digester configurations available for a CSTR displayed in Figure 2.9 with its capability to digest sludge and produce methane needs to be evaluated which are summarised in Table 2.4.

This table illustrates that the two-stage and two-phase digester configurations are able to achieve a much higher OLR compared to the single stage digester configuration. It was for this reason that only two-stage and two-phase digester configuration were considered for the conceptual layouts at Gammams WWTP. Thermophilic digestion as well as temperature phase digestion was excluded from plant due to the reaction sensitivity and the recurring problem of scum accumulation inside the digesters (Moo-Young, 2011).

General flow of the different AD conceptual layouts

In each of the three conceptual layouts the feedstock was first pre-heated with the effluent from the AD plant in the outlet sump. A double tube pre-heat exchanger was used to recover this heat from the effluent by circulating the influent and effluent through the pre-heat exchanger. The additional heat needed to match the feedstock temperature to that of the digester operating temperature will be added with a post-heat exchanger. The heat heated water from the post-heat exchanger will be recovered from the CHP units that generate. This will be covered in detail in section 3.1.3 and a detailed illustration of the pre- and post-heat exchanger is shown in Figure 3.6. The detailed illustration of the CHP unit is shown in Figure 3.19 and will be covered in detail to come.

The supernatant (SN) in each of the three concepts was drained from the middle of the digesters after the rest period of the intermittent mixing schemes. The SN was drained by gravity to a clarifier to recover the trapped solids in the SN which will be displayed in each concept flow diagram. The underflow of the supernatant clarifier was directed back to the feedstock sump to increase the SRT/HRT ratio, and the overflow was directed to the ASP, TFs or the A series channel, depending on the plant load.

The environmental and process operating condition of each concept was specified and the quality of the digestate effluent had to have a 50 % reduction in VS reduction to comply with the relevant regulations. This reduction in VS was not a problem – as can be seen in Table 2.4, all digester plant layouts could deliver a reduction in VS of more than 50 % in stable operation.

Concept 1

In the first concept for the AD plant layout, the thickened sludge was treated in a two-stage digester configuration with a 3/2 layout. The first three digesters were operated as high-rate CSTRs, where they were mixed and heated internally to maintain the operating temperature set point. The second two digesters were operated as post-digesters and were only mixed internally. The biogas in this concept was captured at all five of the digesters and conveyed to the gas storage tank before sending it to the CHP units. The process flow diagram for the concept can be seen in Figure 3.3 and the plant operating conditions selected for the concept are illustrated in Table 3.2.

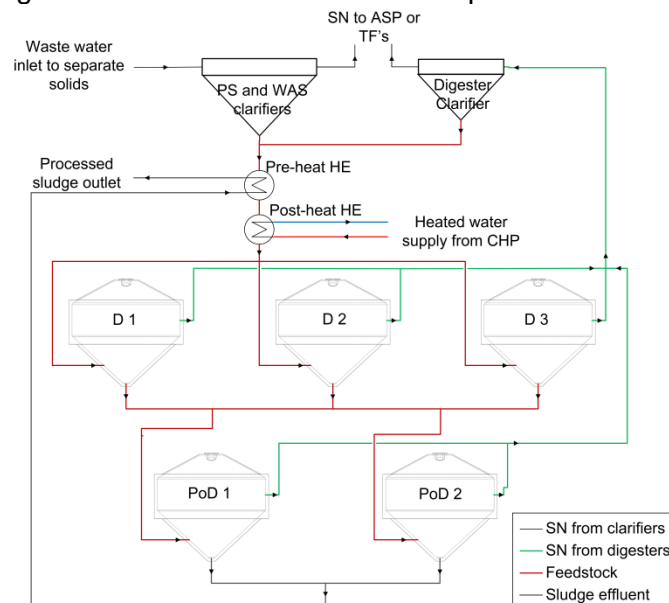


Figure 3.3: Sludge and SN process flow diagram for AD plant - concept 1

Table 3.2: Plant operating conditions for concept 1

Plant operating conditions	3 CSTR digesters	2 post-digesters
Operating temperature (°C)	37	Unheated
HRT (days)	19.9	13.3
Feeding frequency (/day)	4 x	8 x
Volume fed per feeding schedule (m ³)	21.31	15.98
OLR (kgVS/m ³ day) at 4, 6, 8 and 10 % TS	1.8, 2.6, 3.5, 4.4	2.7, 4.0, 5.3, 6.6
Operating pH	6.9–7.0	6.9–7.3
Mix interval; mix (h), unmixed (h)	3.5, 0.5	3.5, 0.5
DVTT (min), UP (W/m ³) and G (s ⁻¹)	60, 5.5, 70	60, 5.5, 70

Concept 2

In the second concept the thickened sludge from the plant was treated in a 4/1, two-stage digester configuration. The sludge was fed to four high-rate CSTRs that were mixed and heated internally to maintain the operating temperature. The sludge was then sent to a single post-digester that was only mixed. The biogas generated by the

digester was captured from all five the digesters and conveyed to the gas storage tank before sending it to the CHP units.

The process flow diagram of the second concept of the AD plant can be seen in Figure 3.4 below, and the plant operating conditions selected are tabulated in Table 3.3.

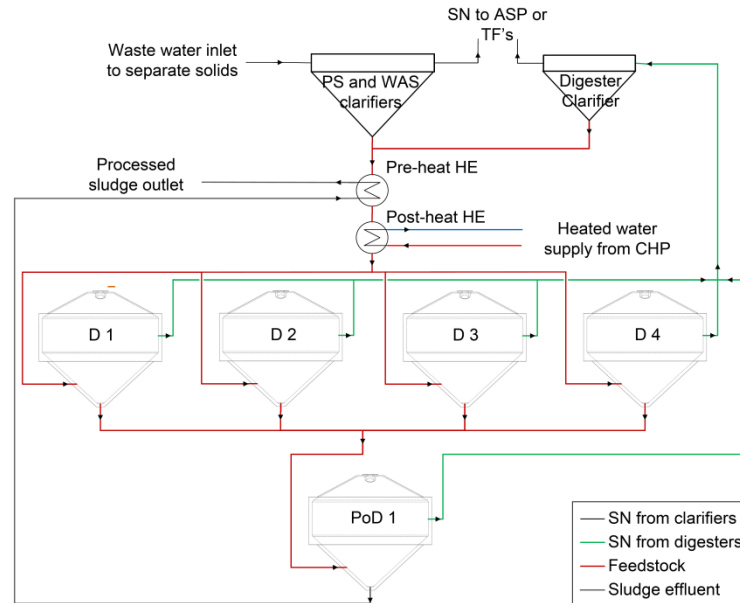


Figure 3.4: Sludge and SN process flow diagram for AD plant - concept 2

Table 3.3: Plant operating conditions for concept 2

Plant operating conditions	4 CSTR digesters	1 post-digester
Operating temperature (°C)	37	Unheated
HRT (days)	24.3	6.1
Feeding frequency (/day)	3 x	12 x
Volume fed per feeding schedule (m ³)	23.31	23.31
OLR (kgVS/m ³ day) at 4, 6, 8 and 10 % TS	1.5, 2.2, 2.9, 3.6	5.8, 8.7, 11.5, 14.4
Operating pH	6.9–7.0	6.9–7.3
Mix interval; mix (h), unmixed (h)	3.5, 0.5	3.5, 0.5
DVTT (min), UP (W/m ³), G (s ⁻¹)	60, 5.5, 70	60, 5.5, 70

Concept 3

The third concept was the most modern configuration used for anaerobic digestion plant layout. The raw thickened sludge was first pumped to a pre-digester that was internally mixed and heated. The sludge from the pre-digester was then pumped to four high-rate CSTRs that also were internally mixed and heated.

The aim with the pre-digester (Pre-D) and the other four CSTR digesters (D1 to D4) was to split the biological decomposing steps of anaerobic digestion into two separate controlled environments, as discussed in the literature review (section 2.2.2). The biogas generated was only tapped off from the four main CSTRs, as the gas produced by the pre-digester contains mainly CO₂ that will be burnt in a flare. By not capturing the pre-digester's gas, the ratio of CH₄/CO₂ is increased, thereby increasing the quality of the fuel supplied to the CHP units. The process flow diagram for this concept can be seen in Figure 3.5 and the plant operating conditions selected are tabulated in Table 3.4.

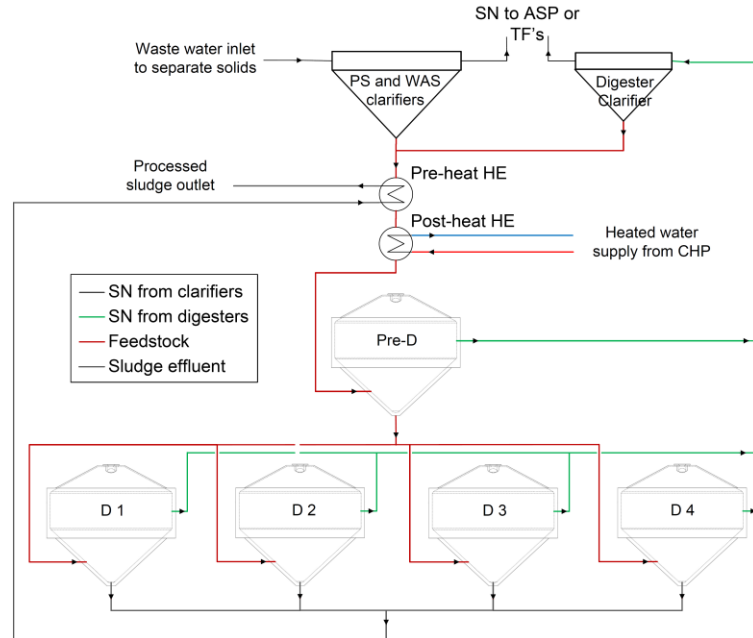


Figure 3.5: Sludge and SN process flow diagram for AD plant - concept 3

Table 3.4: Plant operating conditions for concept 3

Plant operating conditions	1 pre-digester	4 CSTR digesters
Operating temperature (°C)	37	37
HRT (days)	3.2	18.03
Feeding frequency (/day)	12x	6x
Volume fed per feeding schedule (m ³)	33.13	16.56
OLR (kgVS/m ³ day) at 4, 6, 8 and 10 % TS	10.1, 15.1, 20.1, 24.8	2.1, 3.1, 4.1, 5.0
Operating pH	6.5–6.7	6.8–7
Mix interval; mix (h), unmixed (h)	3.5, 0.5	3.5, 0.5
DVTT (min), UP (W/m ³), G (s ⁻¹)	60, 5.5, 70	60, 5.5, 70

The expected performance of the three different conceptual AD plant layouts was estimated and is tabulated in Table 3.5. These expected performance parameters were obtained from similar case studies covered in the literature review and were summarised in Table 2.4.

Table 3.5: Expected plant layout performance of different concepts

Plant performance	Concept 1	Concept 2	Concept 3
AD plant capacity per day (m ³ /day)	255.71	279.69	397.50
Percentage volume of plant sludge treated at TS content of 4, 6, 8 and 10 %	26, 39, 52 and 65 %	28, 43, 57 and 71 %	40, 61, 81 and 100 %
Avg VS reduction of PS and WAS (%)	63	61	60
Biogas yield (m ³ /kgVS)	0.89	0.96	1.1
CH ₄ in biogas (%)	62	65	65

Table 3.5 shows that there is a large difference between the concepts in terms of the sludge-handling capacity. Concept 3 is able to treat 55.4 % more and concept 2 9.3 % more sludge per day compared to concept 1. It is also shown that, by increasing the TS of the feedstock, a larger portion of the available sludge can be treated while still keeping the HRT of the concept constant.

3.1.3 Heat, energy and electrical balance on AD plants

The different plant layouts proposed had to be evaluated using a heat, energy and electrical balance to compare them with each other. For the overall heat, energy and electrical balance, the following points had to be considered:

- Energy requirement to heat up the incoming feedstock to match the digester operating temperature
- Energy requirement to maintain the digester at constant temperature
- Energy produced by digester
- Electrical power generated by CHP conversion units
- Available waste heat to be recovered from CHP
- Parasitic plant energy losses

The objective of the overall heat, energy and electrical balance is to compare and evaluate the different concepts at the selected TS contents over a year, based on the energy demand and energy production of the plant. To simplify this comparison, the mass and energy balance were conducted only at the two solstices and equinoxes in a typical year.

Energy required for feedstock:

Heating the feedstock to the required digester operating temperature is necessary so that the micro-organisms inside the digester do not get a thermal shock when new feedstock is added to the digester (pointed out by Bombardiere *et al.*, 2007).

To calculate the energy requirement for the incoming feedstock, an explicit transient mass and energy balance numerical model was developed for the inlet and outlet sumps, together with the pre- and post-heat exchangers. The process flow diagram of the sumps, pre- and post-heat exchanger can be seen in Figure 3.6. The inlet sludge was first heated by the effluent from the digesters and then heated additionally with the post-heat exchanger to match the digester temperature within a time frame of two hours. Both of the pre- and post-heat exchangers were connected in a counter-flow configuration.

The assumptions made for the numerical model on the feedstock energy requirement were:

- Fluid properties of water were used
- No energy losses to the environment of the sump were included
- Sumps were fully mixed by the pumps, creating a homogenous solution with an even temperature distribution throughout the sumps
- The design of the double-tube pre- and post-heat exchangers was fixed
- The wastewater inlet temperature at the works for the different time intervals of the year was taken as presented in Table 3.6 below:

Table 3.6: Inlet raw wastewater temperature during the year

	Solstice (20 March)	Equinox (21 June)	Solstice (23 Sept)	Equinox (21 Dec)
Sludge temperature (°C)	19.20	16.01	15.83	19.71

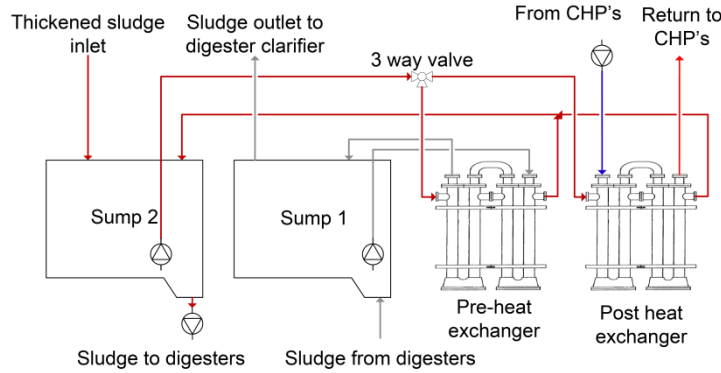


Figure 3.6: Process flow diagram for the heating the feedstock

The discretisation diagram used to develop the numerical model of the energy required for the feedstock is illustrated in Figure 3.7, with the input values for the numerical model tabulated in Table 3.7. The effluent temperature from the post-digester of concepts 1 and 2 was obtained from the digester numerical model, and can be seen in Figure 3.14.

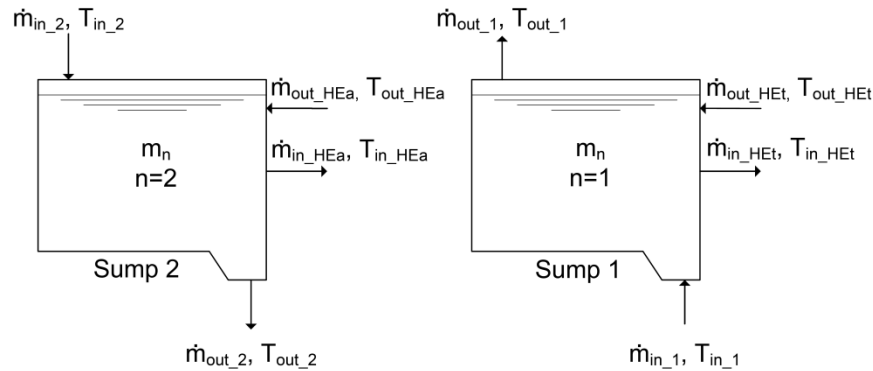


Figure 3.7: Discretisation diagram of sumps at AD plant

Table 3.7: Input values for numerical model of feedstock energy requirements

Name	Symbol	Units	Value
Tube internal diameter	d_i	m	0.11
Tube external diameter	d_o	m	0.12
Thermal conductivity of tube	k_t	W/mK	60
Annulus internal diameter	D_i	m	0.165
Annulus external diameter	D_o	m	0.172
Thermal conductivity of annulus	k_a	W/mK	0.4
Number of hairpins	N_{HP}		20
Number of tubes in annulus	N_t		1
Length of Hairpins	L_{HP}	m	5.7
Mass flow rate tube	\dot{m}_t	kg/s	16
Mass flow rate annulus	\dot{m}_a	kg/s	10
Fouling resistance	R_f	W/m^2K	0.00018
Volume of sumps	V_n	m^3	36
Sump 1 inlet and outlet mass flow rate	$\dot{m}_{in1}; \dot{m}_{out1}$	kg/s	62.3; 25
Sump 2 inlet mass flow rate	$\dot{m}_{in2}, \dot{m}_{out2}$	kg/s	24.7; 25

The formulations for the mass and energy balance of the sumps are provided below. The model used for the double-tube heat exchanger was the log mean temperature difference (LMTD) method formulated by Lui and Kakac (2002).

Mass balance (kg/s)

$$\frac{dm_n}{dt} = \sum (\dot{m}_{in} - \dot{m}_{out})_n + \sum (\dot{m}_{in} - \dot{m}_{out})_{HE_n} \quad (3.1)$$

$$m_n^{t+\Delta t} = \left(\sum (\dot{m}_{in} - \dot{m}_{out})_n + \sum (\dot{m}_{in} - \dot{m}_{out})_{HE_n} \right)^t \Delta t + m_n^t \quad (3.2)$$

Energy balance (W)

$$\frac{dE_n}{dt} = \sum \left(\dot{m} \left(\hat{h} + \frac{v^2}{2} + gz \right)_{in} - \dot{m} \left(\hat{h} + \frac{v^2}{2} + gz \right)_{out} \right)_n + \sum (\dot{Q}_{in} - \dot{Q}_{out})_n + \sum (W_{in} - W_{out})_n \quad (3.3)$$

$$T_n^{t+\Delta t} = \frac{(\dot{m}c_p T_{in} - \dot{m}c_p T_{out})_n + (\dot{Q}_{in} - \dot{Q}_{out})_{HE_n}}{\dot{m}c_p} \Delta t + T_n^t \quad (3.4)$$

The rest of the numerical model with the solar balance and ground temperature profile is presented in Appendix A.1.2.

A sample of the results obtained from the numerical model of the feedstock energy requirement can be seen in Figure 3.8 below. The figure illustrates the volume and sludge temperatures of concept 3 on 20 March, where heat was recovered for 59 min and additional heat was added by the post-heat exchanger for 35 min before it was pumped to the digester for 1 h 35 min to be empty for the next feeding.

The average heat recovered in a day from the effluent exiting the different conceptual AD plants at the four different time intervals in a typical year are summarised in Figure 3.9 below. The averaged additional heat that needs to be added to the feedstock to obtain the digester temperature is displayed in Figure 3.10.

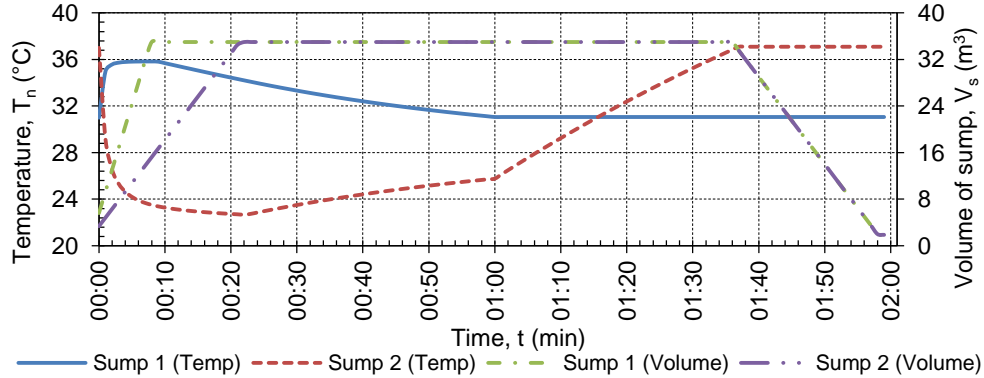


Figure 3.8: Volume and sump temperatures of concept 3 on 20 March

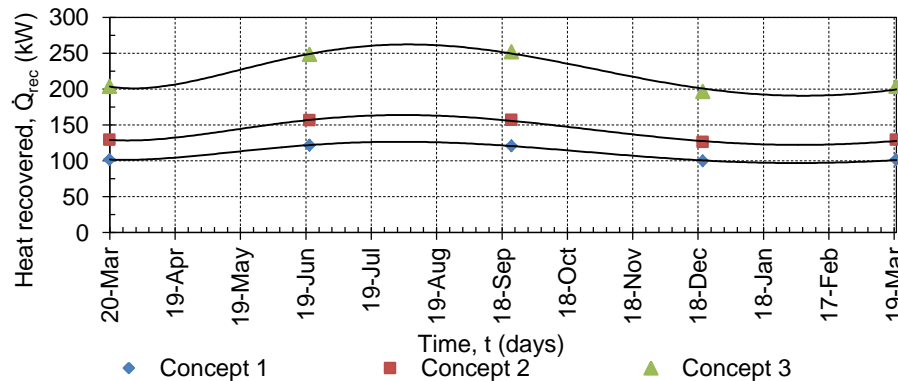


Figure 3.9: Average heat recovered per day from the effluent in a typical year

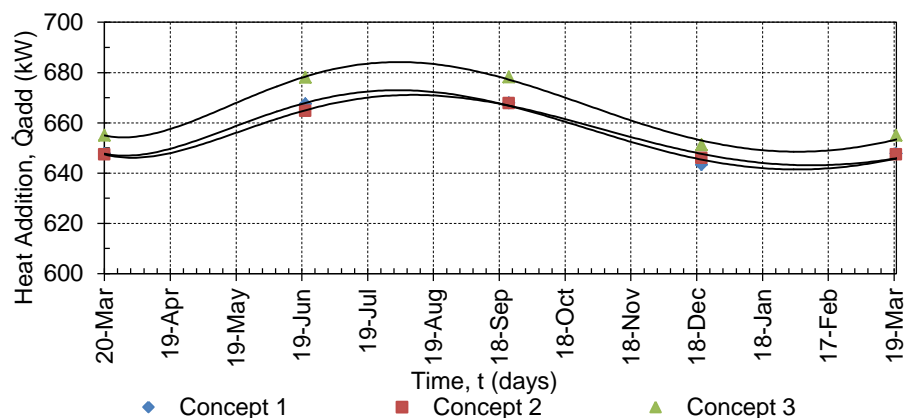


Figure 3.10: Average additional heat needed per day for feedstock in a typical year

The results in Figure 3.9 indicate that the most heat can be recovered from concept 3, followed by concept 2 and then concept 1. The reason for this is that all the digesters in concept 3 are heated, only four in concept 2 and three in concept 1. The averaged results in Figure 3.10 shown that a larger difference in additional heat is not needed, even with the volume per feeding of concept 1 at 21.31 m^3 , 2 at 23.31 m^3 and 3 at 33.13 m^3 . Concept 3 needs 1.37 % more and concept 2 0.02 % less heat on average throughout a typical year even with the large difference in sludge feeding volume compared to concept 1.

Energy required by digesters:

A constant digester-operating temperature is needed to keep the microbial colony in a healthy balance and to increase the gas production rate. A temperature fluctuation of more than $0.6 \text{ }^\circ\text{C}$ from operating point inhibits the acetogenesis bacteria, as these are the most sensitive to environmental changes. A fluctuation of $1 \text{ }^\circ\text{C}$ in less than 24 hours usually results in a toxic reactor (Turovskiy & Mathai, 2006). Therefore, additional heat is needed to make up for the environmental losses. The environmental losses for a digester include radiation, reflection, convection losses, conduction losses to the ground and energy losses through mass transfer.

To calculate the environmental losses of a digester and to determine the digester energy demand, an explicit numerical transient mass and energy balance model was constructed. The numerical model was used to provide additional insight into which section of the digester loses the most heat.

The discretisation diagram used to construct the numerical model for the digester is illustrated in Figure 3.11. In the discretisation of the digester, the digester was divided into five different sections, namely the cone gas area (CGA), cone water area (CWA), side water area (SWA), side ground area (SGrA) and cone ground area (CGrA). The top cone area (CGA, CWA) was subdivided into three layers: a 250 mm reinforced concrete layer, a 10 mm insulation layer and a 6 mm concrete screed on top of the insulation layer. The ground sections (SGrA, CrGrA) were divided into 1 m sections, as can be seen in Figure 3.11.

Selection of the time step used for the explicit numerical model of the energy required by the digesters is presented in Appendix A, section A.1.2, where a time step of one hour was selected.

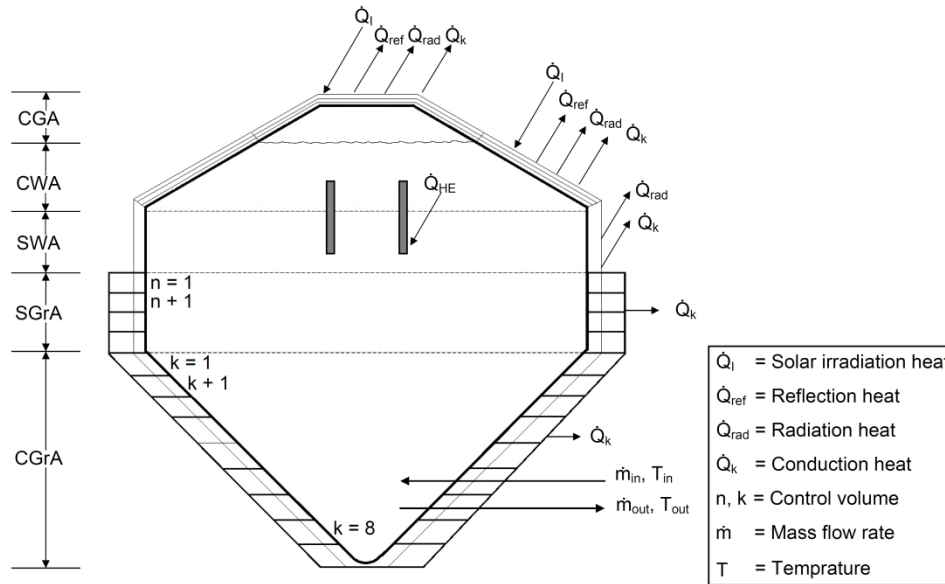


Figure 3.11: Discretisation diagram of digester

The input constants used for the numerical model are tabulated in Table 3.8 and the weather data in a minute interval for the case study (GHI, DHI, DNI, T_a and wind speed) was obtained from the local weather services (NWN, 2011).

Table 3.8: Input constants for numerical model of digester energy requirements

Name	Symbol	Units	Value
Altitude	Z_{lt}	m	1700
Longitude, Latitude	L_{st}, ϕ	deg	22.57, 17.08
Time zone Longitude	L_{Loc}	deg	30
Diffused reflection surroundings	ρ_{gr}	-	0.2
Air pressure	P_a	Pa	82501.29
Gas pressure	P_g	Pa	825012.9
Delta x ground	Δx_g	m	0.028571
Ground thickness	t_{gr}	m	1
Thermal conductivity of insulation	k_{ins}	(W/mK)	0.09
Thermal conductivity of cement	k_{cem}	(W/mK)	0.55
Emissivity outside of digester	ϵ_{out}	-	0.93
Thermal absorptivity outside of digester	α_D	-	0.7
Average air temperature	$T_{m(a)}$	$^{\circ}C$	17.3
Average ground temperature	$T_{m(gr)}$	$^{\circ}C$	19.1
Ground temperature differential	ΔT_m	$^{\circ}C$	1.8
Vegetation coefficient	k_v	W/mK	1
Amplitude of annual air temperature wave	AM	$^{\circ}C$	10.5
Average annual thermal diffusivity ground	α_{gr}	m^2/s	0.0034
Phase shift of air temperature wave	PS	days	40

The assumptions made for the mass and energy balance of the digesters were:

- The sludge inside the digester was taken as water and the biogas as air
- The digester was taken as a well-mixed reactor with an even temperature distribution throughout
- No work done on the digester was taken into account
- The ground temperature was calculated from the curve fit (Equation A.26)
- The ground around the digester is dry and the water table is much lower
- No shade effect on the digesters was taken into account in the numerical model

The numerical model constructed for the digester's energy requirements is presented below:

Mass balance (kg/s)

$$\frac{dm}{dt} = \sum (\dot{m}_{in} - \dot{m}_{out}) + \sum (\dot{m}_{in} - \dot{m}_{out})_{HE} \quad (3.5)$$

$$m^{t+\Delta t} = \left(\sum (\dot{m}_{in} - \dot{m}_{out}) + \sum (\dot{m}_{in} - \dot{m}_{out})_{HE} \right) \Delta t + m^t \quad (3.6)$$

Energy balance (W)

$$\frac{\Delta H}{\Delta t} = \sum \left(\dot{m} \left(\hat{h} + \frac{v^2}{2} + gz \right)_{in} - \dot{m} \left(\hat{h} + \frac{v^2}{2} + gz \right)_{out} \right) + \sum (\dot{Q}_{in} - \dot{Q}_{out}) \quad (3.7)$$

$$+ \sum (W_{in} - W_{out})$$

$$T_D^{t+\Delta t} = \frac{(\dot{m}c_p T_{in} - \dot{m}c_p T_{out} + \sum \dot{Q}_{in} - \sum \dot{Q}_{out})^t \Delta t + \dot{m}c_p T_D^t}{\dot{m}c_p^{t+\Delta t}} \quad (3.8)$$

where Q_{in} and Q_{out} in equation 3.8 were taken as:

$$\sum \dot{Q}_{in}^t = \sum \dot{Q}_{I_i}^t + \dot{Q}_{HE}^t \quad (3.9)$$

$$\sum \dot{Q}_{out}^t = \sum \dot{Q}_{ref_i}^t + \sum \dot{Q}_{rad_i}^t + \sum \dot{Q}_{h_i}^t + \sum \dot{Q}_{k_i}^t \quad (3.10)$$

The results obtained from the numerical model on the environmental losses of a digester were used to calculate the average heat demand per day. The averaged heat demand for the different concepts in a typical year is presented in Figure 3.12.

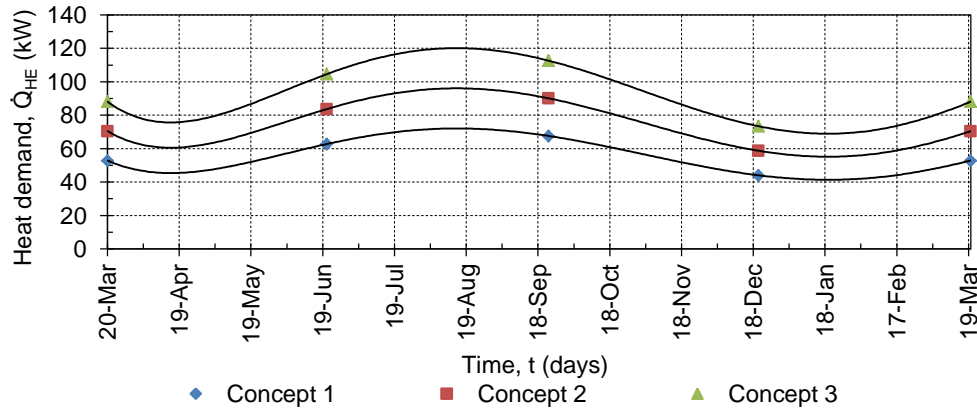


Figure 3.12: Daily averaged heat demand of heated digesters in a typical year

The results displayed in Figure 3.12 indicate that concept 1 had the lowest heat demand, as only three digesters were heated, followed by concepts 2 and 3. The figure also indicates that the peak heat demand was between 19 August and 19 September. This peak is different from that of the feedstock energy demand, which peaks between July and August. From the results it was calculated that, on average throughout a typical year, concept 3 requires 44.03 % and concept 2 33.3 % more heat compared to concept 1.

The numerical model of the digesters was used to determine the temperature fluctuation for the unheated post-digesters in concept 1 and concept 2. The results for concepts 1 and 2 from 20 to 23 June are illustrated in Figure 3.13. The average digester temperatures over 3 days for concepts in a year are displayed in Figure 3.14.

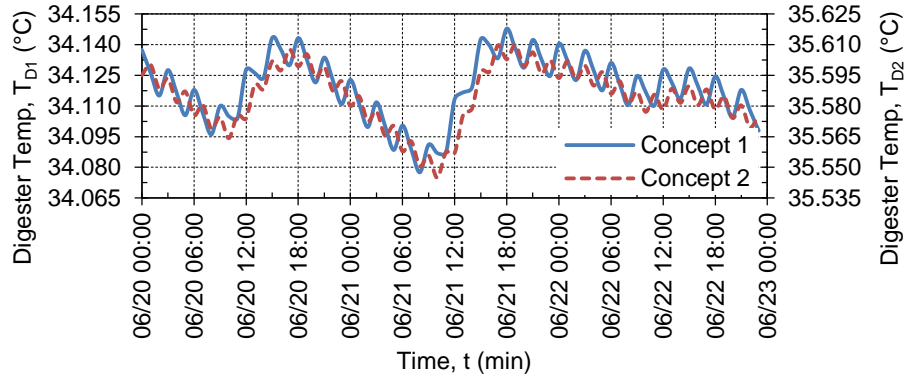


Figure 3.13: Post-digester digestate temperature fluctuations from 20 to 23 June

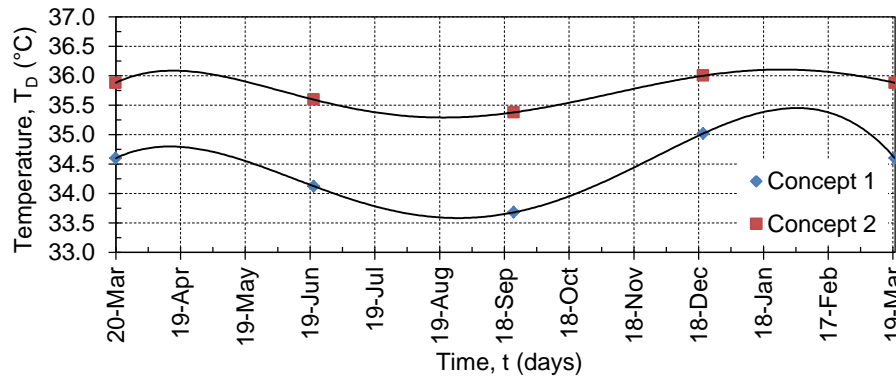


Figure 3.14: Averaged post-digester digestate temperature in a typical year

Figure 3.13 illustrates that the temperature fluctuation inside the post-digesters due to ambient conditions and feeding intervals of concepts 1 and 2 was less than 0.6 °C. The largest temperature fluctuation was in concept 1, with 0.063 °C within seven hours. This is a very small fluctuation compared to the 0.6 °C described in section 2.2.1, and should not have an effect on the acetogenesis bacteria. From the average post-digester temperature presented in Figure 3.14, the lowest temperature peaks between 19 August and 19 September, which correlates with the peak energy demand of the heated digesters. The reason for the lower digester temperature in concept 1 is due to the lower daily sludge throughput. The numerical model was also used to predict the heat loss by type and by section as discretised. The results of this simulation are illustrated in Figure 3.15 by type and in Figure 3.16 by section for the three-day period from 22 to 25 September.

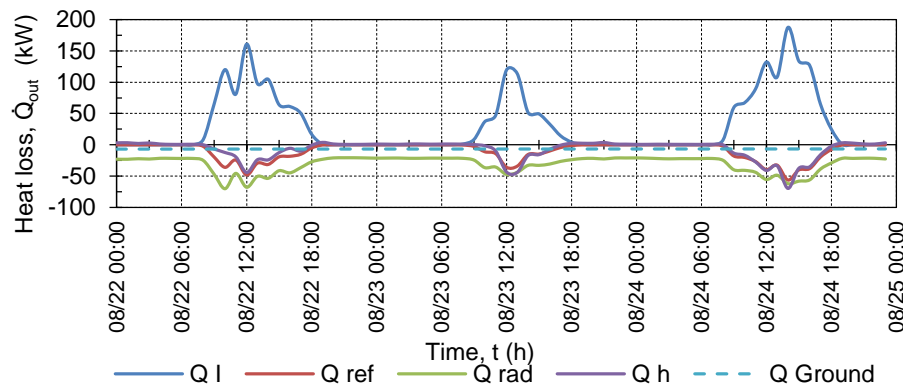


Figure 3.15: Heat losses by type of single heated digester from 22 to 25 September

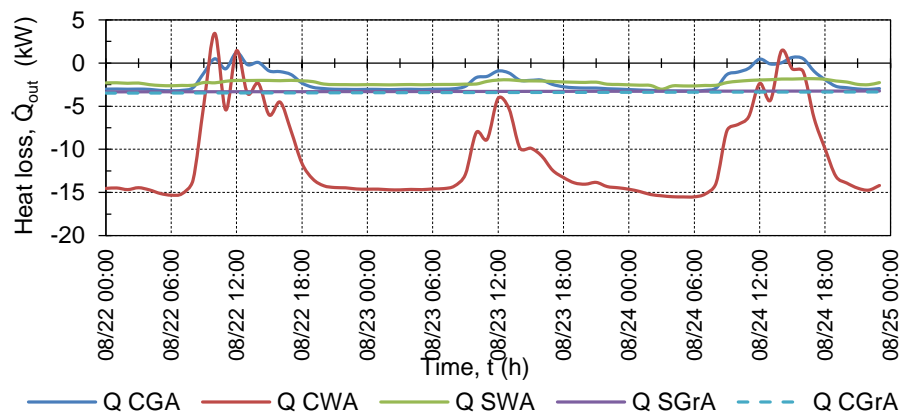


Figure 3.16: Heat losses by section of single heated digester from 22 to 25 September

The results in Figure 3.15 illustrate that the biggest heat loss was the radiation loss, followed by reflection, convection and then conduction to the ground. The results in Figure 3.16 show that the largest environmental heat losses were in the CWA section. This indicates that, if the digester energy demand due to environmental losses needs to be decreased, this section, the CWA, needs to be focused on.

Energy produced by digesters

Modelling the anaerobic digestion process to predict biogas production to gain a better understanding of the process dynamics has been done since the early 1960s. Since the anaerobic process is a chain of interconnected biological reactions in which colonies of micro-bacteria break down organic matter, predicting it is a challenge. The most detailed mathematical model to date is the ADM1 model. This model was developed by the IWA Task Group and was first published in 2001. Many alterations and variations have been made to the model to date, and it consists of 27 input variables.

As this is such a complicated field of study, a decision was made to model the biogas production only on one variable, volatile solid reduction. From the volatile solid reduction in the digester, the energy produced in the different AD plant layouts at the different TS contents can be calculated. The input parameters for the numerical model were obtained in Table 3.5. The additional parameters used for the numerical model are illustrated in Table 3.9. The biogas yield from the WAS, was estimated from experimental studies by Azbar and Speece (2001), Schafer *et al.*, (2002) and Bolzonella D. (2009). It should be noted that the digestion parameters selected in Table 3.9 were conservative, especially concept 3's biogas yield from WAS and the percentage CH₄ in biogas.

Table 3.9: Input parameters for numerical model of digester's energy production

Name	Symbol	Units	Value
Volatile solid reduction of PS (concept 1, 2, 3)	VS _{Red PS}	%	58, 57, 57
Volatile solid reduction of WAS (concept 1, 2, 3)	VS _{Red WAS}	%	67, 65, 62
Biogas yield for PS (concept 1, 2, 3)	Y _{PS}	m ³ /kg	0.88, 0.95, 1.1
Biogas yield for WAS (concept 1, 2, 3)	Y _{WAS}	m ³ /kg	0.62, 0.65, 0.6
Methane concentration in biogas	CH ₄	%	62, 65, 60
Methane density	ρ _{CH4}	kg/m ³	0.6556
Lower heating value of methane	LHV _{CH4}	MJ/kg	50.009

In the numerical model for the digester's energy production, the PS and the WAS were calculated separately as i 'th value, indicated below:

The solids flow rate, \dot{m}_{TS} (kg/s), was calculated using equation 3.11

$$\dot{m}_{TS_i} = \dot{m}_i TS_i \quad (3.11)$$

The volatile solids mass flow rate, \dot{m}_{VS} (kg/s)

$$\dot{m}_{VS_i} = \sum (\dot{m}_{TS_i} VS_i) \quad (3.12)$$

Total volatile solids digested from PS and WAS, \dot{m}_{VS_D} (kg/s)

$$\dot{m}_{VS_{D_i}} = \sum (\dot{m}_{VS_i} VS_{Red}) \quad (3.13)$$

Total volume flow rate of the biogas generated, \dot{V}_B (m³/s)

$$\dot{V}_B = \sum (\dot{m}_{VS_{D_i}} Y_i) \quad (3.14)$$

Total volume flow rate of the methane generated, \dot{V}_{CH_4} (m³/s)

$$\dot{V}_{CH_4} = \dot{V}_B CH_4 \quad (3.15)$$

Total mass flow rate of the methane generated, \dot{m}_{CH_4} (kg/s)

$$\dot{m}_{CH_4} = \rho_{CH_4} \dot{V}_{CH_4} \quad (3.16)$$

Total power available from digesters, P_{Bio} (W)

$$P_{Bio} = \dot{m}_{CH_4} LHV_{CH_4} \quad (3.17)$$

The results from the model of power available from the different conceptual AD plant layouts at the selected TS contents are presented in Figure 3.17 below:

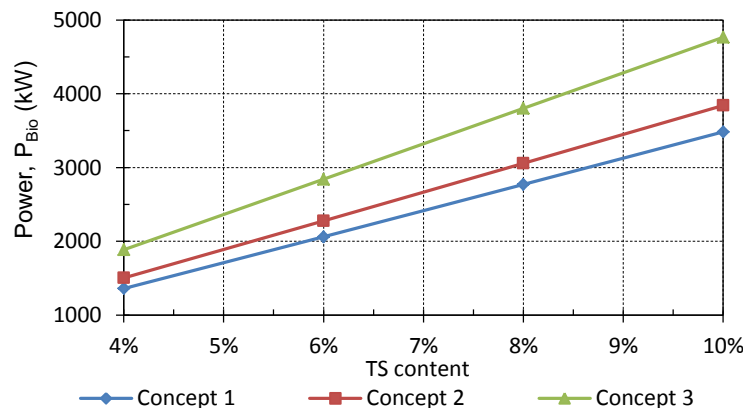


Figure 3.17: Power available from digesters in the different concepts as a function of TS content

In the results presented above it is shown that concept 3 is able to produce more power from the feedstock. The reason for this difference in power is mainly because concept 3 is able to process 55.4 % more sludge, whereas concept 2 can only process 9.4 % more sludge compared to concept 1.

The interesting aspect of the calculated results is that concept 3 is able to produce 38.71 % more power at 4 % and 36.81 % more at 10 % TS content compared to concept 1.

Electric power generated by CHPs

The biogas produced by the different AD plant layouts was pumped to combined heat and power (CHP) internal combustion (IC) units to generate electricity.

To calculate the electrical power generated in the different concepts, the following assumptions were made:

- The CHP power plants will be running on base load mode
- Biogas production rate of the digesters will equal the consumption rate of the CHP units unless the load on a CHP unit is less than 10 %

For the calculation, the power output capacity (200kW) and thermal efficiency (equation 3.19) was obtained from experimental work done by CAE Ltd (CAE, 2014) where the alternator efficiency was obtained from the supplier (equation 3.22).

The calculation used to determine the electric power generated by the CHP's was an iterative calculation. In the first iteration, the total energy possible to generate from biogas (E_{CHP_i}) was calculated at a full load of 200 kW power (P_i) and thermal efficiency (η_{Therm}) to determine the number of CHPs needed. In the following iterations the thermal efficiency of the number of units was calculated separately. The iterative loop in the calculation is from equations 3.18 to 3.20.

Total possible power to generate from biogas, P_{CHP} (W)

$$P_{CHP_i} = P_{Bio} \eta_{Therm_i} \quad (3.18)$$

where the thermal efficiency of the i 'th CHP, η_{Therm} (%), with an R^2 value of 0.9136 is

$$\eta_{Therm_i} = -81.04 \times 10^{-9} P_i^4 + 42.72 \times 10^{-6} P_i^3 - 8.46 \times 10^{-3} P_i^2 + 794.4 \times 10^{-3} P_i - 862.2 \times 10^{-3} \quad (3.19)$$

Number of CHP needed for plant, N_{CHP} (units)

$$N_{CHP} = P_{CHP_i} \div 200 \times 10^3 \quad (3.20)$$

Total generation capacity from plant, P_{elec} (W)

$$P_{elec} = \sum (N_{CHP_i} \eta_{alt_i}) \quad (3.21)$$

where efficiency of alternator, η_{alt} (%), with an R^2 value of 0.9938 is

$$\eta_{alt_i} = 16.67 \times 10^{-9} P_i^3 - 8.7 \times 10^{-6} P_i^2 + 1.363 \times 10^{-3} P_i + 873 \times 10^{-3} \quad (3.22)$$

The calculated electric power generated by the different concepts at the corresponding TS contents is illustrated in Figure 3.18 below:

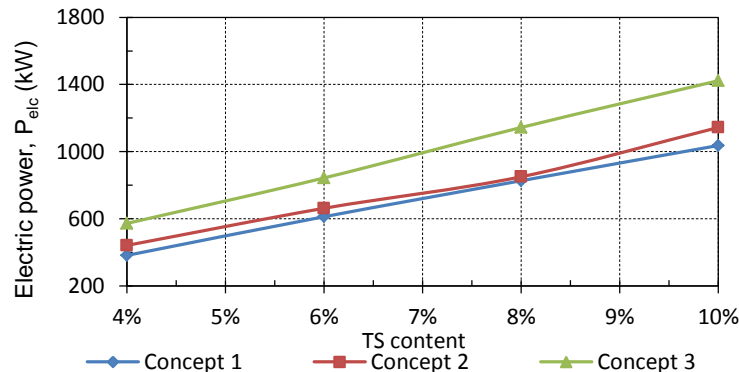


Figure 3.18: Electric power generated by concepts at different TS content

From the results illustrated in Figure 3.18, a significant gain in generated power can be achieved by changing the digester configuration. Concept 3 is able to generate 50 % more at 4 % and 37.26 % more at 10 % solid content compared to concept 1.

Available waste heat recovered from CHPs

The waste heat from the CHPs was used to heat the incoming feedstock and the digesters, as described before and illustrated in Figure 3.3 to 3.5, 3.6 and 3.11. The waste heat available to recover from an IC engine of a typical CHP unit is on the coolant side, engine oil and on the exhaust side.

The IC engine used in this case had an internal oil cooler and a water-cooled exhaust manifold that was cooled by the coolant passing through the engine. To recover the waste heat from the CHP unit, it had to be equipped with a plate heat exchanger on the coolant side and a shell tube heat exchanger on the exhaust gas line. The process flow diagram of the CHP unit with these heat-recovery heat exchangers installed can be seen in Figure 3.19 below:

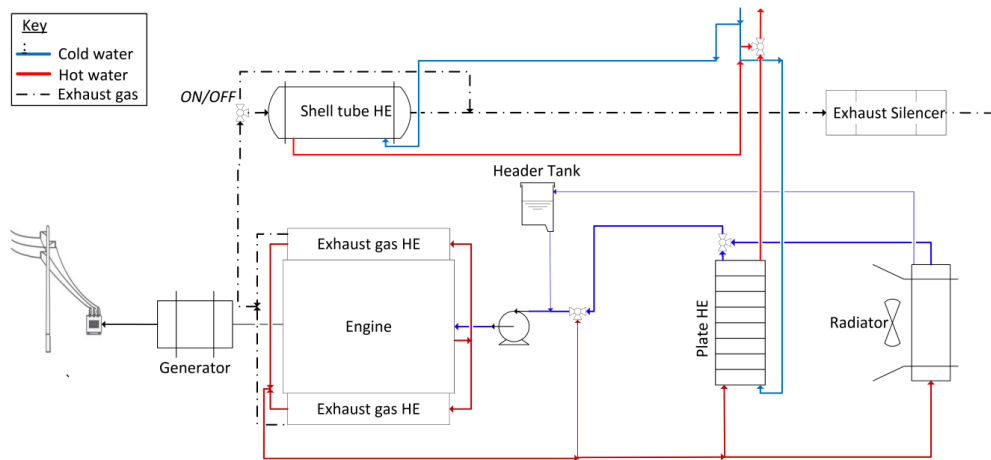


Figure 3.19: CHP process flow diagram

The coolant flow rate required by the engine was 10 kg/s and it was controlled to 85 °C on the engine outlet. After the coolant passed through the engine block, it was directed to the water-cooled exhaust manifold and then to a plate heat exchanger, or the radiator, or both, controlled by the three-way valve.

The exhaust gas exiting the exhaust manifold was conveyed to an on/off three-way valve before it passed through the shell and tube heat exchanger. The exhaust gas passed through the shell tube heat exchanger and was controlled to a minimum outlet temperature of 110 °C. This minimum temperature was to ensure that no condensation formed in the shell tube heat exchanger, as the exhaust gas contains high levels of sulphur (S^{2+}) and forms sulfuric acid (H_2SO_4) when it comes into contact with water.

The heat recoverable on the coolant side using the plate heat exchanger was calculated by a curve fit equation that was obtained experimentally (CAE, 2014) and is formulated below.

The curve fit equation for heat available from each CHP unit on coolant side at a load, \dot{Q}_{CHPC} (W), with an R^2 value of 0.9896

$$\dot{Q}_{CHPC_i} = -144.8 \times 10^{-6} P_i^2 + 983.9 \times 10^{-3} P_i - 365.7 \times 10^{-3} \quad R^2 = 0.9896 \quad (3.23)$$

Total heat available from each CHP unit's coolant side, \dot{Q}_{CHPTC} (W)

$$\dot{Q}_{CHPTC} = \sum \dot{Q}_{CHPC_i} \quad (3.24)$$

The results obtained for the available heat to be recovered from the concepts at the different TS content feedstock are plotted in Figure 3.20 below.

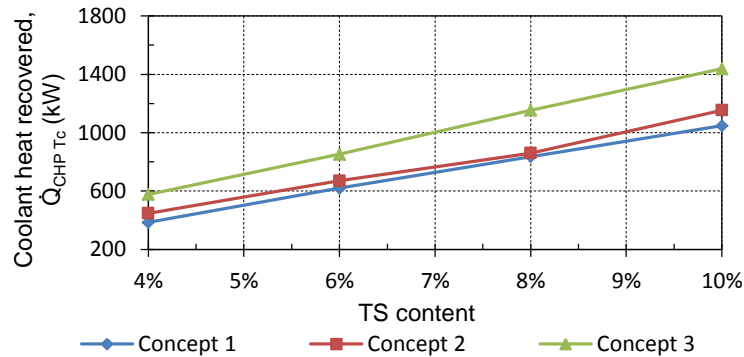


Figure 3.20: Coolant heat recovered from AD plant concepts at different TS content

The available heat to be recovered from the exhaust gas using the shell tube heat exchanger was calculated with two curve fits – the gas mass flow rate and gas temperature. These curve fits were also obtained from the experimental work conducted by CAE (2014). The calculation for heat recovered from exhaust gas is as follows:

The curve fit for mass flow rate of exhaust gas at a load, \dot{m}_{exh} (kg/s), with an R^2 value of 0.9879

$$\dot{m}_{exh_i} = -944.7 \times 10^{-6} P_i + 39.44 \times 10^{-3} \quad R^2 = 0.9879 \quad (3.25)$$

Curve fit for temperature of exhaust gas at a load, T_{exh} ($^{\circ}\text{C}$), with an R^2 value of 0.9935

$$T_{exh_i} = -49.44 \times 10^{-9} P_i^4 + 47.43 \times 10^{-6} P_i^3 - 13.97 \times 10^{-3} P_i^2 + 1.8614 P_i + 467.44 \quad (3.26)$$

Heat available from exhaust gas at each CHP unit, $\dot{Q}_{CHP e}$ (W)

$$\dot{Q}_{CHP e_i} = \dot{m}_{exh_i} c_p (T_{exh_i} - T_{out}) \quad (3.27)$$

Total heat available from each CHP unit's exhaust side, $\dot{Q}_{CHP T_e}$ (W)

$$\dot{Q}_{CHP T_e} = \sum \dot{Q}_{CHP e_i} \quad (3.28)$$

The calculated heat available to be recovered from the CHP unit using the shell and tube heat exchanger of the concepts is presented in Figure 3.21.

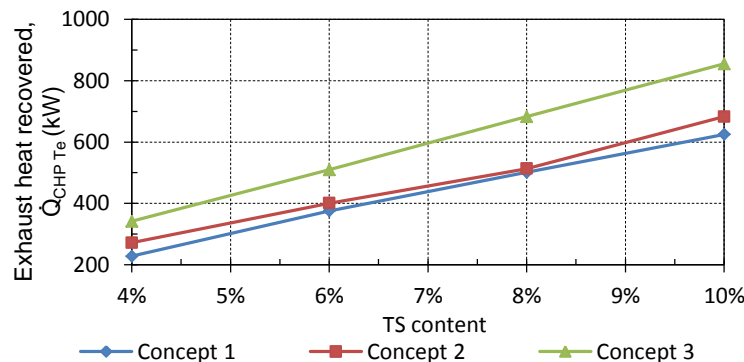


Figure 3.21: Exhaust heat recovered from AD plant concepts at different TS content

From the calculations done, the available waste heat recovered from the CHP units with the configuration illustrated in Figure 3.19 was 96.2 % on the coolant side and 56.9 % on the exhaust gas side of the engine electrical power if the engines were generating load at full load.

Parasitic load of AD plant

The parasitic load of the AD plant had to be included, as it can be a significant percentage of the power generated, especially in the northern hemisphere.

The parasitic load of the Gammams plant as well as that of the CHP units are listed in Table 3.10 below. The values obtained in the table were taken from CAE (2014), the design department for the Gammams WWTP upgrade project. The assumption made for the overall electric energy balance of the different concepts was that the parasitic loads were running on a continuous basis to obtain the worst-case scenario.

Table 3.10: Parasitic load of the AD plants

Location	Name of load	Size (kW)	Number of units	Total (kW)
Plant load	Slurry pump	9	1	9
	Liquid ring blowers	5.5	5	27.5
	Heat circulation pump	3.2	2	6.4
	Heat recovery pump	3.2	2	6.4
	Heat exchanger slurry pump	5.5	1	5.5
	Heat exchanger effluent pump	5.5	1	5.5
	Other	10	1	10
CHP load per unit	Ventilation fan	2.2		
	Coolant pump	3.5		
	Lateral channel blowers	2.2		
	Other	1.62		

Overall energy balance of conceptual AD plant layouts

To evaluate the different concepts against each other in a typical year at different TS contents, a balance of the heat, energy and power generation was drawn up.

Overall heat balance

For the overall heat balance calculation for the different concepts in a typical year at the different TS contents, the summation of the heat demand, available recovered heat and heat losses were taken into account for a minute time interval using equation 3.29 below.

$$\dot{Q}_{Bal} = \dot{Q}_{In_{HE_{Feed}}} + \dot{Q}_{In_{HE_D}} + \dot{Q}_{CHP_{T_c}} + \dot{Q}_{CHP_{T_e}} \quad (3.29)$$

A sample of the heat balance for concept 1 at 4 % TS content at the two solstices and equinoxes are plotted in Figure 3.22 below.

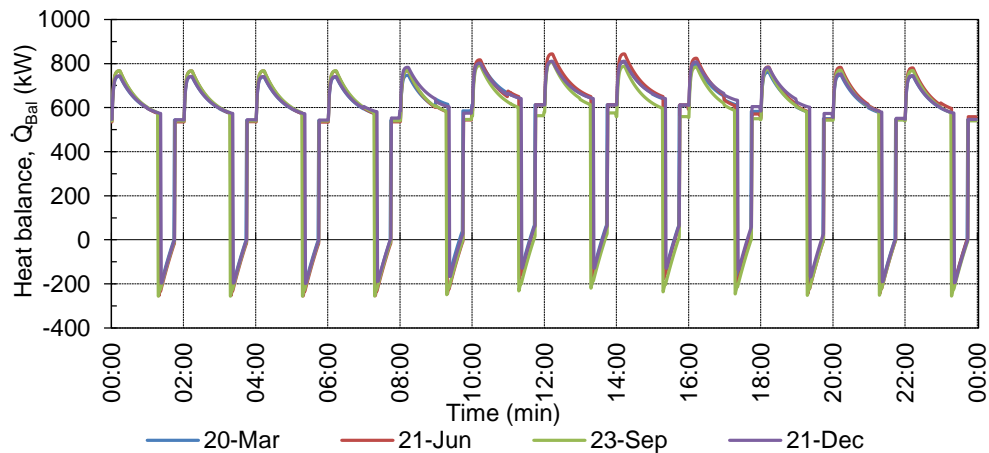


Figure 3.22: Heat balance of concept 1 at 4 % TS on the solstices and equinoxes

The results of the heat balance plotted in Figure 3.22 for concept 1 at 4 % TS contents indicate that there is a heat shortage for 19 minutes with a peak on 23 September of 255.94 kW. The heat balance for concept 2 and 3 look similar, but the heat shortage becomes less. In concept 2, the peak heat shortage is 183.17 kW and lasts for 18 minutes, and in concept 3 the heat shortage peaked at 51.47 kW and only lasted for 7 minutes on 23 September at 4 % TS content. The results indicate that, at increased TS contents higher than 4 %, there were no more heat shortages. The heat balances for the concepts was averaged per day and are displayed in Figure 3.23.

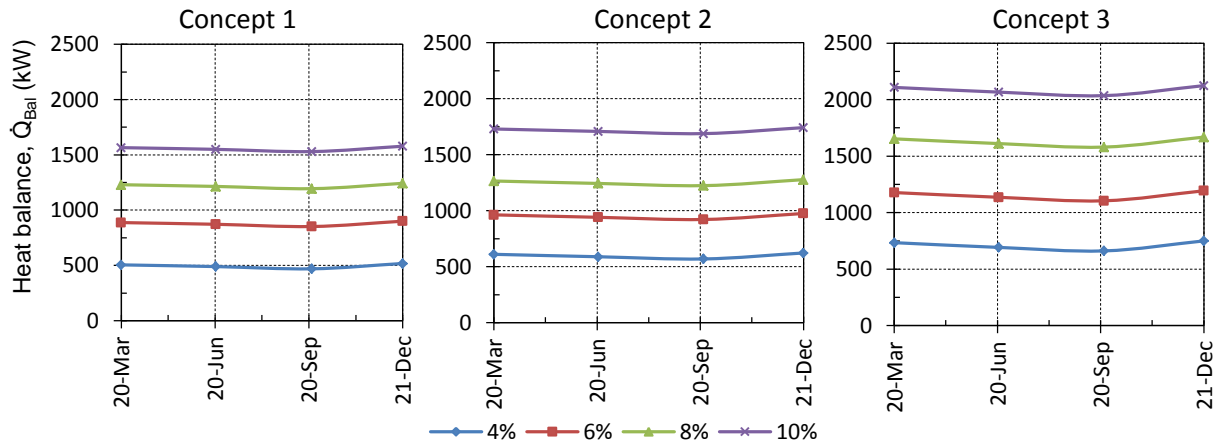


Figure 3.23: Average heat balance of concepts at TS contents in typical year

From the calculated average daily heat balance, it is shown that all concepts have surplus heat available and that the surplus heat increases with the increase in TS contents. It also indicates that the highest energy demand by the concepts is on 23 September from the points calculated. From the results it was calculated that concept 3 had 35.45 % more and concept 2 had 10.48 % more surplus heat available compared to concept 1.

Overall energy balance

The overall energy balances of the concepts were calculated at hourly intervals and averaged per day, and are displayed in Figure 3.24 below.

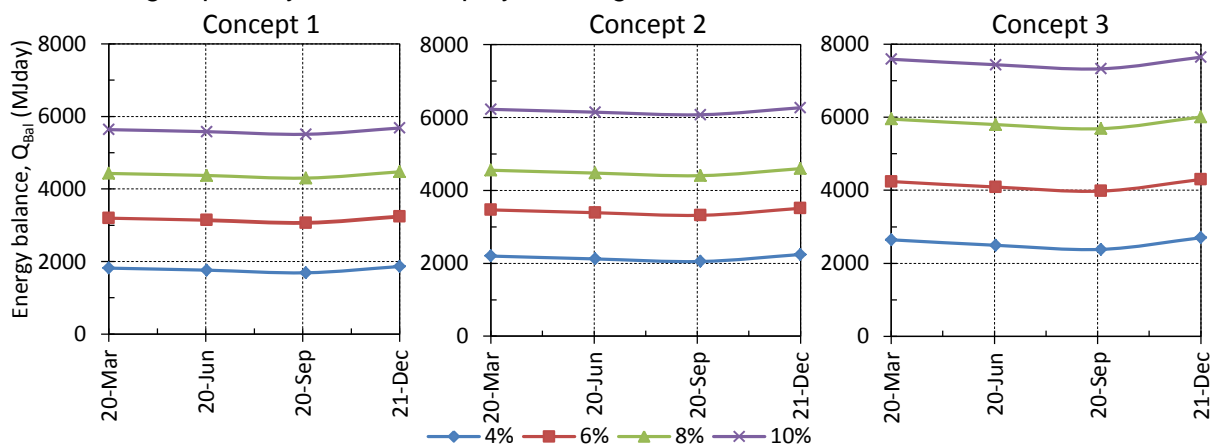


Figure 3.24: Averaged overall energy balance of concepts at TS contents in typical year

In the daily averaged energy balance the same trend lines can be seen as in the heat balance in Figure 3.23, with concept 3 outperforming the other two concepts.

Overall electrical balance

The overall electrical balance of the three concepts simply involved the summation of the electrical energy produced, the parasitic load of the plant and the parasitic load of the CHP units. The results obtained from the balance are illustrated in Figure 3.25 for TS contents between 4 and 10%.

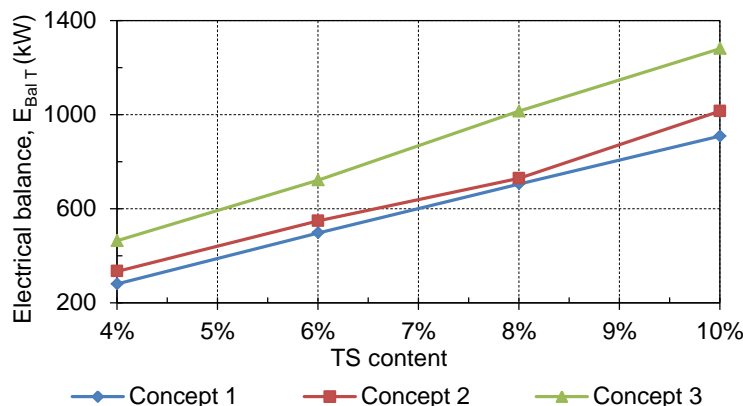


Figure 3.25: Overall electricity balance of AD plants at different TS contents

The results of the overall electrical balance calculated show that concept 3 is able to generate 52 % more and concept 2, 38 % more net electrical power compared to concept 1. Figure 3.25 show the importance of increasing the TS content of the feedstock as the net electrical power of concept 3 can be increased by 276 % when increasing the TS from 4 to 10 %.

3.2 Digester mixing system

An effective mixing system for a digester is essential on the biological side to increase the rate of micro-bacterial productivity and on the hydraulic side to increase the effective volume.

On the biological side, it was found from a review of case studies that an intermittent mixing scheme of 2 hours on and 2 hours rest obtained an 18 % increase in biogas production compared to a continuous mixing scheme. A gentle mixing intensity with minimal shear on the microorganism was indicated to work best to create a healthy internal environment inside the digester for the case studies reviewed.

In the case studies reviewed, it was found that the most effective mixing method was mechanical draft tube mixing in an upward direction. This mixing method has, as has been pointed out inherent maintenance problems, because the digester needs to be opened to clear blockages exposing personal to hazardous working environment arising from the presence of biogas. The second most effective method, according to the comparative studies reviewed, was the gas recirculation bubble column, with a 29 % increase in UP. From the knowledge gained on a confined mixing system (section 2.3), it was found that the plug flow two-phase flow regime was a more effective regime to convey liquids compared to the bubble flow regime.

The aim of this section was to come up with a mixing system concept for a CSTR. The design was based on the gas recirculation bubble piston method, together with the accompanying numerical model that can predict the volume flow rate of the mixing system.

The objectives that were set for this section were to generate and evaluate three different concepts to generate a plug-flow regime inside a draft tube. The second objective set out was to construct a transient numerical model that could predict the total volume flow rate of the mixing system in a plug-flow regime.

3.2.1 Design criteria and limitations for mixing system

To generate three different concepts for the mixing system, the design criteria and limitations first had to be set and are listed below:

- There may not be any moving parts inside the digester
- The mixing system needs to be able to operate in a TS content of 4 to 10 %
- The rate of the mixing system must be able to be adjusted
- The load on the gas compressor needs to remain as constant as possible
- The mixing system may not create the possibility of a gas explosion
- The mixing system must be able to be unblocked/cleaned without opening the digester
- The mixing system needs to fit through the middle opening of a digester with a diameter of 600 mm

3.2.2 Concepts for mixing system

The objective was to generate three different concepts using the gas recirculation bubble piston method. Each concept's main function was to generate a plug in a vertical draft tube based on the design criteria and the limitations set out. The three different concepts were evaluated in an evaluation matrix to find the best-suited option.

Concept 1

The first concept was based on a gas accumulator with a series of pressure vessels connected in parallel, where the compressed gas in the vessels is released in batches by automated valves to form a plug. A schematic process flow diagram of the concept can be seen in Figure 3.26 below.

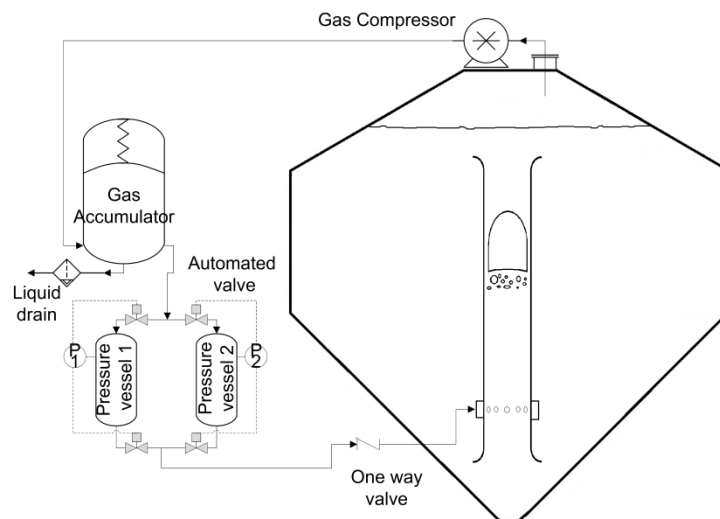


Figure 3.26: Concept 1 – Pressure vessel with automated valve outside digester

In this concept, the compressor supplies the accumulator with a constant flow rate and the accumulator ensures that the gas supply pressure stays constant.

The pressurised gas in the accumulator was then used to fill the two pressure vessels in batches by opening the inlet automated valves individually. As the pressure vessel reaches the set pressure, the inlet valve closes and the outlet valve opens. The pressurised gas is conveyed through a one-way valve before it reaches the set of nozzles at the bottom of the draft tube, creating a plug.

The set of nozzles located in the draft tube run the risk of becoming blocked. If this happens, the gas delivery line after the outlet automated valves has to be disconnected and flushed with highly pressurised water. If the pressurised water does not unblock the nozzles, the drawback of the concept is that the digester needs to be emptied and the nozzles have to be cleaned manually.

Concept 2

The second concept to generate a plug was derived from concept 1 by placing the gas accumulator at the bottom of the draft tube. This concept releases the gas plugs into the draft tube by a U-tube configuration. The process flow diagram for this concept can be seen in Figure 3.27 below.

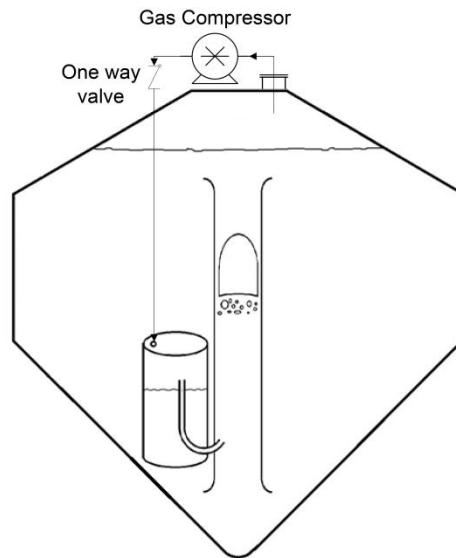


Figure 3.27: Concept 2 – Gas accumulator with U-tube inside digester

The gas supplied from the compressor passes through the one-way valve into the gas accumulator at the bottom of the draft tube. This gas accumulator is open at the bottom and is connected with a U-tube to the draft tube. As the pressurised gas fills the gas accumulator, it displaces the digestate through the bottom of the gas accumulator and through the U-tube. When the gas has displaced all the digestate up to the lowest point of the U-tube, the gas escapes through the U-tube into the draft tube. As the gas escapes through the U-tube, the digestate level in the gas accumulator rises until it floods the U-tube and the cycle starts all over.

With this concept, the delivery pressure of the compressor will stay nearly constant, as the major factor determining the pressure is the hydrostatic pressure. The frequency of this mixing system can also be changed by just varying the gas supply flow.

The drawbacks of this concept are blockages of the gas accumulator and the U-tube. The gas accumulator can be flushed, but the U-tube, on the other hand, poses a problem as it cannot be flushed or pressurised inside the accumulator, as the bottom is open.

Concept 3

The third concept used the idea of the gas accumulator inside the digester, but consisted of a series of chambers that also worked on the U-tube principle. The aim with the series of channels was to decrease the chances of blockages compared to a single U-tube and to be able to flush the gas accumulator when needed.

The gas accumulator, also known as a plug-flow generator, was supplied with pressurised gas and released the accumulated gas into the draft tube in plugs. The flow diagram of the third concept is illustrated in Figure 3.28 below.

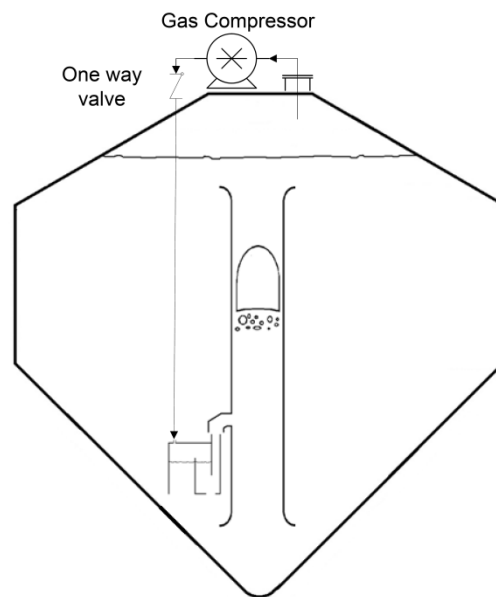


Figure 3.28: Concept 3 – Plug-flow generator

The pressurised gas supplied from the compressor first passes through a one-way valve and then to the plug-flow generator. The pressurised gas fills the plug-flow generator and displaces the digestate out through the bottom of the open chambers.

When the displaced digestate level reaches the level just below that of the bottom of the first chamber (on the right-hand side in Figure 3.28), the accumulated gas escapes through this chamber and enters the draft tube as a plug. With the accumulated gas escaping in the first chamber, the digestate level in the third chamber (large chamber on the left-hand side) will rise to a point and the bottom of chamber two will be flooded.

In this concept there are no mechanical or moving parts in the digester. The system also keeps the load on the gas compressor constant and, by varying the gas flow rate, the frequency of plug formation changes. The series of chambers in this concept provides an advantage over the U-tube of concept 2, as they can be bigger in size and a high-pressurised water line can be incorporated with a set of nozzles to flush the plug-flow generator.

Concept evaluation

The three concepts generated for the mixing system were assessed in an evaluation matrix based on a selected set of installation, operation and maintenance criteria.

In the evaluation matrix criteria, an importance factor was assigned based on a scale from 1 to 5, with 5 being the highest. A rating was assigned to each criterion on a scale from 1 to 5, with 5 being the highest again. The importance factor and the rating giving to the concept were then multiplied to get a score. The scores of each concept were summed to get a total score for each concept, and these can be seen in Table 3.11 below.

Table 3.11: Mixing concept evaluation matrix

Evaluation criteria	Importance	Concept 1		Concept 2		Concept 3	
		Rating	Score	Rating	Score	Rating	Score
Risk of blockage	5	5	25	2	10	4	20
Ease of cleaning	4	4	16	2	8	4	16
Maintenance	4	3	12	5	20	5	20
Manufacturing cost	3	1	3	5	15	4	12
Ease of installation	2	4	8	3	6	3	6
Design complexity	4	1	4	5	20	5	20
Operating live time	4	3	12	5	20	5	20
Total			80		99		114

Based on the concept elevation matrix presented above, concept 3 seemed to be the most promising option. This concept was used for the scale experimental. The numerical model to predict the mass displaced by the draft tube was also based on this concept.

3.2.3 Numerical model of draft tube

Different case studies were reviewed in the literature review (section 2.3.2) on methods to convey liquids in a confined section using two-phase flow. The numerical models used in these studies to predict the liquid volume flow rate displaced were one-dimensional (1D) steady-state mass and momentum balance models (Kassab et al., 2009; Mahrous, 2012). From the reviewed case studies it was observed that the 1D steady-state numerical models used could predict the mass flow rate displaced with fairly good accuracy. Using a steady state model for concept 3, one would not obtain the same accuracy, as the system is highly time dependent.

The aim with the numerical model is to capture the full cycle of the plug, from where it is injected into the draft tube until it escapes at the top and the draft tube's motion returns to rest. To capture this phenomenon with a numerical model it needs to be time dependent and a transient model is needed.

A further review was done to look for a transient numerical model that could capture the cycle of the plug in the draft tube. Among the numerical models that were found that possibly could predict this phenomenon were:

- The transient 1D slug flow model on a Eulerian grid base with a mass and momentum balance (De Henau & Raithby, 1994)
- A transient 1D plug flow model on a Lagrangian grid base with a mass and momentum balance assuming incompressible flow (Kjeldbly, 2013)

From reviewing these models listed above it became clear that most plug flow models are 1D mass momentum balance models with the following uncertainties; the liquid film thickness that surround the rising plug, the downward velocity of the liquid film and the interface shear stress between gas and liquid. In 2005, Taha and Cui investigated the motion of a plug rising in a vertical tube using a 2D axis symmetrical transient CFD Fluent model and also could not come up with a correlation for the liquid film thickness, the velocity of the liquid film or the interface shear stress.

A decision was then made to construct a new model that would capture the full cycle of the plug rising in the draft tube, where the shear forces acting on the plug would be determined by experimental work in terms of a friction multiplier (FM). The model was limited to a 1D transient explicit mass and momentum balance model based on a Lagrangian grid with three control volumes to simplify the complexity of the two-phase flow. The assumptions made while constructing the numerical model were:

- Isothermal expansion of plug was assumed using the ideal gas law
- The properties of air were used for the gas plug
- The instantaneous velocity of the liquid above the plug, the velocity of the plug and the velocity of the liquid below the plug were assumed to be the same
- A friction multiplier was used for the plug and the liquid below the plug
- The plug's initial velocity was taken as zero

With the assumptions made, the geometry of the draft tube was discretised into the three controlled volumes illustrated in Figure 3.29 a). The discretisation diagram of the momentum balance over the three controlled volumes is presented in Figure 3.29 b), with the forces acting on the controlled volumes.

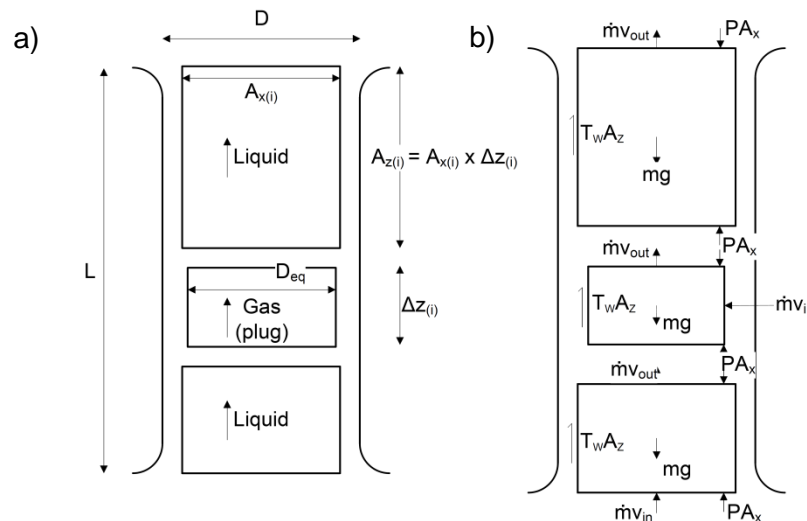


Figure 3.29: Discretisation diagram of two-phase model of a) geometry and b) momentum balance

The mass balance for the i 'th controlled volume in the discretisation diagram was derived using equations 3.30 and 3.31 below:

$$\frac{d}{dt} \int_i^{i+1} \rho dV = \int_i^{i+1} \rho v dA_x \quad (3.30)$$

$$\frac{d}{dt} \rho A_{x_i} \Delta z = \sum \rho v A_{x_i} - \sum \rho v A_{x_i} \quad (3.31)$$

where

$$A_{x_{L1,L2}} = 0.25\pi D^2 \quad (3.32)$$

$$A_{x_p} = 0.25\pi D_{eq}^2 \quad (3.33)$$

and the equivalent plug diameter D_{eq} is

$$D_{eq} = D - \% \delta D \quad (3.34)$$

The momentum balance i'th controlled volume was derived using equations 3.35 and 3.36:

$$\frac{d}{dt} \int_i^{i+1} \rho v dV = \int_i^{i+1} \rho v v dA_x - \int_i^{i+1} P dA_x - \int_i^{i+1} \rho g dV - \int_i^{i+1} \tau_w dA_z \quad (3.35)$$

$$\frac{d}{dt} \rho A_x \Delta z v = \sum \rho v v A_x + \sum \rho g h A_x - \rho g A_x \Delta z - \tau_w \pi d \Delta z \quad (3.36)$$

where the shear force, τ_i , for each i'th controlled volume is calculated by

$$\tau_i = \frac{1}{2} \lambda_i \rho v^2 \quad (3.37)$$

The friction factor, λ_i , for the i'th controlled volume is

$$\lambda_i = FM_i C_{f_i} \quad (3.38)$$

where the friction multiplier, FM for control volume L1, was taken as

$$FM_{L1} = 1 \quad (3.39)$$

and the FM for control volume P and L2 obtained from the experimental work as

$$FM_{P,L2} = e^{(-0.18393(\ln P_e)^8 + 4.93657)} \quad (3.40)$$

The friction coefficient, C_f , for the plug in turbulent flow

$$C_{f_p} = 0.316 R_e^{-0.25} \quad \text{if } R_e > 2300 \quad (3.41)$$

The friction coefficient, C_f , for the controlled volume L1 and L2 in turbulent flow:

$$C_{f_{L1,2}} = 0.079 R_e^{-0.25} \quad \text{if } R_e > 2300 \quad (3.42)$$

The friction coefficient, C_f , for the i'th controlled volume in laminar flow:

$$C_{f_i} = \frac{64}{R_e} \quad \text{if } 1 > R_e > 2300 \quad (3.43)$$

$$C_{f_i} = 16 \quad \text{if } R_e < 1 \quad (3.44)$$

The plug ratio, P_e used was defined as height over diameter of plug;

$$P_e = \frac{z_p}{D_p} \quad (3.45)$$

Equations 3.30 and 3.31, 3.35 and 3.36 and 3.41 to 3.44 were obtained from White (2011) with the $\% \delta$ in equation 3.34 taken as 5%. Equations 3.37 to 3.39 were obtained from Kjeldbly *et al.* (2013) and 3.40 was obtained from the experimental work conducted in this thesis (refer to Appendix A.2.1).

The 1D transient numerical model was used to predict the summation of liquid displaced for a full-scale mixing system. The time increment used for the simulations was 0.06 s. The selection of the time increments for the simulations is discussed in detail in Appendix A.2.2. The full-scale mixing system geometrical construction consisted of a 13 m long draft tube with an internal diameter of 364 mm. The top clearance between the outlet of the draft tube and the liquid level was taken as

600 mm, and the bottom clearance between the inlet of the draft tube and the floor of the digester as 1.2 m. The plug inlet was placed 1.2 m above the inlet of the draft tube, with a plug ratio of $1.2P_e$. The inlet and outlet of the draft tube were configured with a Bell mouth, with an entrance and exit loss coefficient of 0.25 and 0.3 respectively. This geometry was used as the base case for the rest of the simulations.

The results obtained from the simulation are illustrated in Figure 3.30 and Figure 3.31 below. Figure 3.30 shows the velocity profile of the fluid moving inside the draft tube. The summation of the mass displaced is displayed on the secondary axis in Figure 3.30. The results of the acceleration and mass flow rate of the draft tube are illustrated in Figure 3.31.

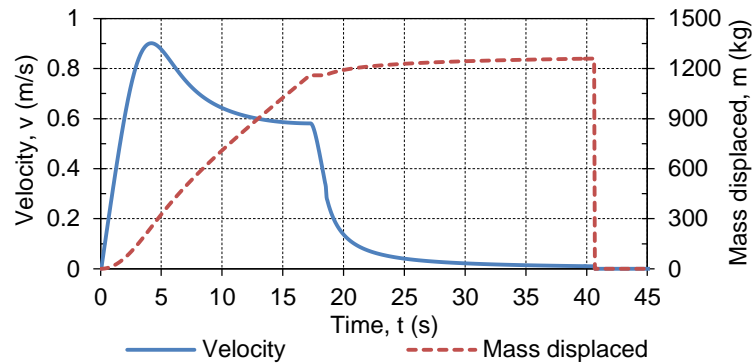


Figure 3.30: Velocity profile and the mass of liquid displaced over time from a 365 mm draft tube with a plug ratio of $1.2P_e$

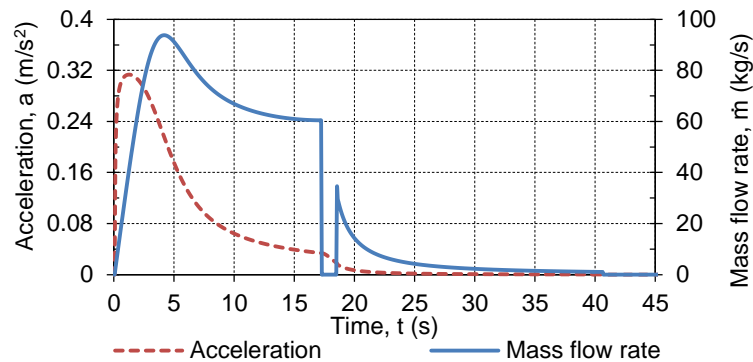


Figure 3.31: Acceleration profile and mass of liquid displaced over time from a 365 mm draft tube with a plug ratio of $1.2P_e$

The results illustrated in Figure 3.30 show that the velocity profile increased sharply from rest to 0.9 m/s up to 4.2 s, and then started to decline at 0.33 m/s when the plug exited the draft tube at 17.28 s. From this point onwards, a sharp decrease in the velocity can be seen, with a long tail until the cycle ends. The results of the mass displaced on the secondary axis of Figure 3.30 show a steady increase in the mass displaced until the plug exits the draft tube. This is followed by a plateau in the trend for 1.32 s as the plug exits the draft tube, followed by the tail until the motion ends with a total of 1 260 kg of liquid displaced.

The acceleration profile illustrated in Figure 3.31 increased sharply to a maximum of 0.313 m/s^2 after 1.26 s. From this point onwards, a large deceleration is displayed until the plug exited the draft tube. While the plug exited the draft tube there was another sharp deceleration, followed by a long tail that correlated with the velocity

profile. On the secondary axis of Figure 3.31 the trend of the mass flow rate from draft tube is illustrated, peaking at 91 kg/s after 4.2 s. The rest of the profile is similar to the velocity profile, but decreases to almost 0 when the plug exits the draft tube due to the difference in density.

In the second set of simulations using the numerical model, the effect of the plug frequency on the mass and mass flow rate displaced was studied. The same geometrical configuration as the base case was used, but the plug frequency was varied between 0.019 Hz to 0.054 Hz for five consecutive cycles. A sample of the results obtained for a plug frequency of 0.048 Hz and a plug ratio of $1.2P_e$ is illustrated in Figure 3.32 below, in which the mass displaced and the velocity profile are plotted. For the rest of the results obtained on the plug frequencies, only the last four cycles were taken into account. These results were averaged and are plotted in Figure 3.33. The reason for eliminating the first cycle from the results was that equilibrium was only obtained after the second cycle.

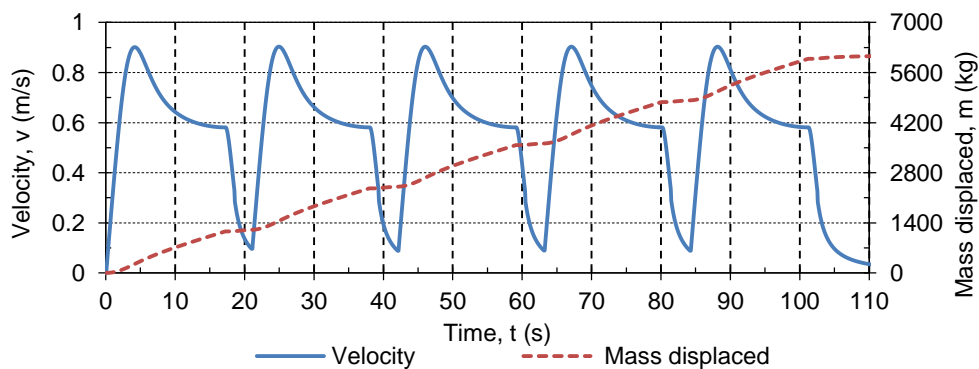


Figure 3.32: Velocity profile and the mass displaced over time of five cycles with a plug frequency of 0.048 Hz

From Figure 3.32, the same trend in the mass displaced and velocity profile up to 21 s, where the velocity is 0.12 m/s, can be seen compared to Figure 3.30, but from this point onwards a repetitive cycle is shown.

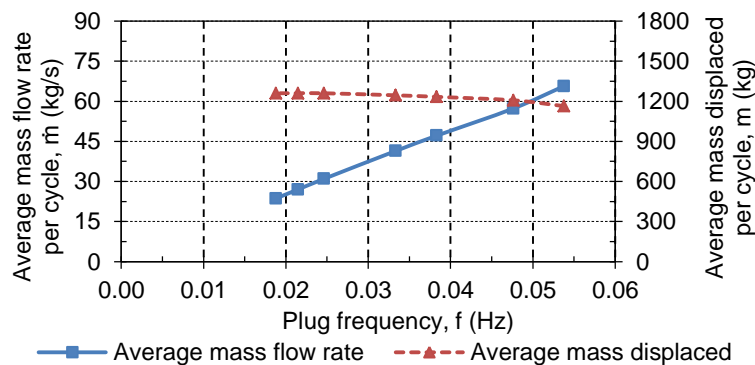


Figure 3.33: Effect of plug frequency on the average mass flow rate and average mass displaced per cycle

The averaged results presented in Figure 3.33 indicate that an increase in plug frequency led to an increase in the averaged mass flow rate. The result of the mass displaced on the secondary axis in Figure 3.33 shows a trend line that follows a parabolic shape, peaking at 0.025 Hz. At this frequency a plug was introduced just after the motion of the draft tube returned to rest.

In the third set of simulations, a sensitivity analysis of the geometrical construction of the mixing system was conducted. In the sensitivity analysis the internal diameter of the draft tube was varied from 176 to 516 mm, the top clearance from 0.2 to 1.2 m, the bottom clearance from 0.6 to 2.2 m and the plug ratio from 0.7 to 1.4 P_e .

The results obtained from the different simulations were normalised against the base case and the effect of the geometrical construction on the mass displaced is presented in Figure 3.34 and on the mass flow rate in Figure 3.35.

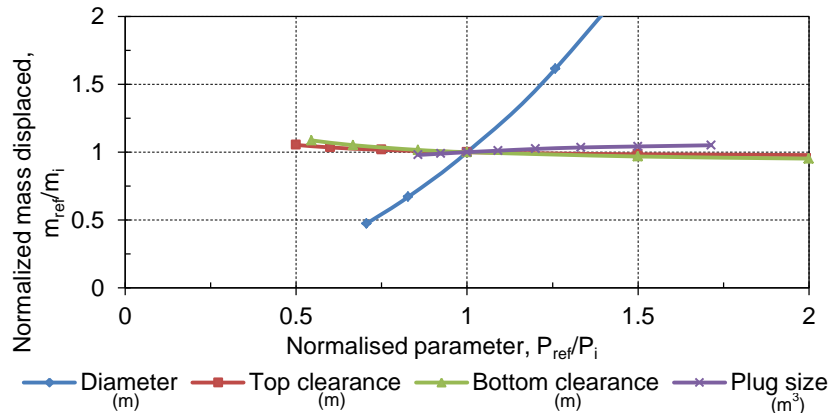


Figure 3.34: Sensitivity analysis of mass displaced of mixing system based on geometrical construction

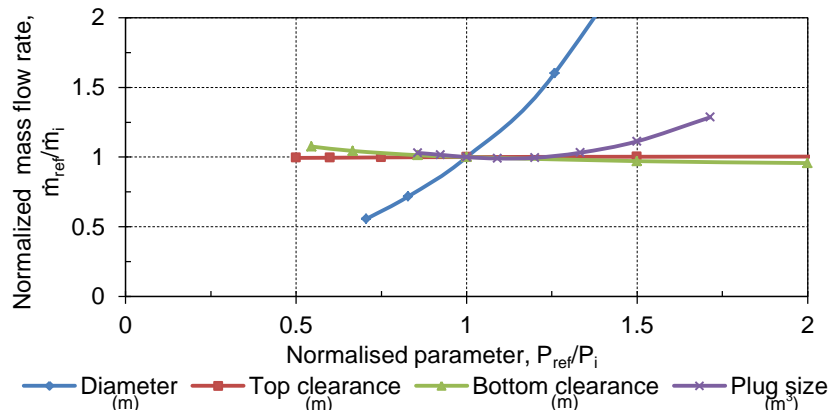


Figure 3.35: Sensitivity analysis of averaged mass flow rate of mixing system based on geometrical construction

From the normalised results obtained in Figure 3.34 and Figure 3.35, it is clear that the diameter of the draft tube is the only parameter that has a major effect on the mixing system. The sensitivity study also indicates that the top and bottom clearance had a very limited effect on the mixing system, where an increase in the top and bottom clearance led to a decrease in the amount of mass displaced, as well as in the mass flow rate. The results show that the increase plug ratio leads to a linear increase in mass displaced (Figure 3.34), but to a parabolic trend of increased mass flow rate (Figure 3.35). From this parabolic trend an optimum plug size could be determined for this geometrical configuration to increase the mass flow rate of the mixing system.

From the three sets of numerical simulations of the mixing system, enough knowledge was gained in order to derive a proposed design for a full-scale mixing system for a CSTR using the gas recirculation method in a plug-flow regime.

3.3 Conclusion

The methodology of this study was divided in two main sections. In the first section the focus was placed to determine; the available sludge and disposable method used at Gammams WWTP, to draw up three different plant layout concepts to treat the available sludge and the numerical modeling of the heat energy and electricity balance on the conceptual plants. In the second section the focus was placed to propose a mixing system for a 1 600 m³ CSTR.

At Gammams WWTP there are two available sludge streams that need to be treated, the first from the primary settling tanks (PSTs) known as primary sludge (PS) and the second from the secondary settling tanks (SSTs) known as waste activated sludge (WAS). The combined volume of sludge available at Gammams WWTP was 983.741 m³/day at TS contents of 4 % which volume can be reduced significantly if dewatered and was illustrated in Figure 3.2. The PS was selected to be treated first before adding the WAS as PS places higher load on WWTP (Thornton et al., 2009).

Three different conceptual AD plant layouts were drawn up based on the available infrastructure and sludge disposal method used at Gammams WWTP (refer back to Figure 3.26, 3.4 and 3.5 for illustrations). In each concept the feedstock TS was ranging from 4 % to 10 %, but the hydraulic retention time (HRT) was kept constant for each concept.

The general concept model used for the three different conceptual AD plant layouts was that the feedstock stream entering each concept was first pre-heated by the effluent from the AD plant using a double tube pre-heat exchanger. The feedstock entering was then heated further to the digester operating temperature by another double tube post-heat exchanger of which the heat was recovered from the CHP units (refer back to Figure 3.6 for flow diagram and Figure 3.19 for CHP flow diagram). The biogas generated from each of the digester layout concepts were then conveyed to internal combustion CHP units where electricity was generated for the WWTP and nearby suburbs in Windhoek.

The first concept consisted of a 3/2 two-stage digester configurations which could treat 65 % of the available sludge at the WWTP at TS content of 10 %. Concept 2 consisted of a 4/1 two-stage digester configuration which could treat 71 % of the available sludge and concept 3 digester was configured in a two-phase configuration able to treat 100 % of the available sludge at the WWTP at TS content of 10 %.

The three different conceptual AD plant layouts were then evaluated based on a numerical overall heat, energy and electricity balance. The numerical model included the feedstock heat requirements, the digesters heat requirements, digester energy production, net electric power generated and available heat to be recovered from CHPs. The results of the numerical model indicated that concept 3 outperformed the other two by far. In the overall heat balance it was found that there was a heat shortage at 4 % TS content for all concepts, but at increased TS contents there was an abundance of heat available. The results on the net electric power generated by concept 3 increased by 276% with increasing the TS from 4 % to 10%. On average concept 3 produced 52 % more net electric power and concept 2, 38 % more compared to concept 1. These results indicated the impotence of increasing an AD plant TS contents.

In the second section of the methodology the design criteria and limitations for CSTR mixing system were set and based on it, three different conceptual mixing systems were drawn up. The three different concepts were evaluated based on a concept evaluation matrix and a numerical model was derived for the selected mixing system.

The main design criteria set for the development of the mixing system for a CSTR in this study was, that there should be no moving parts inside the digester, should be able to operate in TS contents up to 10 % and mixing rate must be adjustable (all listed in section 3.2.1). Based on the design criteria and limitations set for the mixing system three different concepts were drawn up using the confined gas recirculation in a plug flow regime mixing method.

The first mixing concept was based on gas accumulator with a series of pressure vessels connected in parallel that reassess the pressured gas in batches to and from gas plugs. The second concept was derived from concept 1 by placing the gas accumulator working on U-tube principle at the bottom of the draft tube and in the third concept the gas accumulator was also placed at bottom of draft tube, but worked on a series of U-tubes to release gas plug (refer back to Figure 3.26, 3.27 and 3.28 for illustrations). These three mixing concepts were then evaluated in a concept evaluation matrix and based on the results concept 3 was selected.

Based on the selected concept a, 1D transient explicit numerical model using a three control volume Lagrangian mass momentum balance was derived. The numerical model was developed to predict the liquid mass displaced out the top of the draft tube by a certain plug volume and to perform a sensitivity analysis on the mixing system geometry. For the numerical model a friction multiplier was used that was determined by experimental work and using a multi-linear regression model using MS Excel.

The results of the mixing system numerical model illustrated that an increase in plug frequency leads to an increase in the liquid mass flow rate displaced (refer back to Figure 3.33). The sensitivity study conducted on the mixing system geometry indicated, that the only major parameter affecting the performance of the mixing system was the draft tube diameter. It also indicated that an optimum plug size can be determined for a diameter of a draft tube (refer back to Figure 3.34 and 3.35).

The methodology of this study illustrated the benefits in selecting the digester configuration evaluating the three concepts in an overall heat, energy and net electrical production balance at increasing TS contents of the feedstock through a typical year. The numerical model derived from the selected mixing system for the CSTR illustrated it is possible to convey large volumes using a plug flow two-phase flow regime and that the effectiveness can be increased with the correct plug size.

4. EXPERIMENTAL WORK

The experimental work in this thesis focused on an evaluation of the confined gas mixing system using concept 3 selected in the methodology section to mix the digester.

The aim of the experimental work was to use the data gathered from the scale model to predict the performance of the plug-flow generator, to determine a correlation for the friction multiplier (FM) and to verify the numerical two-phase flow model.

The objectives for the work discussed in this chapter were to determine the effect of the different geometrical variations on the plug-flow generator for it to displace liquid from the top of the draft tube. In order to achieve these objectives, the experimental work was broken into two different sections. In the first section, the focus was on the ability of the plug-flow generator to generate a selected plug size by varying the geometry of the plug-flow generator itself under different gas supply flow rates and hydrostatic pressures.

In the second section, the focus was on obtaining the liquid mass displaced for a selected plug-flow generator and the averaged liquid mass flow rate at different gas supply flow rates and hydrostatic pressures. It was also used to gather data to construct an explicate equation for the FM for the two-phase numerical model.

4.1 Plug size

In the first section of the experimental work, the emphasis was to investigate the ability of the plug-flow generator to generate a volume of plug by varying the geometry. A descriptive picture of the plug generator's geometry from a front and side section view (A-A) can be seen in Figure 4.1. The different geometrical parameters that were varied in this work were the volumes, areas of chambers 1 to 3, and the orifice area plate.

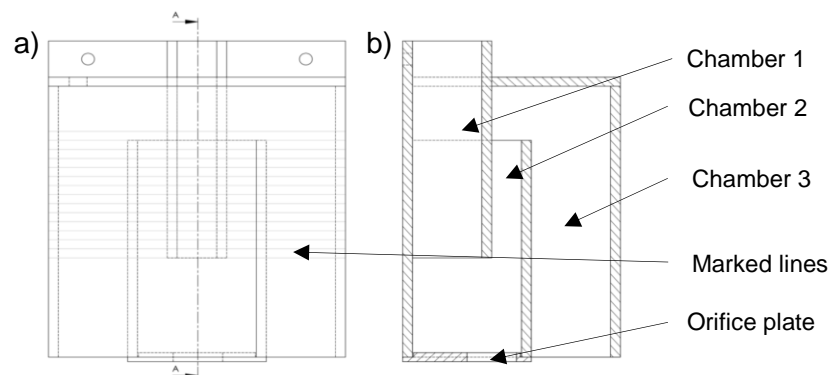


Figure 4.1: Plug-flow generator a) front and b) side section view

On the plug generators, a set of lines was scratched on the front view of chamber 3, as illustrated in Figure 4.1. These lines were scraped with a vernier high-gauge scale from the bottom level of chamber 1 upwards at a spacing of 5 mm to the top level of chamber 2, with an accuracy of 0.02 mm. This set of 5 mm spaced lines was used for two purposes – initially to calibrate the air flow meter (refer to Appendix B.1 for more detail on calibration), and secondly to determine the plug size released by the plug-flow generators.

For the experimental work, seven different geometrical variations in the plug generators were built using Perspex sheets. The dimensions of the seven plug generator variations were measured with a vernier calliper (accuracy of 0.02 mm) after each one was built. Each of the seven plug-flow generators built also had a set of three different orifice plates for the bottom of section 2. The areas and active volumes measured for the different plug-flow generators were calculated and are tabulated in Table 4.1 below:

Table 4.1: Measured data from the different plug-flow generators

Plug generator	Cross section area (m ²)			Active volume (m ³)			Orifice area (m ²)		
	A ₁	A ₂	A ₃	V ₁	V ₂	V ₃	A ₀₁	A ₀₂	A ₀₃
1.1.1	700E ⁻⁶	2.10E ⁻³	9.80E ⁻³	66.5E ⁻⁶	2.90E ⁻³	3.63E ⁻³	201E ⁻⁶	415E ⁻⁶	804E ⁻⁶
1.1.2	455E ⁻⁶	2.45E ⁻³	9.80E ⁻³	43.2E ⁻⁶	2.93E ⁻³	3.63E ⁻³	201E ⁻⁶	415E ⁻⁶	804E ⁻⁶
1.1.3	94.6E ⁻⁶	3.00E ⁻³	9.80E ⁻³	8.98E ⁻⁶	2.98E ⁻³	3.63E ⁻³	201E ⁻⁶	415E ⁻⁶	804E ⁻⁶
1.2.1	700E ⁻⁶	3.26E ⁻³	8.50E ⁻³	66.5E ⁻⁶	3.43E ⁻³	3.63E ⁻³	201E ⁻⁶	415E ⁻⁶	804E ⁻⁶
1.2.2	700E ⁻⁶	4.78E ⁻³	6.81E ⁻³	66.5E ⁻⁶	4.09E ⁻³	4.28E ⁻³	201E ⁻⁶	415E ⁻⁶	804E ⁻⁶
1.3.1	700E ⁻⁶	2.10E ⁻³	5.40E ⁻³	66.5E ⁻⁶	2.90E ⁻³	3.21E ⁻³	201E ⁻⁶	415E ⁻⁶	804E ⁻⁶
1.3.2	700E ⁻⁶	2.10E ⁻³	14.0E ⁻³	66.5E ⁻⁶	2.90E ⁻³	4.03E ⁻³	201E ⁻⁶	415E ⁻⁶	804E ⁻⁶

4.1.1 Effect of geometric construction

The initial experimental test work in the first section was to determine the ability of the seven different geometrical variations of plug generators to generate plugs. The experimental setup used for these tests consisted of a compressed air supply line, a pressure regulator, a pressure vessel, a moisture trap, an air flow meter, a testing tank, the plug-flow generators and a high-speed video camera. A schematic flow diagram of the setup used is illustrated in Figure 4.2 below.

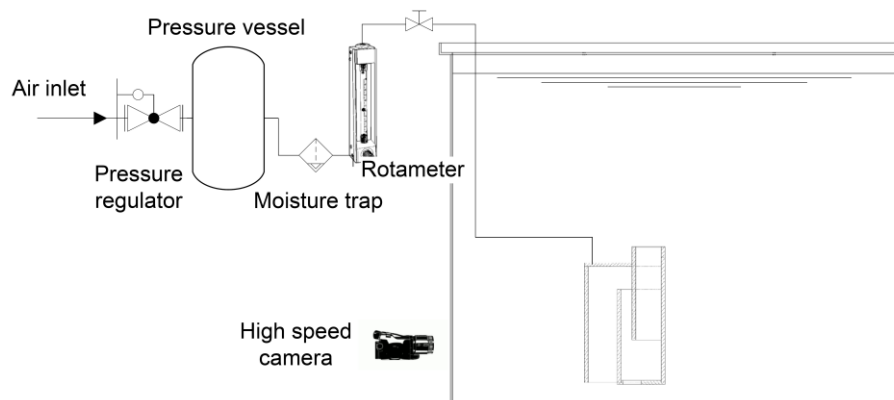


Figure 4.2: Experimental setup for effect of geometry, pressure and calibration

In the experimental setup used, the compressed air was supplied by a centrifugal air compressor at a constant pressure of 7 bar. A pressure regulator was installed next in line to reduce the line pressure to the desired set point. The outlet of the pressure regulator was connected to a pressure vessel (10 L capacity) to ensure that a constant flow rate and pressure were achieved from this point onwards to the rest of the instrumentation. An air service unit as installed after the pressure vessel to supply the air flow meter with condensation, oil and any debris-free air. The air flow meter used for the experiments was a National Instrument rotameter with a gas flow range of 0.05 to 2.5 Nm³/h. The calibration of the rotameter is discussed in Appendix B.1.

From the gas flow meter, the air supply line passed through a manual shut-off valve before it was connected to the plug-flow generator in the testing tank. The testing tank had a capacity of 1 500 L, with a diameter of 1 m and workable depth of 1.5 m. Two inspection windows made from a Perspex sheet were installed 180° apart to locate the high-speed camera outside the testing tank, focusing on the plug generator box. The camera was a GoPro 3 Hero edition at a video setting of 100 frames per second and a pixel frame size of 1050 x 960. The captured videos were converted to picture frames and edited in Adobe Photoshop CS6 to eliminate the effect of the wide angle lens to improve the accuracy of the data captured.

The experiments conducted on the seven plug-flow generators with their three different orifice plates to determine the effect of the geometry variation were done at a volumetric air supply flow rate of 0.1 to 1.9 m³/h. The experimental procedure used to determine the effect of the geometrical constriction is listed below:

1. Install the plug-flow generator at a liquid depth of 700 mm, 200 mm away from the inspection window
2. Level the plug generator's x and y direction
3. Set up the high-speed camera 200 mm away from the inspection window so that the middle of the lens is level with that of the bottom of chamber 1
4. Set the pressure regulator feeding the gas supply line to 1 bar and open the gas supply valve
5. Set rotameter to the required flow rate
6. Close the air shut-off valve
7. Disconnect the gas supply line after the shut-off valve so that the accumulated air inside the plug-flow generator can escape and connect hose again
8. Start the video recording on the camera
9. Open the shut-off valve
10. Record three cycles of the plug-flow generator
11. Repeat steps 6 to 10 another eleven times at increasing air flow supply rates
12. Change the orifice plate of the plug-flow generator
13. Repeat steps 5 to 12 twice to complete testing for one variation of the plug-flow generator with three different orifice plates
14. Install a next plug-flow generator and follow steps 1 to 14

From the experimental work conducted on the effect of the geometrical constriction and by analysing the results, the working principal of the plug-flow generator was better understood. In the section below, the working principle is described, followed by the results obtained on the effect of the geometrical constriction.

Working principle of plug-flow generator

From the experimental work conducted and data obtained, it was observed that the plug-flow generator cycle consisted of three steps. These three steps are schematically illustrated in Figure 4.3.

In the first step, the air supplied to the plug-flow generator displaces the liquid in chambers 2 and 3 from the bottom openings. As the air is supplied continuously at a constant flow rate, the liquid level in chambers 2 and 3 reaches the level of the bottom opening of chamber 1 (see Figure 4.3, image a). With the continuous addition of air, the liquid level in chambers 2 and 3 drops below the bottom opening of chamber 1 and the accumulated air, and what is still being supplied starts to escape through the bottom opening of chamber 1.

As the air starts escaping, it marks the start of the second step of the plug-flow generator cycle. As the accumulated air in the plug-flow generator escapes, the liquid level in chamber 3 starts to rise, while that in chamber 2 remains stationary. The rise of the level of the liquid in chamber 3 forces the accumulated air from the opening in chamber 1 to form a plug. The plug formation ends when the liquid level in chamber 3 rises to a certain height (at position z_{3b} refer to Figure 4.3 image b), while the liquid level in chamber 2 rises to position z_{2b} and closes the bottom of the opening of chamber 1. This marks the end of the second step.

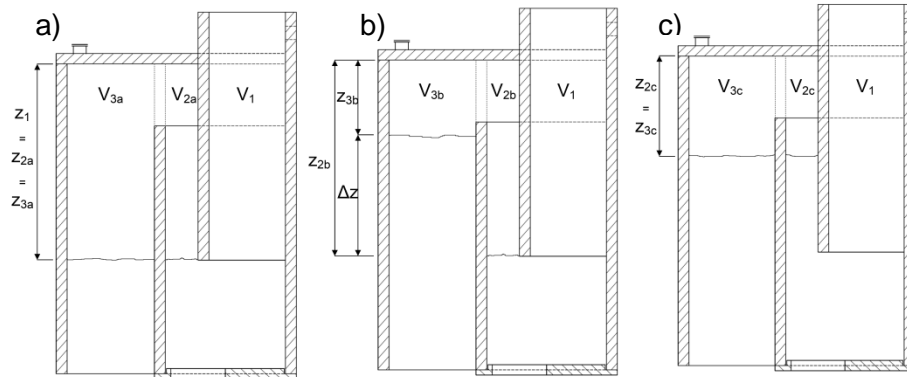


Figure 4.3: Schematic cycle of a plug-flow generator a) step 1, b) step 2 and c) step 3

In the third step after plug formation, with air still being supplied at a continuous rate, the liquid level in chamber 2 rises to point z_{2c} and the level in chamber 3 drops to z_{3c} (refer to Figure 4.3, image c). When the liquid level of chambers 2 and 3 are at the same level, the plug-flow generator cycle repeats. A full cycle captured in the experimental work of plug-flow generator 1.1.1 with an orifice area of $415 \times 10^{-6} \text{ m}^2$ at a volumetric air flow rate of $0.7 \text{ Nm}^3/\text{h}$ is presented in Appendix B.3.

From the results in the experimental work, it was found that the function of the orifice plate is to restrict the liquid flow rate entering the bottom of chamber 2 and to prolong the time period for the volume of air in chamber 3 to escape. Therefore, by decreasing the orifice area, a larger plug volume can be released, but at a slower rate if the air supply rate is kept the same.

Results of geometrical construction

The results of the experimental work on the effect of the geometrical construction was obtained by recording the following parameters:

- Air supply volume flow rate
- Volume of plug generated
- Time interval between plugs

The volume of the plugs, V_p , in m^3 , generated by the different variations in plug-flow generators, was calculated using the photos captured by the camera and equations 4.1 to 4.3 below:

$$V_p = V_{acc} + V_{supply} \quad (4.1)$$

where the accumulated volume of air, V_{acc} , and the volume of air supplied, V_{supply} , in m^3 were

$$V_{acc} = A_3(\Delta z_{3b}) \quad (4.2)$$

$$V_{supply} = \dot{v}_a t \quad (4.3)$$

In equation 4.2, A_3 is the area of chamber 3 of the plug-flow generator in m^2 , and Δz_{3b} is the height difference in the plug-flow generator in m. In equation 4.3, \dot{v}_a is the air supply volume flow rate in m^3/h and t is the time period from when the plug started escaping chamber 1 until it stopped, in seconds.

The volume of the plugs formed by the different plug-flow generators is presented in Figure 4.4 to Figure 4.6. The mean data of the experimental work is tabulated in Appendix E, Table E.1.

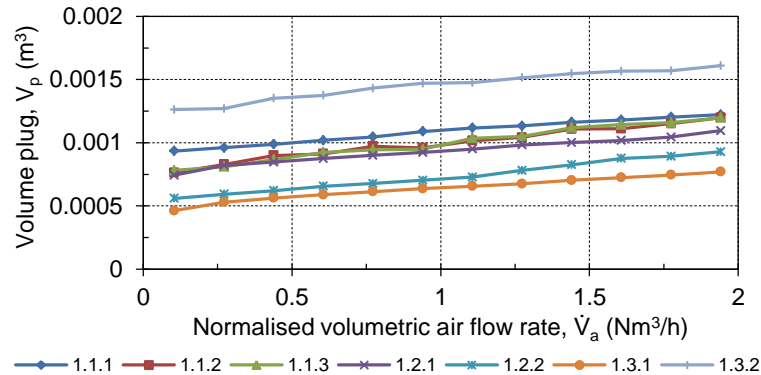


Figure 4.4: Volumes of plugs generated as a function of air flow rate with an orifice area of $201 \times 10^{-6} m^2$

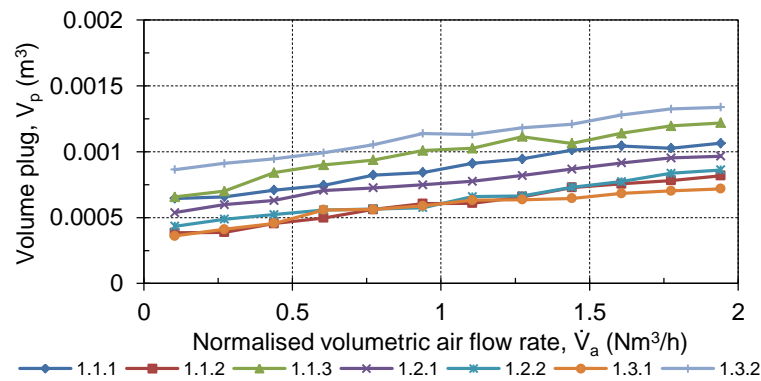


Figure 4.5: Volumes of plugs generated as a function of air flow rate with an orifice area of $415 \times 10^{-6} m^2$

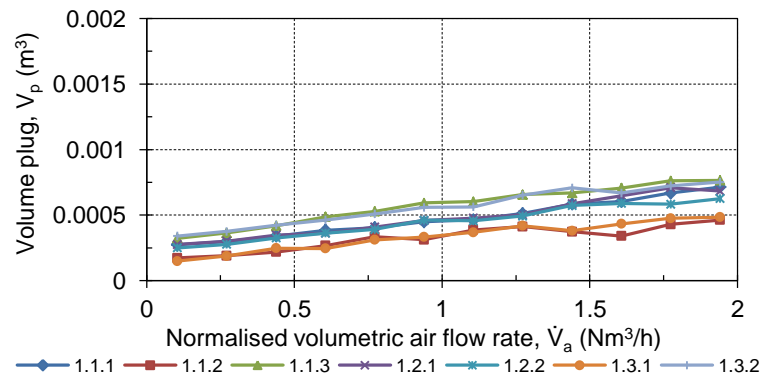


Figure 4.6: Volumes of plugs generated as a function of air flow rate with an orifice area of $804 \times 10^{-6} m^2$

In the results obtained for the volume of plugs generated, presented in Figure 4.4 to Figure 4.6, it is shown that the plug volume decreases with an increase in orifice area. The results also indicate that the volume of plug generated increases on a steady gradient as the air supply flow rate is increased.

The results of the time frequency between the plugs were obtained by taking the inverse of the time period between plugs formed. The time period between plugs was calculated by summing the number of frames from when the air started to escape into chamber 1 until it recurred in the next cycle and dividing it by 100.

The calculated plug frequency of the plug generator with an orifice area of $201 \times 10^{-6} \text{ m}^2$ can be seen in Figure 4.7 below. The results for the orifice area of $415 \times 10^{-6} \text{ m}^2$ and $804 \times 10^{-6} \text{ m}^2$ have not been plotted, but the mean data can be seen in Appendix E, Table E.1.

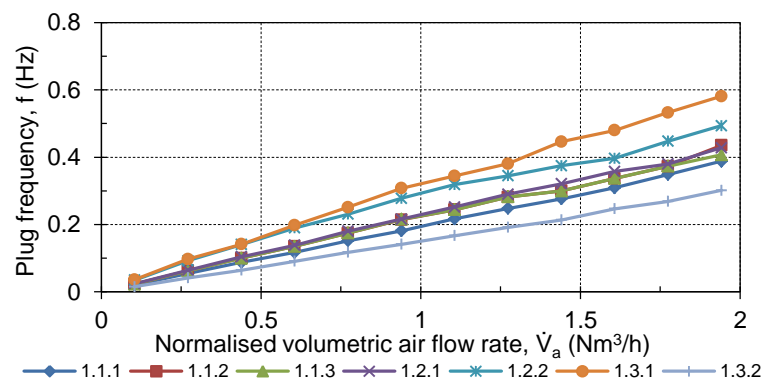


Figure 4.7: Plug frequency as a function of air flow rate with an orifice area of $201 \times 10^{-6} \text{ m}^2$

Figure 4.7 above shows that, with an increase in air supply flow rate, the plug frequency increase on a linear trend. From the mean data in Appendix E, Table E.1 it can be seen that an increase in orifice area also leads to an increase in plug frequency.

4.1.2 Effect of hydrostatic pressure

To determine the effect of hydrostatic pressure on the capability of the plug-flow generator to generate a plug, the liquid level in the testing tank had to be varied for the second set of experimental work. The liquid levels in this experiment were varied to two additional heights. The liquid level in the original experiment was set at 0.7 m and was varied to 0.85 m and then to 1 m above the plug-flow generator in this experiment. From these three different heights, the effect of the hydrostatic pressure on the plug-flow generator was visible.

For this second set of test work, only one of the plug generators was used, namely 1.1.1, with an orifice area of $201 \times 10^{-6} \text{ m}^2$. The reason for testing only one of the plug-flow generators with a single orifice plate was that the effect of hydrostatic pressure would be similar on the rest of the plug-flow generators.

The experimental setup used for the study on the effect of the hydrostatic pressure was the same setup previously illustrated in Figure 4.2, but only this time the liquid level was varied, as mentioned above. The liquid level was measured each time before a test using a steel ruler with an accuracy of 1 mm. The air supply flow rates selected for the experimental work was again between 0.1 and 1.9 Nm³/h.

The experimental testing procedure followed to determine the effect of the hydrostatic pressure on the plug-flow generator was as follows;

1. Set liquid level to 0.85 m above the plug-flow generator
2. Follow steps 1 to 11 of the effect of the geometrical constriction of the plug-flow generator
3. Change the liquid level in the testing tank to 1 m and repeat steps 1 to 11 of the geometrical test procedure

To obtain the result of the experimental work on the effect of the hydrostatic pressure, the same parameters were recorded, as pointed out in the previous set of test work.

Results on the effect of hydrostatic pressure

The volumes of the plugs generated at the different liquid levels of the plug-flow generator configuration 1.1.1 with an orifice area of $201 \times 10^{-6} \text{ m}^2$ are displayed in Figure 4.8 below. The mean data of the experiment can be seen in Appendix E, Table E.2.

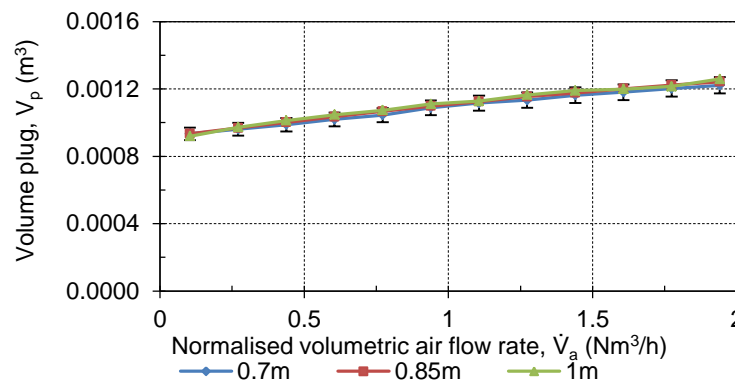


Figure 4.8: Volumes of plugs at different hydrostatic pressures as a function of air flow rate using plug generator 1.1.1 and an orifice area of $201 \times 10^{-6} \text{ m}^2$

The results presented in the figure above show that there is almost no effect of hydrostatic pressure on plug formation by a plug-flow generator. In order to evaluate the magnitude, vertical error bars were included in the figure above at a deviation of $\pm 4\%$ from the original case tested at 0.7 m. With the vertical error bars of $\pm 4\%$ include in Figure 4.8 it is shown that all the measured data points lies within these bars and illustrate that the effect of hydrostatic pressure on the generator's negligibly. With the volume of plug generated at different hydrostatic pressures being nearly constant, the time period under normalised air flow rate also stayed constant, of which the mean data are presented in Appendix E, Table E.2.

Predicting the behaviour of the plug-flow generator

With the data obtained on the volume and frequency of the plug generated by the different geometrical construction plug-flow generators, mathematical relationships had to be derived to predict these for the full-scale model. To derive a mathematical relationship to predict the volume of the plug generated and the plug frequency based on the geometrical construction, a multi-linear variable regression model was used. The method used in this instance was the Microsoft Excel ANOVA model. A total of 252 data points were imported of the different geometry configurations at the corresponding air supply flow rate for the volume as well as for the frequency, but the volumes of the plug were converted to mass, as the mass is not affected by depth and makes it easier to scale.

Mass of plug

The best mathematical relationship obtained from the ANOVA analysis for the mass of the plug generated by the plug-flow generator is presented in empirical equation 4.4.

$$m_p = 232.974 \times 10^{-6} \dot{m}_{air} - 1.089A_{or} + 84.318V_2 + 821.712 \times 10^{-3}V_3 - 3.2A_1 - 8.308A_2 - 1.943 \times 10^{-3} \quad R^2 = 0.9085 \quad (4.4)$$

where \dot{m}_{air} is the mass flow rate of the air supply rate in kg/h, A_{or} is the area of the orifice in m^2 , V_2 is the active volume of chamber 2 in m^3 , V_3 is the active volume of chamber 3 in m^3 , A_1 is the area of chamber 1 and A_2 the area of chamber 2 in m^2 . The accuracy of the mathematical relationship obtained is illustrated in Figure 4.9, with a R^2 value of 0.9098.

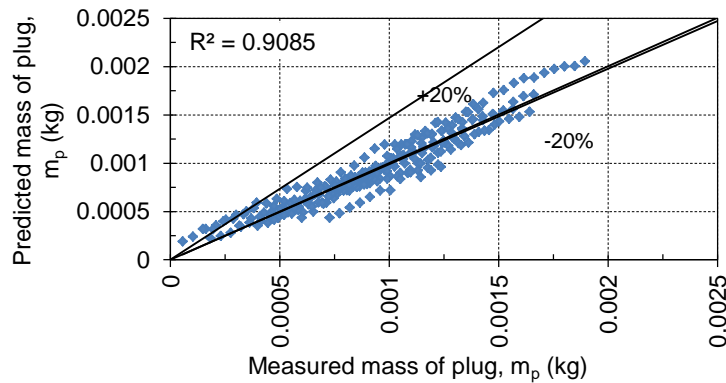


Figure 4.9: Multiple linear regression analysis of mass of plug with R^2 of 0.9098

In the figure above, the predicted and measured mass of the plug generated were plotted against each other and a deviation envelope of $\pm 20\%$ was included to indicate the accuracy of the relationship. The figure illustrates that only 28 data points of 252 lie outside the deviation envelope. A linear curve fit was placed through the data points, forcing it through the origin. From the curve fit it is clear that the empirical equation 4.4 captures the data well and runs through the mean of the data points.

Plug frequency

The best equation obtained from the ANOVA method for the plug frequency generated is presented in equation 4.5. The predicted results with the equation were again plotted against the measured results in Figure 4.10 to illustrate the accuracy of the mathematical relationship.

$$f = e^{(1.107 \ln \dot{m}_{air} - 892.263 \times 10^{-3} \ln m_p - 7.653)} \quad R^2 = 0.9894 \quad (4.5)$$

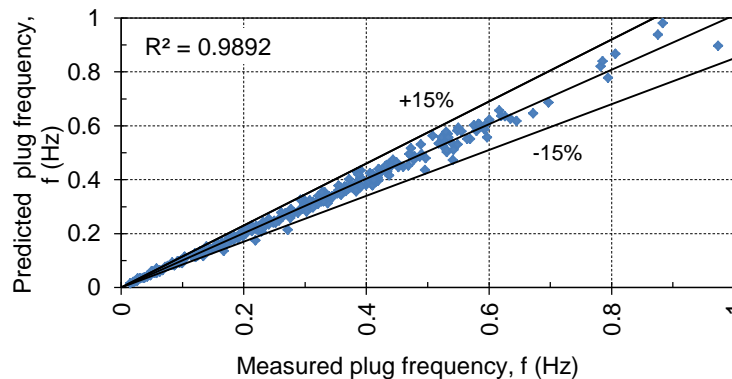


Figure 4.10: Multiple linear regression analysis of plug frequency with R^2 of 0.9894

In Figure 4.10, the predicted and measured plug frequency were plotted with a deviation envelope of $\pm 15\%$. The figure illustrates that only four of the 252 data points fall outside the deviation envelope. A linear curve fit was again placed through the data points, forcing it through the origin, and a R^2 value of 0.9894 was obtained. The incline of the linear curve fit indicates that empirical equation 4.5 lies well on the mean, which means the linear curve fit are a good approximate.

With these two empirical equations of the mass of the plug and the plug frequency for different geometries, a design could be drawn up for the full-scale plug-flow generator.

4.2 Mass displaced

In the second section of experimental work, the objective was to determine the liquid mass displaced by a plug from the draft tube and this was subdivided into two sets: the effect plug size (4.2.1) and the effect hydrostatic pressure (4.2.2). The result of this experimental work was used to determine the FM and to validate the numerical two-phase flow model constructed in this thesis.

4.2.1 Effect of plug size

To determine the effect of the plug size released on the amount of liquid displaced from the draft tube, the geometry of the plug-flow generator had to be varied again and the mass displaced had to be measured. With the volume of the plugs already known, only the displaced liquid had to be measured.

Plug generator 1.1.1, together with its three different orifice plates, were used for this work. The experimental setup used for this was the same as used previously, only this time the following items were added: a draft tube, a container to capture liquid displaced, a liquid outlet line, a beaker and an electronic scale. The schematic flow diagram of the setup used can be seen in Figure 4.11.

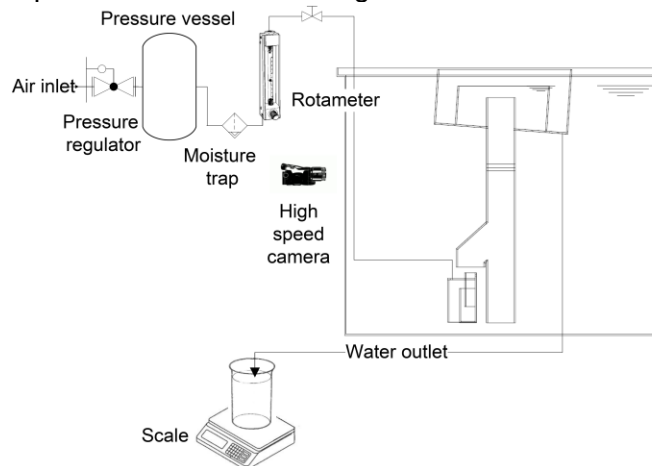


Figure 4.11: Experimental setup used to measure liquid mass displaced

The draft tube made of Perspex tubing was installed vertically with its outlet 1D from the surface of the water level and its bottom inlet 1D from the floor of the testing tank. The total length of the draft tube was 800 mm, with an internal diameter of 100 mm. A plug inlet was added to the draft tube 210 mm from the bottom inlet, consisting of a 'y' junction with two 45° angled sections made from the same Perspex tubing. The plug-flow generator was installed with 10 mm below the plug inlet of the draft tube at a total liquid depth of 0.7 m.

At the top of the draft tube, a container was installed to separate the liquid and air phases. The container consisted of a sloped floor, two separate compartments and a liquid drain at the lowest point in the outer compartment's floor. The container's internal compartment sides were at the same level as that of the liquid level in the testing tank. The outer compartments' sides were raised so that no liquid transfer was possible from the tank to the container or vice versa (see Figure 4.11).

The container worked on the following principle: As the plug inside the draft tube displaces the liquid out of the top, the liquid level of the inner compartment overflows into the outer compartment while the air escapes to the atmosphere. The liquid in this outer compartment flows to the lowest point, where the drain is located. The liquid drains from the container into a beaker placed on top of an electronic scale. The electronic scale used to measure the mass of displaced water was a GE electronic scale with an accuracy up to 1×10^{-3} kg.

The experimental procedure for the set of tests on the liquid mass displaced was:

1. Ensure that the draft tube is installed vertically
2. Ensure that the container is installed so that the meniscus of the liquid level in the middle compartment is level all around the top of the lid
3. Follow steps 1 to 4 of the geometrical test procedure
4. Run the experiment and let a plug form to make sure that the entire volume of plug released is captured by the plug inlet of the draft tube
5. Follow steps 5 to 19 of the geometrical test procedure
6. Start experiment and record five cycles of plugs forming
7. Close the shut-off valve after the fifth plug and let all the water in the container drain into the beaker placed on top of the scale
8. Let the scale stabilise before taking a reading
9. Empty the beaker back into the testing tank and make sure that the liquid level is back at the original level
10. Repeat procedure for the three different orifice plates of the plug generator

To obtain the results for the effect of the plug size on the liquid mass displaced from the draft tube, the flowing parameters were recorded:

- Volumetric air flow rate
- Mass of liquid displaced by a plug
- Time period of a cycle
- Liquid level tested at

Results of volume of plug

The results of the liquid mass displaced from the draft tube are displayed in Figure 4.12. The mean data obtained in this set of work was tabulated in Appendix E, Table E.2.

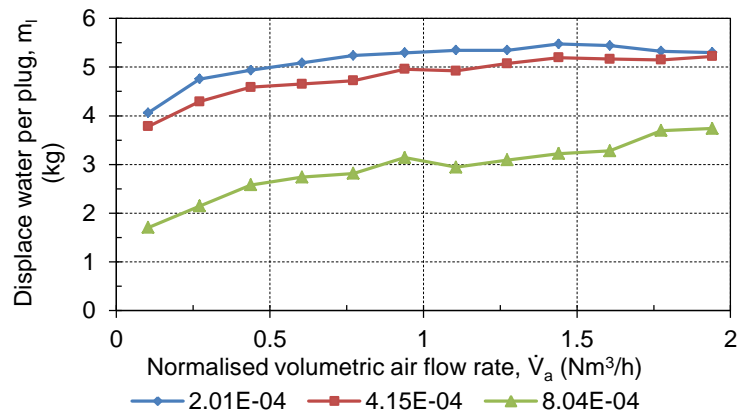


Figure 4.12: Liquid mass displaced from the draft tube per plug as a function of air flow rate using plug-flow generator 1.1.1 with its different orifice plates

The results plotted of the liquid mass displaced per plug illustrate that the mass of liquid displaced is largely affected by the volume of plug generated. With an increase in orifice area, the plug volume of the plug decreased and this also led to a reduction in liquid mass displaced per plug.

To obtain the average mass flow rate displaced from the draft tube per cycle, the total liquid mass displaced by a plug was divided by the time period between the plugs. The averaged mass flow rates calculated for plug generator configuration 1.1.1 with its three different orifice plates are plotted in Figure 4.13 and the mean data of the experiment can be seen in Appendix E, Table E.2.

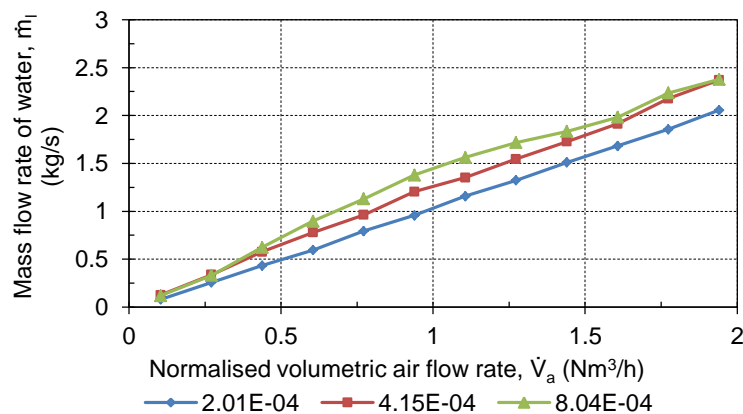


Figure 4.13: Liquid mass flow rate of mixing system as a function of air flow rate with plug-flow generator 1.1.1 using different orifice plates

The results in the figure above show that an increase in air supply flow rate leads to an increase in liquid mass flow rate displaced per cycle. They also illustrate that the largest orifice area obtained a higher mass flow rate per cycle. This was expected, as the large orifice area plate leads to a higher plug frequency and therefore an increase in mass flow rate.

4.2.2 Effect of hydrostatic pressure

The second set of experimental work was focused on determining the effect of the hydrostatic pressure on liquid displaced from the draft tube. In order to determine the effect of the hydrostatic pressure on the liquid displaced from the draft tube, the level inside the testing tank had to be varied.

The experimental setup that was used for this study was the same as previously illustrated in Figure 4.11, but only this time the liquid level in the testing tank was varied, as well as the length of the draft tube.

For the test work, only plug generator 1.1.1 was used with a single orifice plate with an area of $415 \times 10^{-6} \text{ m}^2$. The liquid level was varied to 0.85 to 1 m above the plug-flow generator, with the draft tube ending 1D below the liquid level in the tank each time. The liquid level of the tank was again measured with a stainless steel ruler.

The experimental testing procedure followed to determine the effect of the hydrostatic pressure on the liquid displaced from the draft tube was as follows:

1. Set liquid level to 0.85 m above the plug-flow generator
2. Follow steps 1 to 13 of the effect of volume of plug in section 4.2.1
3. Change the liquid level to 1 m and repeat steps 1 to 13 of the same test procedure

Results of hydrostatic pressure

The results of the effect of the hydrostatic pressure on the liquid displaced from the draft tube are displayed in Figure 4.14 below. The mean data obtained are tabulated in Appendix E, Table E.3.

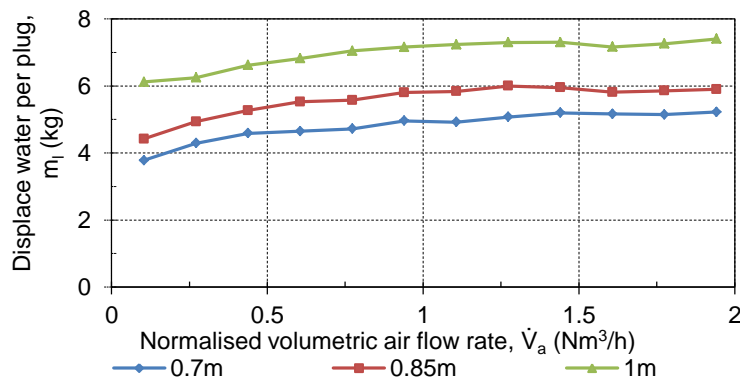


Figure 4.14: Liquid mass per plug displaced at different hydrostatic pressures as a function of air flow rate using plug-flow generator 1.1.1 with an orifice area of $415 \times 10^{-6} \text{ m}^2$

The results of the liquid displaced at different hydrostatic pressures presented in Figure 4.14 illustrate that the increase in hydrostatic pressure on the mixing system leads to an increase in the amount of water displaced.

The mass flow rate of the liquid displaced per cycle was calculated in the same manner as that of the effect of volume of plug on mass flow. The averaged mass flow rates per cycle calculated from the results are displayed in Figure 4.15 below and the mean data are tabulated in Appendix E, Table E.4.

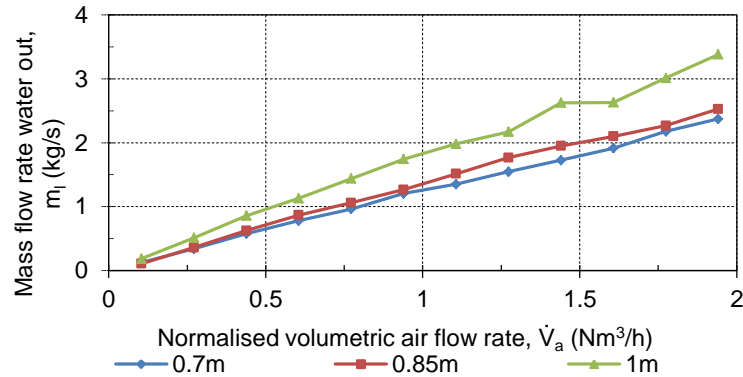


Figure 4.15: Liquid mass flow rate displaced at different hydrostatic pressures as a function of air flow rate using plug-flow generator 1.1.1 with an orifice area of $415 \times 10^{-6} \text{ m}^2$

The figure above shows that an increase in hydrostatic pressure on the mixing system leads to an increase in mass flow rate displaced from the top of the draft tube. The results show that a 21 % increase in hydrostatic pressure leads to an average of 7 % increase in mass flow, where a 43 % increase in hydrostatic pressure leads to an average 45 % increase in mass flow.

It can be concluded that the basic design of a plug flow generator to be used in a CSTR digester was proposed and correlations for its key geometry parameters and flow performance were developed from measured data in the experimental work. The correlations estimated from the observed data obtained could predict the mass of plug generated up to an accuracy of $\pm 20 \%$ and the plug frequency up to $\pm 15 \%$. These correlations can be used to develop a full-scale gas regulation mixing system operating in a plug-flow regime. The results on the effect of the hydrostatic pressure on the liquid displacement from the draft tube can be used to determine the friction multiplier for the numerical model.

5. ANALYSIS AND PROPOSED DESIGN

The anaerobic digestion of complex organic substances such as PS and WAS is very sensitive to environmental conditions and the process operating conditions under which the different sets of micro-bacteria have to perform. The case studies reviewed on the digester show that a change in the plant conditions can lead to an increase or decrease in the digester's performance to treat the quantity of sludge, to deliver the desired quality of effluent and to regulate the biogas production rate. Therefore, selecting a suitable plant layout with the correct operating conditions is very important.

This chapter proposes the most suitable design layout, together with a mixing system, for the WWTP AD plant to treat the quantity of sludge available to the required quality and to generate power from it.

This chapter is divided into two sections – the proposed design layout for the AD plant (5.1) and the proposed design for the digester mixing system (5.2). The objectives set for the first section were to analyse the results obtained from the comparison study on the different conceptual layouts and to propose a suitable AD plant layout. The second set of objectives set out were to analyse the results obtained from the two-phase flow numerical model and the experimental work done and to propose a digester mixing system for the AD plant.

5.1 Proposed design layout for AD plant

To propose a design layout for an AD plant, the WWTP's general plant flow needed to be revised as well as the infrastructure available for an upgrade. The general plant wastewater flow was reviewed in section 2.1 and the infrastructure available in section 3.1.2. Based on the quantity, quality of the sludge, environmental and process operating factors and infrastructure available, three conceptual AD plant layouts were drawn up. The three different conceptual AD plant layouts were evaluated in a comparison study based on a heat, energy and electrical balance, with the feedstock for the layouts ranging from 4 to 10 % TS content in a year.

The results obtained from each numerical model were presented after each section and the overall balance was presented at the end of section 3.1.3. The comparative results of the different concepts obtained will be analysed below in section 5.1.1, and a proposed design layout will be drawn up in section 5.1.2.

5.1.1 Analysis of conceptual layouts of AD plant

In the comparison study it was shown that, by increasing the TS content of the feedstock, the energy and electrical production of the AD plant could be increased. Increasing the TS content fed to the digester also increased the OLR, as more VS are introduced per volume. The OLR was calculated for each concept at the corresponding TS content by keeping the HRT constant for the different concepts, as mentioned. The calculated OLRs for the different concepts were illustrated in the plant operating conditions for each concept from Table 3.2 to Table 3.4.

When comparing the calculated OLRs with the maximum OLRs presented in Table 2.4 for the different types of AD plant layouts, it can be seen that the OLRs for concept 1 with TS contents ranging from 4 % to 10 % all fall below the maximum OLR prescribed for the digester configuration. In concept 2, the OLR at a solid content of 10 % for the post-digester was approaching the maximum, with an OLR of

14.4 kgVS/m³day compared to the maximum of 16 kgVS/m³day, but it could still work. The high OLR will only be a problem if the plant's capacity has to increase in the future.

The OLR in concept 3 at a solid content of 10 % for the pre-digester of 24.8 kgVS/m³day exceeded the prescribed maximum of 22 kgVS/m³day. If the concept was fed with 8.8 % TS content sludge, the OLR would be at the maximum for a concept. Therefore, it is recommended that concept 3's thickened feedstock does not exceed a solid content of 8 % so that the OLR is maintained at 20.1 kgVS/m³day.

By feeding concept 3 with 8 % TS content feedstock, it was possible to treat 81 % of the WWTP sludge available compared to 57 % and 52 % in concept 2 and 1 at the same feedstock solid content (refer back to Table 3.5) or 71 % and 65 % in concept 2 and concept 1 at 10 % TS content feedstock. Based on sludge treatment capacity, concept 3 is the more suitable option, as it will treat the most sludge and will decrease the load on the Otjomuize WWTP the most.

The quality to which the digesters treated the sludge all exceeded the 50 % VS reduction required by the regulations set out for disposal. The VS reduction selected for concepts 1 and 2 in this thesis correlate with the effect of HRT on the percentage reduction in VS in Figure 2.7. Even if the VS reduction selected for concept 2 is for a single-stage mesophilic digester it can be considered conservatively.

The VS reduction of concept 3, on the other hand, does not apply to the values displayed in Figure 2.7, as it is a more advanced digester configuration in which the biological process is split into two reactors. The VS reduction of 60 % in the third concept was obtained from Schafer *et al.* (2002), but the HRT in this case study was only 17 days. With the HRT in concept 3 being 21.2 days it can also be considered conservative. Therefore, as the VS reduction selected for all concepts are conservative and the energy production of the digesters mainly calculated from the VS reduction, the overall energy production of the concepts will be highly possible to obtain in reality.

From the overall heat balance of the different conceptual AD plants it was observed that there was a heat shortage at 4 % TS contents in all three of the concepts based on the minute interval time step. It also was observed that the heat shortage could be eliminated by increasing the TS of the feedstock, and the net energy production of the plant could be increase, as mentioned.

To solve the heat shortage if the plant was selected to operate at a 4 % TS content or lower, three alternative methods could be applied. The first alternative was decrease the digester feeding frequency from four times to three times or even twice to allow more time to heat the incoming feedstock to the required digester temperature.

The second alternative was to eliminate the pre-heat exchanger and only heat the incoming feedstock with the post-heat exchanger. This alternative would also provide more time for the post-heat exchanger to heat the incoming feedstock. The third alternative was to store heat in a buffer tank so that, when the AD plant's heat demand exceeds the supply, the stored heat can make up for it.

By increasing the TS contents of concept 3 to 8 % it was proven that the heat supply exceeded the heat demand by a large quota, and it might be possible to eliminate some of the components to save on capital costs. In order to eliminate components,

the heat balance of concept 3 was plotted in Figure 5.1 on a minute time step at a solid content of 8 % for 23 September, as this is where heat demands peak.

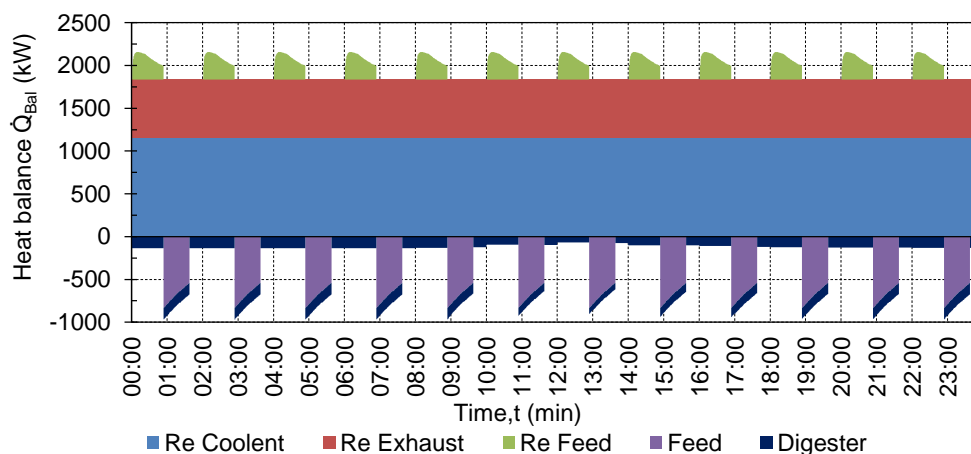


Figure 5.1: Heat balance of concept 3 at 8 % TS contents on 23 September in minute intervals

Figure 5.1 illustrates that the heat recovered from the exhaust shell and tube heat exchanger could be eliminated and that it might be possible to eliminate the pre-heat exchanger. If this would be possible, the complexity, parasitic load and capital cost of the AD plant could be reduced.

5.1.2 Proposed design layout for AD plant

The two-phase digester configuration of concept 3 proved to be a more suitable option to use for the proposed design layout. This configuration was able to process a larger volume of sludge per day and produce a higher net electrical power output, and the effluent leaving the AD plant met the regulations set out. But, it was also mentioned in the analysis section that concept 3 should only be operated up to a solid content of 8 % due to the high OLR in the pre-digester. It is for these reasons that a two-phase digester configuration at a solid content of 8 % was selected for the proposed design layout.

Determining the layout of the proposed design

For the proposed plant layout it is clearly illustrated in Figure 5.1 that the shell tube heat exchanger recovering waste heat from the exhaust gas of the CHP units can be eliminated. What was not certain was if the pre-heat exchanger could be eliminated from recovering the heat from the effluent and heating the influent.

For the proposed design, the feedstock heat requirement numerical model was edited by eliminating the pre-heat exchanger and only heating the incoming feedstock with the double tube post-heat exchanger. The heat transfer rate of the post-heat exchanger was limited by reducing the mass flow rate through the heat exchanger. The aim with this modified feedstock heat requirement model was to simulate if this configuration was possible without the shell tube and the pre-heat exchanger.

Using this feedstock heat requirement numerical model, several simulations were run to determine the minimum mass flow rate through the post-heat exchanger in order to heat the influent to the required temperature in the set time period. The rest of the input values used for this model are presented in Table 3.7, also at a feeding frequency of twelve times per day. The minimum mass flow rate obtained from these

simulations was a flow rate of 7.9 kg/s. The feedstock temperature and volume profile heated by the post-heat exchanger at this mass flow rate of 7.9 kg/s are presented in Figure 5.2 below.

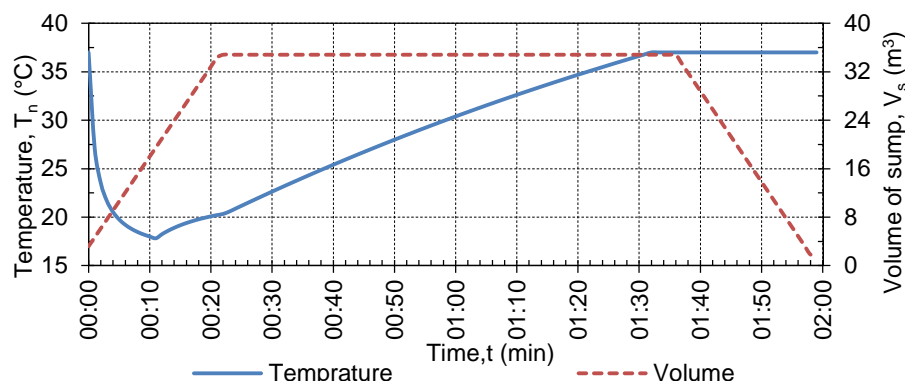


Figure 5.2: Volume and sump temperatures of proposed design layout on 23 September

From the results published in Figure 5.2 it is illustrated that it is possible to heat the incoming feedstock into sump 2 with the post-heat exchanger only at a mass flow rate of 7.9 kg/s in the set time period of 1 h 30 min with 4 min to spare before the sump needs to be emptied to feed the pre-digester.

The heat balance of the proposed design without the tube heat exchanger, pre-heat exchanger and lowered mass flow rate of 7.9 kg/s in the post-heat exchanger was also simulated and the results obtained on 23 September at 8 % TS contents are plotted in Figure 5.3 below.

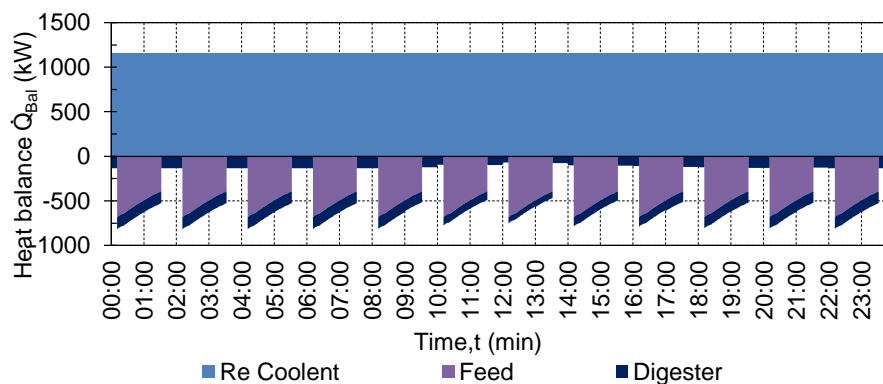


Figure 5.3: Overall heat balance of the proposed design on 23 September in minute intervals

From the calculated overall heat balance the averaged peak demand on 23 September was 812.79 kW, where the total heat recovered from the CHP units was 1154.5 kW. This heat balance proves that it is possible to eliminate the shell tube heat exchanger and pre-heat exchanger from the plant layout, and it also provides a heat reserve of more than 25 % if needed.

The daily averaged heat demand for the incoming feedstock of the proposed design was also calculated again at the two solstices and equinoxes and is illustrated in Figure 5.4. For comparison, the heat demand for the feedstock of concept 3 at the same TS contents heated by the post-heat exchanger operating at a mass flow rate of 10 kg/s was included in the figure.

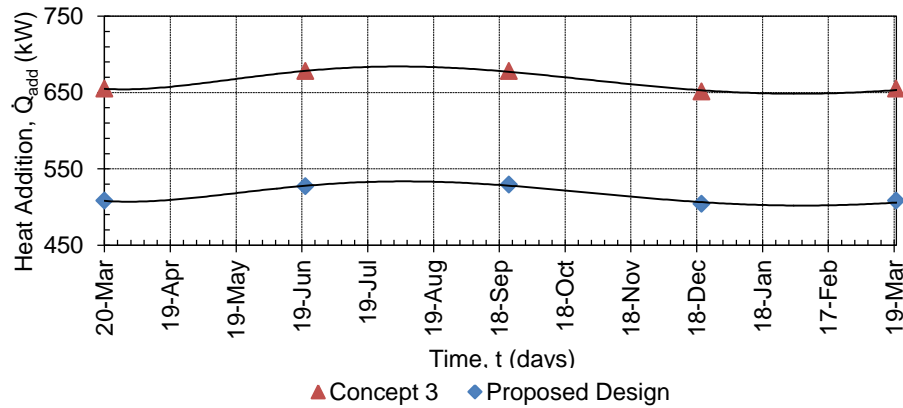


Figure 5.4: Daily averaged heat addition needed for the proposed design in a typical year

From the plotted average daily heat demand in Figure 5.4 it is clear that the heat addition of the proposed design is lower than concept 3 due to the decrease in mass flow rate of the post-heat exchanger. On average throughout the year, the proposed design layout has a 29 % lower heat demand compared to concept 3 for the calculated values.

With these results, the overall heat and energy balance was calculated for the proposed design. The daily averaged values calculated for the balances are presented in Figure 5.5 below, together with concept 3 at 8 % TS content.

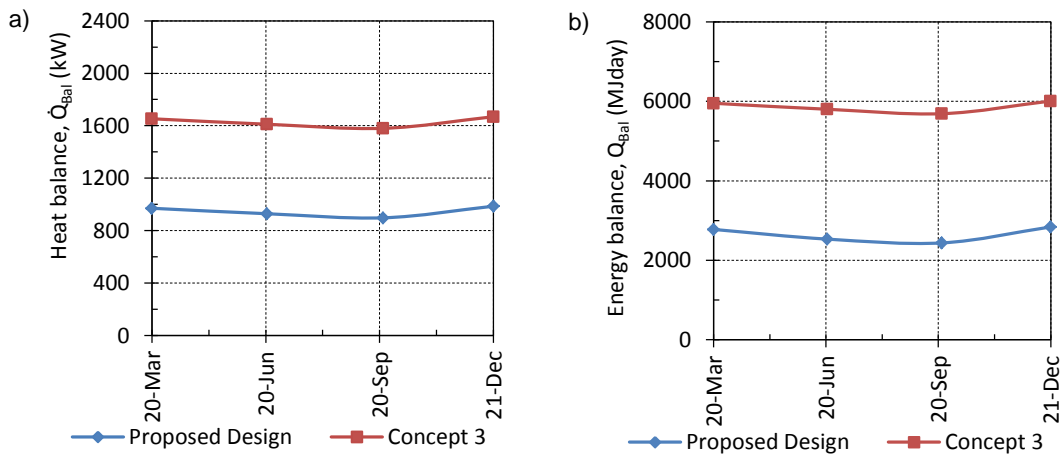


Figure 5.5: a) Averaged daily heat and b) energy balance of the proposed design layout in typical year

The overall heat and energy balance results presented in the figures above indicate that the amount of additional heat and energy available have been decrease compared to that of concept 3. Even if the results in the overall heat and energy balance still seem a lot, it was calculated that there only was 25 % additional heat capacity at the peaks. This additional capacity calculated is even less in reality, as the assumption of no heat losses was included in the calculations for the heat circulation system, and the environmental losses at the sumps and the shadow effect on the digesters for the plant were not included.

The proposed design

The proposed design consists of the five 1 600 m³ digesters in a two-phase layout, with one digester used as the pre-digester and the other four as high-rate CSTRs. The proposed design would be fed with a volume of 986.742 m³/day, of which the TS would be increased to 8 %, which will reduce the volume to 398.416 m³/day. By operating the plant at this TS content, as much as 81 % of the total available raw sludge at Gammams WWTP could be treated. The estimated VS reduction selected for the proposed design was 60 % and, with this reduction, a total 1.293 MW net electrical power could be generated with seven CHPs rated at 200 kW.

The schematic flow diagram for the proposed design layout is illustrated in Figure 5.6. Only one CHP unit and one digester were include in the flow diagram to decrease the complexity of the diagram.

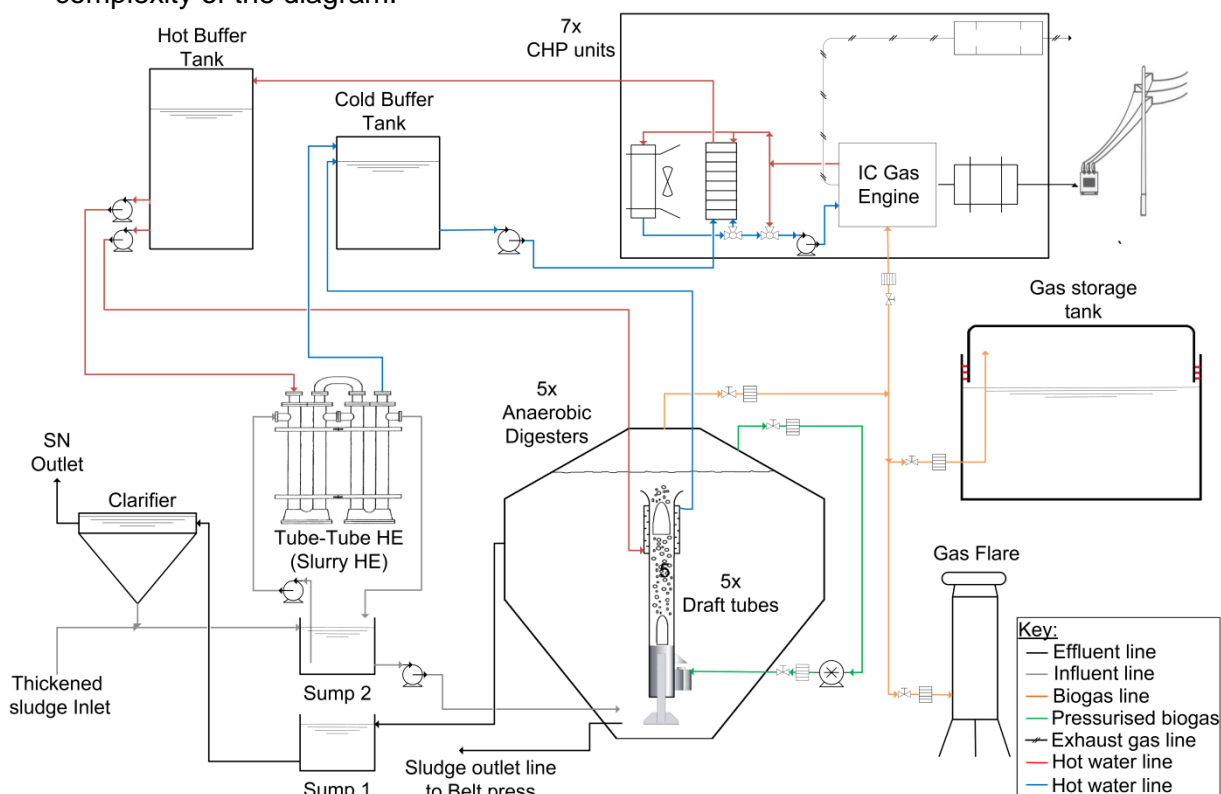


Figure 5.6: AD plant proposed design layout for the WWTP case study

The thickened influent will enter the plant at sump 2, where it will be heated to 37 °C with the double tube heat exchanger. Heated sludge from sump 2 will be pumped to the pre-digester twelve times per day, at 33.13 m³ per feeding. The sludge will be kept in the pre-digester at a HRT of 3.2 days, after which it will be pumped to the other four high-rate digesters. Sludge in the pre-digester will be fed to the four digesters four times per day with a volume of 16.56 m³ per feeding, and it will be kept for a HRT of 18.03 days. The treated sludge for the four digesters will then be pumped to the belt press plant, where it will be dewatered and treated further with a composting process and ultimately sold as fertiliser. Dewatered waste water from the belt press plant will be conveyed to either the TFs of the ASP before it is reclaimed.

The supernatant in the proposed design will only be drawn off from the four high-rate reactors and will be conveyed to sump 1 before it is sent to the digester clarifier. The clarifier will separate the trapped solids, which will be reintroduced to the AD plant, as can be seen in Figure 5.6. The overflow of the clarified SN will then be directed to the TFs or the ASP to be treated and ultimately be reclaimed as potable water.

Biogas generated from the proposed design layout will only be taken from the four high-rate digesters, as the gas generated from the pre-digester is mainly CO₂. The biogas captured from the four digester will be conveyed to gas storage tanks before it is sent to the seven CHPs. Gas generated from the pre-digester will be sent to the gas flair to burn the small portion of CH₄ to reduce the greenhouse gases to CO₂.

The heat recovered from the CHPs will only be from the engine cooling circuit with a plate heat exchanger. The waste heat recovered will be pumped to a hot buffer tank before it is sent to the tube and tube feedstock heat exchanger and the digesters' internal heat exchangers, as illustrated in Figure 5.6. Additional heat left can be supplied to heat the composting process at the belt press plant or it can be discarded into the air using the radiators.

With this proposed design layout, the importance of selecting the correct plant layout was proven in terms of the AD plant energy production, sludge-processing capacity and quality of effluent.

5.2 Digester mixing system for proposed AD plant

Mixing a digester is essential for the following reasons: it prevents a crust layer forming on top of the digestate, it increases the effective volume of the reactor and it acts as the transportation method for microorganisms to the organic substances in the digestate.

The effect of mixing was studied in the literature review, as well as the parameters used to quantify the amount of mixing needed for a digester. The mixing method, intensity and interval selected for the different case studies was reviewed. As the proposed design layout selected for the AD plant is similar to that of concept 3, the same mixing interval and intensity will be used as was tabulated in Table 3.4.

The design criteria and limitations of the digester mixing system were set out in the methodology of this thesis. From these design criteria, three different concepts were drawn up and one was selected. A numerical model was developed based on the selected concept to predict the volume of liquid displaced by the mixing concept.

To verify the numerical model, an experimental study was conducted based on the selected mixing concept. In the experimental study, two empirical equations were obtained (4.4 and 4.5) to be able to predict the plug size released as well as the plug frequency based on the geometrical construction of the plug-flow generator.

Using the verified numerical model, a sensitivity analysis was conducted on the geometrical construction of the selected mixing system presented in Figure 3.34 and the effect of the plug size on the mass and mass flow rate displaced from the top in Figure 3.35. The results obtained from the sensitivity analysis were analysed against the mixing parameters set out to quantify the amount of mixing needed for a CSTR. This analysis is discussed in section 5.2.1 to come and, based on the outcome of the analysis of the mixing system, a design is proposed in section 5.2.2.

5.2.1 Analysis of concepts for digester mixing system

To quantify the required amount of mixing needed to keep the different types of microorganisms in the digester healthy and to eliminate the formation of dead zones, the mixing parameters were defined from experimental studies. These experimental studies conducted on the mixing parameters, namely the DVTT, UP and G, were reviewed in the literature review in section 2.2.2. For this work, the DVTT was used to calculate the volume flow rate required to mix the digester and the UP and G were calculated from the DVTT.

With the DVTT taken as one hour and the volume of the digester as $1\,600\text{ m}^3$, the required volume flow rate calculated with equation 2.4 was $1\,600\text{ m}^3/\text{h}$ or a mass flow rate of 444.44 kg/s assuming a density of $1\,000\text{ kg/m}^3$. This is quite a large flow rate compared to the results obtained from the base case simulated with an internal diameter of 365 mm presented in Figure 3.32 at a plug frequency of 0.048 Hz .

From the sensitivity analysis conducted on the geometrical construction of the mixing system, it could be seen that the only major parameter affecting the mass and mass flow rate displaced was the internal diameter of the draft tube (see Figure 3.34 and Figure 3.35). By increasing the diameter of the draft tube, the mass and mass flow rate displaced can be increased. It should be borne in mind, however, that a limitation of a maximum outside diameter of 600 mm was set in section 3.2.1 for the draft tube to be lowered into the digester.

The raw data of the sensitivity analysis for the effect of the diameter on the mass and mass flow rate displaced from the top of the draft tube is plotted in Figure 5.7 below.

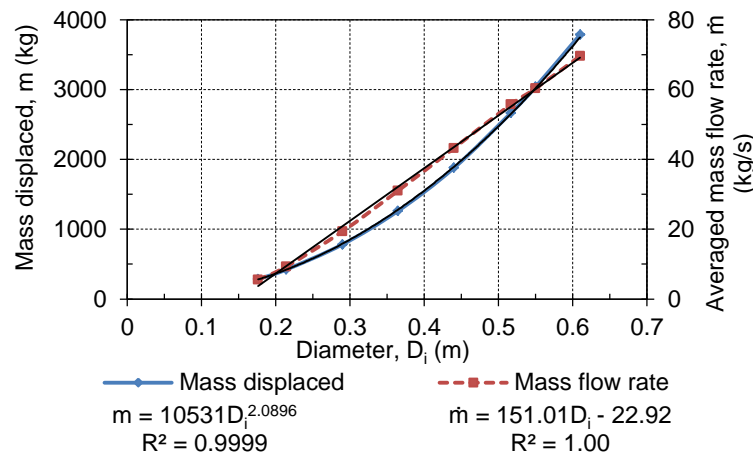


Figure 5.7: Effect of draft tube diameter on the mass and mass flow rate displaced from the top of the digester for a single full-plug cycle at 0.021 Hz and a plug ratio of $1.2P_e$

The results in the figure above illustrates that the mass displaced by the draft tube follows a geometric trend and the mass flow rate a linear trend as the diameter is increased. Based on the limitation and the pipe sizes available, the internal diameter of the draft tube was limited to 518 mm . From Figure 5.7 it can be calculated that the averaged mass flow rate by a 518 mm draft tube is 55.7 kg/s and the mass displaced per cycle is $2\,661\text{ kg}$ at 0.021 Hz and a plug ratio of $1.2P_e$.

With this mass flow rate, a total of eight draft tubes are needed operating at a plug frequency of 0.021 Hz for the mixing system to comply with a DVTT of one hour. This

number of draft tubes can be decreased by increasing the plug frequency and selecting the correct plug size for the draft tube.

By increasing the plug frequency of the mixing system, the mass flow rate can be increased based on the linear trend displayed in Figure 3.33, but the mass displaced per plug cycle decreases, which means the mixing system becomes less effective.

The other option to increase the mass flow rate of the mixing system is to determine the correct plug size for the draft tube, as it follows a parabolic trend, which was observed from the sensitivity analysis conducted on the plug size in Figure 3.35.

From this analysis conducted of the mixing system, the diameter of the draft tube was set to 518 mm. The analysis also indicated that more than one draft tube would be needed for the digester mixing system in order to comply with the mixing parameter set. This meant that two different draft tubes had to be simulated for the proposed design, as only one can be placed in the middle of the digester and the rest on the inclined bank of the digester.

5.2.2 Proposed digester mixing system

The proposed design for the mixing system was divided into three subsections, namely the draft tube, the plug generator and the overall proposed mixing system design for the digester.

In the draft tube section, the number of draft tubes needed for the design were calculated, as well as the plug size; in the plug generator section the dimensions of the plug generator were determined; and in the section on the overall mixing system, a schematic design is proposed for the digester.

Draft tube

In the analyses conducted on the draft tube, the internal diameter of the tube had to be limited to 518 mm with an outside diameter of 530 mm due to the size of the middle opening in the digester. With the internal diameter limited to 518 mm, it became clear that more than one draft tube would be needed to achieve the desired DVTT of one hour.

For the proposed design, the first draft tube was placed in the middle of the digester to suck up all the settled solids from the bottom and displace them to the top of the digester. The additional draft tubes needed to achieve the DVTT were placed on the inclined bank of the bottom cone in the digester.

The plugs from these additional draft tubes placed on the inclined bank should surface at the top liquid level and not run up the side of the top cone in the digester. To avoid this situation, the additional draft tubes had to be evenly spaced on the incline bank at a radius of 2.8 m from the centre of the digester.

To determine the number of draft tubes needed for the mixing system, the geometry of each of the draft tubes first needed to be selected followed by the plug size and the plug frequency at which the different lengths of draft tube would operate at.

The top clearance of the selected draft tubes was taken as 1D below the lowest liquid level between feedings. This resulted in a distance of 915 mm below the full liquid level mark. The bottom clearance for the middle draft tube was selected to be 2D from the bottom of the cone due to a suction pipe ending in the cone at the bottom of the

digester. The bottom clearance for the side draft tubes were selected to be 1D from the incline bank.

These selected dimensions of each draft tube were used in the numerical model to simulate the effect of the different plug sizes on both of the selected draft tube arrangements for a single plug cycle. The summarised results from the numerical model on the effect of the plug sizes for the different draft tubes are illustrated in Figure 5.8.

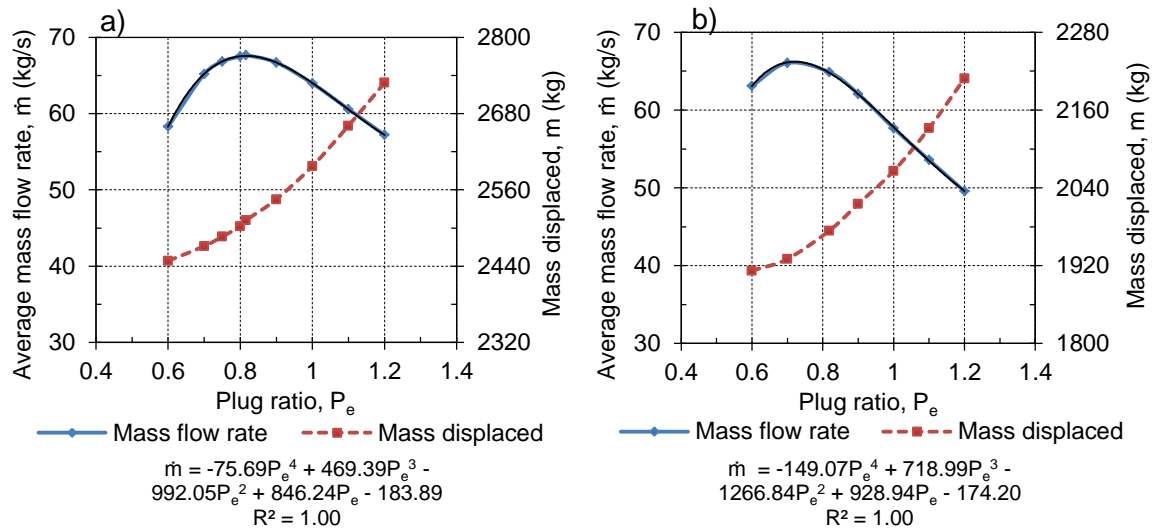


Figure 5.8: Effect of plug size on the average mass flow rate and mass displaced per cycle by the a) middle draft tube and b) side draft tube proposed

In Figure 5.8 the results illustrate that an optimum plug size could be determined to increase the mass flow rate. Parabolic trend lines were placed through each of the figures mass flow rates and the equations obtained together with the R^2 value for each are include below the figures.

To calculate the optimum plug size for the daft tubes in order to increase the mass flow rate, the equations obtained from the curve fits were differentiated and equated to zero. The calculated plug size for the middle draft tube came to $0.818P_e$ and for the side draft tube to $0.724P_e$. With these plug sizes for the selective draft tubes known, the numerical model could be used again to determine the average mass flow rate per cycle at increased plug frequencies.

Several simulations were conducted at increased plug frequency for the selected draft tubes using the calculated plug sizes. Five consecutive cycles were simulated at each plug frequency and only the last four cycles where taken into account.

The averaged results of the last four cycles for the selected draft tubes of the numerical simulations, at an increased plug frequency, are summarised and illustrated in Figure 5.9.

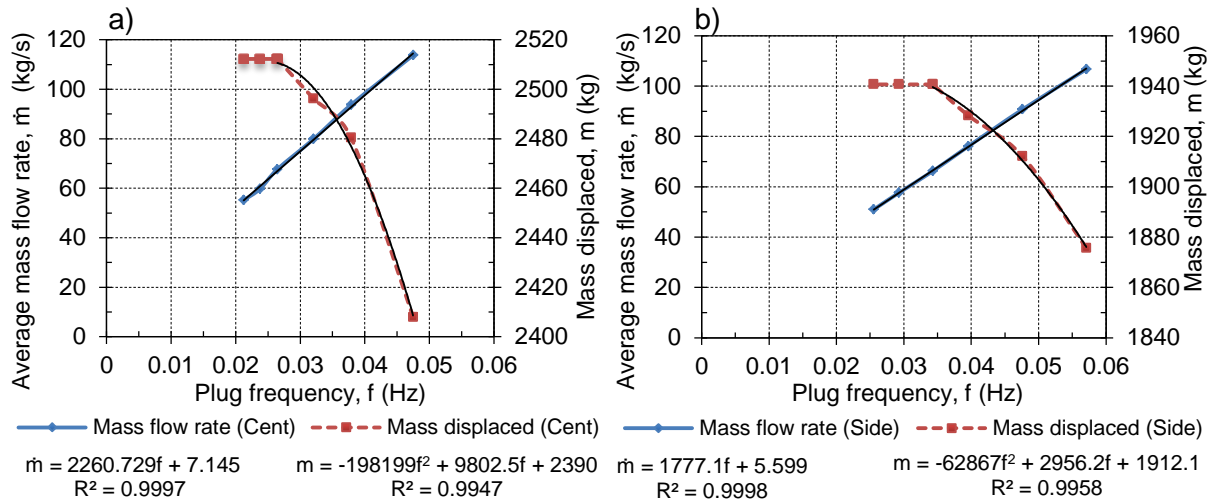


Figure 5.9: Effect of plug frequency on average mass flow rate and mass displaced for the a) middle draft tube with a plug size of 0.818P_e and b) side draft tube a plug size of 0.724P_e

In the results obtained from the numerical simulations on the effect of the plug frequencies on the mass flow rate, it is illustrated that the mass flow rate of the middle tube was almost the same as that of the side draft tubes. It was calculated that the side draft tubes mass flow rate was only 4.7 % lower compared to the middle draft tube. The summation of mass displaced by each plug for the selective draft tubes starts off at a plateau, as can be seen in Figure 5.9, but as the plug frequency increases the mass displaced starts to decrease.

The highest operating point for the draft tubes was selected to be as the initial plug exits at the top the next is injected. Thus, for the middle draft tube, the highest and lowest operating point was at 0.0264 Hz and 0.047 Hz and for the side draft tube was selected to be between 0.034 Hz 0.057 Hz. It should be noted that the draft tube could be operated outside these selected operating ranges, but the numerical model was only validated to predict a single plug rising. With these selected operating ranges for the selective draft tubes known, the number of draft tubes were calculated and the range of DVTT that can be achieved with the number of draft tubes. The calculated number of draft tubes and the range of DVTT that can be achieved are displayed in the Figure 5.10.

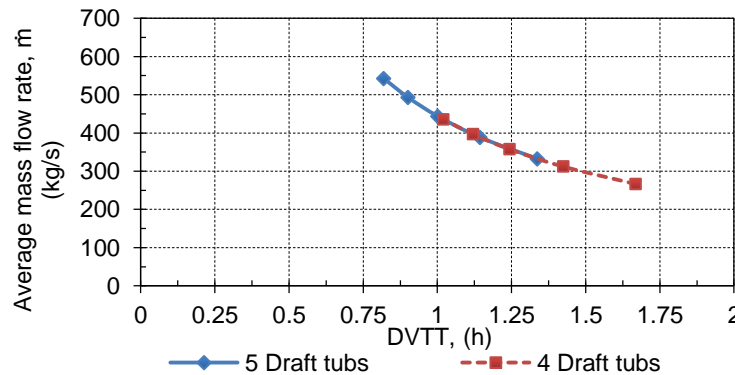


Figure 5.10: Number of draft tubes needed for mixing system vs. range of DVTT in which mixing system can operate

In Figure 5.10 it is shown that it is possible to achieve a DVTT of one hour with four draft tubes, but with all four of the draft tubes are running at full capacity. With five draft tubes it is possible to achieve a DVTT as low as 0.82 h when running it at full capacity, but five draft tubes can achieve a DVTT of one hour running only at 50 % capacity.

A decision on the number of draft tubes to be used for the mixing system had to be based on the volumetric gas flow rate required for the plug generators. This volumetric gas flow rate would then ultimately be related to the power consumption required by the mixing system.

The volumetric gas flow rate required for the draft tubes to operate in the selected operating range could be determined with equation 4.5 obtained in the experimental work. As the operating depth of the draft tubes, plug generates and plug frequency were known, the gas mass flow rate required could be calculated. The calculated gas mass flow rate for the middle and side draft tube was converted back to volumetric gas flow rate and normalised to atmospheric conditions. The calculated results for a single middle and side draft tube are illustrated in Figure 5.11 below.

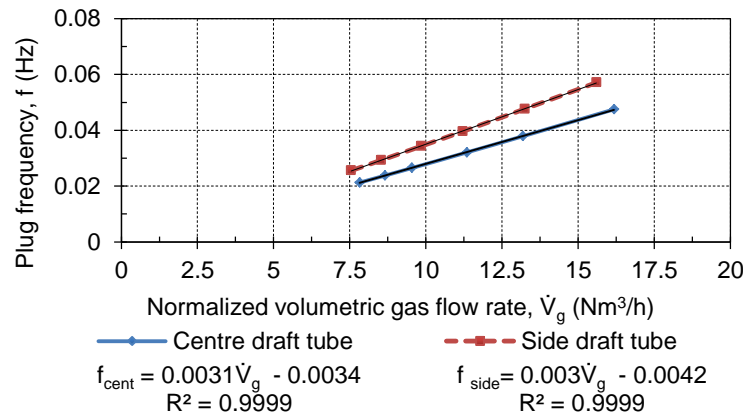


Figure 5.11: Middle and side draft tube plug frequency versus normalised volumetric gas flow rate

From Figure 5.11 it is shown that there was a very small difference in the volumetric gas flow rate required for the middle and side draft tubes. The reason for this is that the side draft tube plug size is slightly smaller than that of the middle draft tube, but it operates at a slightly higher plug frequency, resulting in the small difference.

With the volumetric gas flow rate known for the middle and side draft tubes, the required total volumetric gas flow rate for a digester mixing system consisting of four or five draft tubes could be calculated. The required flow rate calculated for the different digester mixing systems is illustrated in Figure 5.12.

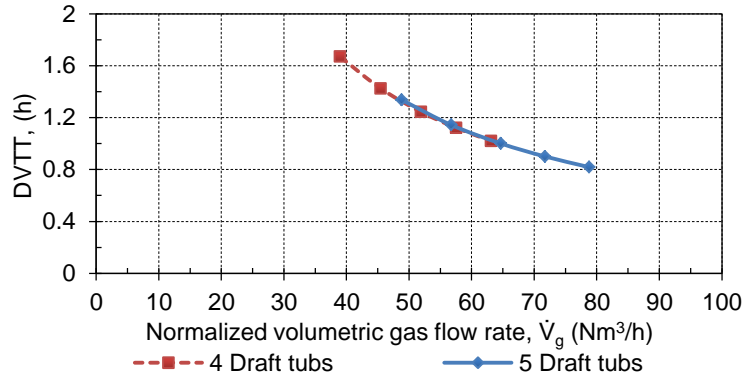


Figure 5.12: Number of draft tubes as a function of DVTT and normalised volumetric gas flow rate needed for mixing system

The figure above illustrates that there was not a large difference in volumetric gas flow rate needed for four and five draft tubes for the mixing system. The calculated difference between four and five draft tubes are was only 1.12 % increase in volumetric gas flow rate, from 64.134 Nm³/h for four draft tubes to 64.852 Nm³/h for five draft tubes at a DVTT of one hour.

The selected DVTT for the proposed design mixing system was taken as 1 hour, but from the case studied in the literature review it could be in the range from 0.8 to 1.2 hours. Based on these results a decision was made to select five draft tubes with an inner diameter of 518 mm for the proposed mixing system.

The calculated volumetric gas flow rate for the proposed mixing system consisting out of five draft tubes was 64.852 Nm³/h and an additional 5 % was added (65.708 Nm³/h) for leakage to select the size of gas compressor required. The gas compressor selected for the proposed design was an Elmo Rietschle 2BV2 071 liquid ring compressor. The data sheet for this compressor is included in Appendix D and the characteristic curve for the compressor at reduced speeds is illustrated in Figure 5.13. It must be noted that the shaft speed can only be reduced to 920 rpm as specified by the supplier.

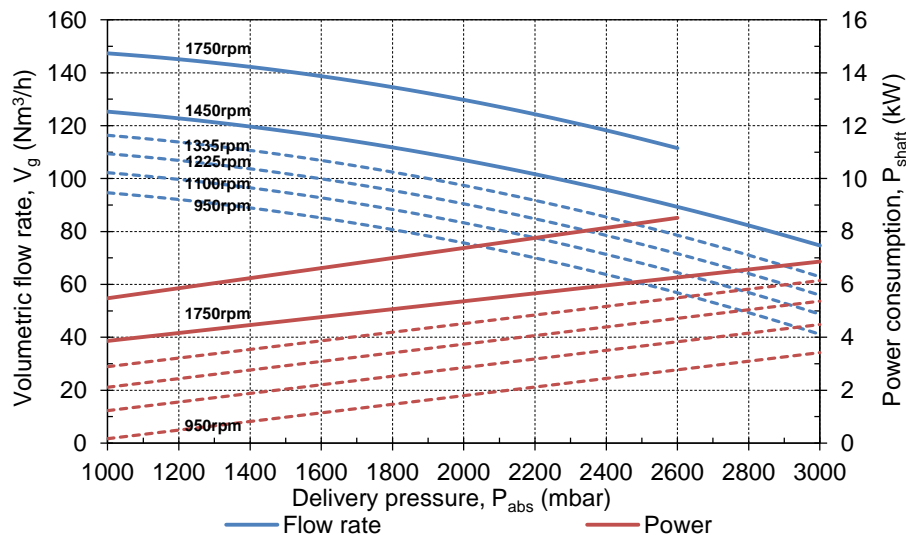


Figure 5.13: Liquid ring blower volumetric gas flow rate and power consumption as a function of delivery pressure head

From the compressor characteristic curve in the figure above, the power consumption at a volumetric gas flow rate of 65.708 Nm³/h and at a delivery pressure of 1.77 bar gauge pressure (2.6 bar absolute pressure) was 3.86 kW, with the compressor shaft spinning at 1 104 rpm. The delivery pressure of 1.77 bar selected allows for a pressure loss of 36 kPa (25 %) due to friction and minor losses in the gas manifold.

In order to compare the proposed mixing system to other mixing systems used, the unit power (UP) and the normalised mixing intensity (G) of the systems had to be determined. The UP and G were calculated using equations 2.5 and 2.6, with the assumption that the fluid medium is water at temperature of 37 °C.

The calculated values for the UP and G were plotted against the operating range of the proposed digester mixing system as a function of DVTT and are illustrated in Figure 5.14.

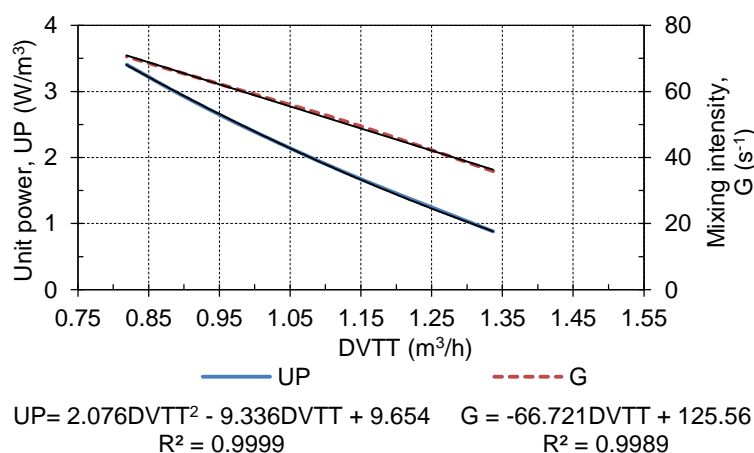


Figure 5.14: Unit power and mixing intensity of the proposed mixing system as a function of DVTT

In Figure 5.14 it is shown that for a DVTT ranging from 0.81 to 1.33 h, the UP lies between 3.41 and 0.88 W/m³ and the G between 70.58 and 35.88 s⁻¹.

When comparing the calculated mixing parameters of the proposed mixing system to that set by Turovskiy & Mathai (2006) of DVTT, UP and G of 0.8 to 1.2 h, 7.9 to 5.2 W/m³ and 85 to 50 s⁻¹ respectively, it can be seen that the UP and G of the proposed design do not correlate well. The lower values for the UP and G indicate that the confined gas recirculation plug-flow regime is a more efficient method in terms of power consumption and can achieve the same DVTT at a lower mixing intensity. It should also be noted that the mixing parameter set by Turovskiy & Mathai (2006) is at increased solid contents and takes cylindrically shaped digester into account.

When the proposed design was compared to mechanical draft tube simulated by Binix (2010a) with both mixing systems operating in water for an egg-shaped digester; the mechanical draft tube archived effective mixing at a DVTT, UP and G of 0.85 h 2.97 W/m³ and 65.5 s⁻¹ respectively, where the proposed design obtains a UP and G of 3.22 W/m³ and 68.84 s⁻¹ respectively, at the same DVTT of 0.85 h.

This shows that the proposed design requires a 7 % increases in terms of power consumption per unit volume compared to the mechanical draft tube method to achieve the same DVTT and G at 0 % TS contents.

This result did not come as a surprise, as compressing gas is not as efficient as a submersed impeller, but at increased TS content in the digester the confined gas recirculation method may outperform the mechanical draft tube as the power requirement of the mechanical draft tube follows a power law trend and the power requirement for the gas recirculation method may not increase as much (Wu B., 2010b).

Therefore it could be concluded that the proposed design of the mixing system using the gas recirculation method operating in a plug-flow regime will satisfy the biological requirement of micro bacteria inside the digester, according to the mixing parameter (DVTT and G) it can achieve. The proposed design provides the benefit above the mechanical draft tube method of no moving parts inside the digester, eliminating downtime due to clogged rotating equipment as it can be flushed. There is also no reduction in biogas production that would normally be experienced when the digester is exposed to air for maintenance on the mixing stems at only a 7 % increases in UP requirement compared to mechanical draft tub.

Plug generator

To develop the plug generators for the two selected draft tubes in the proposed design, the operating depth, plug size and mass flow rate of the gas supplied to the selective plug generator had to be known. As all of the abovementioned parameters for the plug generators were calculated in the previous section, the geometrical construction of the two plug generators could be calculated with empirical equation 4.4 obtained in the experimental work.

By using equation 4.4 to determine the geometrical construction of the two plug generators a number of solutions could be found, some of which might not necessary work. To avoid this situation, the dimensions of plug generator 1.1.1 were used as reference case.

The key depended dimensions of plug generator 1.1.1 were converted into geometrical ratios and these ratios were used to calculate the required dimensions of the proposed plug generators for the two selected draft tubes.

To calculate the dimensions of the two plug generators an assumption had to be made that the A_3/A_2 ratio of plug generator 1.1.1 had to be increased. For the calculation, equation 4.4 with the input data displayed in Table 5.1 was used with a GRG nonlinear solver in Microsoft Excel. In the solver the geometrical ratios of the proposed design plug generators were constrained to be the same as those of plug generator 1.1.1.

Table 5.1: Input data of selective draft tubes for the proposed design plug generators at a DVTT of 1 h

Input parameters	Middle draft tube (1 x)	Side draft tubes (4 x)
Draft tube internal diameter (mm)	518	518
Operating depth (m)	12.7	10.38
Plug ratio (P_e)	0.818	0.724
Mass of plug (kg)	0.235	0.188
Supply gas mass flow rate (kg/h)	16.257	15.071

The results obtained from the solver for the two plug generators geometrical ratios are presented in Table 5.2. The detailed dimensions of the different sections of the two plug generators can be seen in the drawings attached in Appendix C.

Table 5.2: Geometrical ratios of proposed plug generators in comparison with plug generator 1.1.1

Geometrical ratio	Generator 1.1.1	Middle plug generator	% Change	Side plug generator	% Change
W_3/L_3	1.390	1.390	0.00%	1.390	0.00%
W_3/H_3	0.927	0.927	0.00%	0.927	0.00%
A_3/A_2	4.363	8.213	46.88%	9.695	55.00%
A_2/A_1	4.685	4.685	0.00%	4.685	0.00%
V_3/V_2	5.454	13.067	58.26%	16.517	66.98%
V_2/V_1	4.685	4.685	0.00%	4.685	0.00%
A_1/A_0	1.639	1.639	0.00%	1.639	0.00%

From the table it is illustrated that all the geometrical ratios of the proposed plug generators are the same, except for the A_3/A_2 ratio, which led to a change in V_3/V_2 as well.

Overall proposed mixing system design for a CSTR

The proposed confined gas recirculation mixing system for a CSTR with a volume of 1 600 m³ consists of five draft tubes with their associated plug generators, a single gas supply train and a gas compressor. A schematic process flow diagram of the proposed mixing system is illustrated in Figure 5.15 where only two plug generators were included to simplify the diagram.

Gas from the gas storage tank will be supplied to a liquid ring compressor which relies on a ring of water between the impeller and the compressor casing to act as a seal. The compressed gas and liquid mixture from the compressor is conveyed to liquid separator where the gas is separated from the liquid and the liquid directed back to the compressor.

The compressed gas is then directed to the gas -mixing manifold before it is injected to the gas trains of each plug generators. The gas train of each plug generator consists of a needle valve, rotameter, pressure gauge, pressure regulator, a one-way valve and a manual shut-off valve (refer to Figure 5.15).

The function of the needle valve in the gas train is to set the flow rate measured by the rotameter to that required. The pressure gauge displays the line pressure where the pressure regulator function is set at and maintains the same pressure in each gas train for measuring purposes, as the plug generators are located at different liquid depths. Each gas train is also equipped with a one-way valve to prevent sludge from flowing up the gas supply line. A manual shut-off valve is also located after the one-way valve to close it and is then connected to the plug generator.

The pressurised water line that will be used to flush the plug generator is also connected to a manifold before it is split to the five plug-flow generators. At the manifold a shut-off valve is installed to flush the flow generators individually if needed.

In order to control the DVTT of the mixing system, the liquid ring compressor motor will be connected to a variable speed drive (VSD).

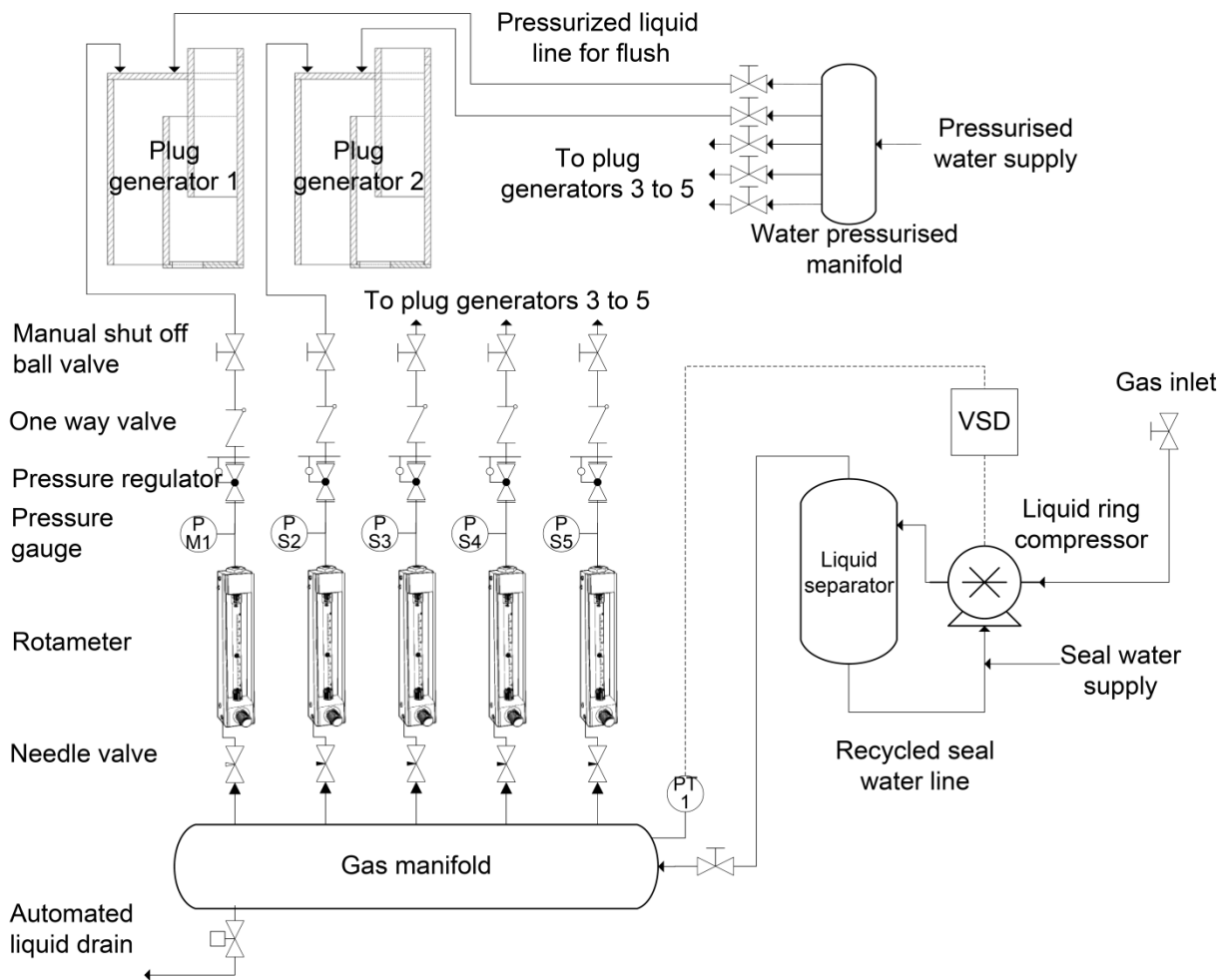


Figure 5.15: Process flow diagram of proposed mixing system

6. DISCUSSION AND CONCLUSIONS

The aim of the thermal modelling of the anaerobic digestion plant was to illustrate the importance of selecting a plant layout in terms of plant process capacity, quality of effluent and energy production. The objective was to generate three different conceptual plant layouts based on the information gained on the biological process, environmental and process factors affecting the anaerobic process from literature.

The case study selected (Windhoek, Namibia) reclaims 35 % (22Ml/day) of the city's portable water demand from secondary effluent of Gammams WWTP and the WWTP has the infrastructure to stabilize the sludge using anaerobic digestion (Du Pisani, 2006). The use of anaerobic digestion for raw municipal sludge stabilization has the capability to address the issue of a sustainable alternative for energy and portable water resource which makes it, one of the ideal treatment processes for the selected case study.

Anaerobic digestion is a complex degradation process, affected by environmental and process operating factors where the organic fraction of the feedstock is decomposed in the absence of air in a chain of events broken up into four main steps. The four main steps are hydrolysis, acidogenesis, acetogenesis and methanogenesis. The first two steps degrade the organic fraction into soluble intermediates and soluble monomers and prefer an acidic environment at a pH of between 5.2 up to 6.3. The second two steps prefer a neutral environment at a pH 6.6 up to 7.2 which tend to be more sensitive to environmental and process operating factors.

Based on the knowledge gained in the literature review (Chapter 2) on anaerobic digestion environmental and process operating factors affecting, the rate of digestion and gas production three concepts were derived. The first concept consisted out of a 3/2 two-stage, the second out of a 4/1 two-stage and the third out of a two-phase digester configuration. The three concepts were evaluated in terms of their overall heat, energy and electrical balances shown in figures 3.23 to 3.25 respectively.

The results shown in the figures 3.23 to 3.25 illustrate that concept 3, the two-phase digester configuration outperformed the other two concepts in terms of heat, energy and electrical production at the different total solids contents. In the overall heat balance it was found that there was a heat shortage at 4 % TS contents at all concepts, but at increased TS contents there was an abundance of heat available. Based on the electric power balance, concept 3 net power increased by 276% with increasing the TS from 4 % to 10%. On averaged concept 3 produced 52 % more net electric power and concept 2, 38 % more compared to concept 1. Concept 3 however had to be limited to feedstock total solids contents of 8 %, due to the high digester organic loading rate discussed in section 5.1.1. At 8 % total solids contents concept 3 was still able to process 81 % of the available sewage sludge at the wastewater treatment plant (refer to Table 3.5) and generate 1.293 MW. Concept 2 was only able to treat 57 % and concept 1 52 % of the available sewage sludge at the same total solid contents of 8 % TS.

Based on the results of the overall heat, energy and electrical balances as well as plant process capacity, concept 3 was selected as the proposed design. Concept 3 was adapted for the proposed design AD plant layout, to see if it was possible to eliminate the slurry pre-heat exchanger as well as the shell and tube heat recovery exchangers on the exhausts, of the combined heat and power plants to simplify the

plant. An overall heat and energy balance was again conducted on the proposed design and the results obtained were presented in Figure 5.3 and 5.5. The results proved that it was possible to eliminate these items and still have a heat reserve of more than 25 % at the peak heat demand point in a typical year. From these results the proposed design layout for the plant was drawn up and presented in Figure 5.6.

The second aim of this thesis was the hydraulic modelling and development of a mixing system for a continuous stirred digester with no mechanical moving parts inside the digester. To develop the mixing system, a review was conducted in chapter 2 on the different mixing systems available, comparative case studies on mixing systems and case studies on the effect of mixing on the biological side of digestion.

The mixing method selected was the confined gas recirculation method, operating in a two-phase plug-flow regime. Figure 2.13 and the case studies reviewed in section 2.3.2 revealed that the two-phase plug-flow regime was the most effective regime in terms of gas mass supply rate versus liquid mass flow rate displaced. With the selected mixing method the objective was to propose three different concepts for the digester mixing system. The three concepts proposed illustrated in Figures 3.26 to 3.28 were evaluated in an evaluation matrix in Table 3.11 and the results of the matrix indicated that concept 3, the plug-flow generator placed at the bottom of the draft tube, was the most promising option and was therefore selected.

With the mixing system selected, the next objective was to develop a one-dimensional, transient two-phase flow numerical model that was able to predict the liquid mass displaced by the draft tube for a defined plug size presented in section 3.2.3. The numerical model was used to conduct a sensitivity study on the geometry of construction of the mixing system with the result presented in figures 3.34 and 3.35. The results indicated that the only major parameter of the geometrical construction affecting the performance was the draft tube diameter and that the plug size can be optimized for a draft tube diameter to increase the mass flow rate of liquid displaced.

An experimental study followed the numerical modelling of the digester mixing system. A scale model of the selected mixing system was constructed with the objective to capture the effect geometrical construction of the plug-flow generator has on the formation of the plug volume released by the plug-flow generator. Two empirical correlations were obtained to capture the effect of the geometrical construction from the results in Figures 4.4 to 4.6 using multi-linear regression. Equation 4.4 was obtained to predict the mass of plug released and equation 4.5 to predict plug frequency at which the plug is released with the accuracies presented in Figure 4.9 and 4.10. The experimental results were also used to define an empirical correlation for the friction multiplier presented in equation 3.40 for the numerical model and to validate the numerical model against the experimental results in Figure A.4.

The results of the numerical sensitivity study and the experimental work were used to develop a mixing system for a continuous stirred digester. With the diameter limited to 518 mm, it was discovered that more than one draft tube was needed. A decision was made to place one draft tube in the middle and the additional ones needed on a radius of 2.8 m from the center of the digester. The plug sizes were determined and the effect of plug frequency of the draft tubes was studied in Figure 5.8 and 5.9. Based on the volumetric gas flow rate calculated in Figure 5.12, five draft tube were selected for the mixing system which requires only a 1.12 % increase in volumetric gas flow rate compared to four draft tubes, but the five draft tube can achieve a DVTT as low as

0.82 The proposed design of the mixing system is presented in Figure 5.15 with its plug-flow generator illustrated in Appendix C.

When the proposed design was compared to the mechanical draft tube at the same digester volume turn over time, the proposed design required 7 % more power per unit volume at 0 % total solid content. The proposed design however provides additional advantages over the mechanical draft tube, as all the mechanical equipment of the systems is located outside the digester and the proposed mixing system can be flushed with pressurised water if it gets blocked. Using the proposed design also eliminates the reduction in biogas production rate when the digester is opened for maintenance and exposed to air.

It can be concluded that the thermal modelling of the anaerobic digestion plant can probably lead to an increase in the electrical production of the plant and still meet the effluent required regulations. The proposed design of the plant finally presented is able to treat 81 % (986.742 m³/day) of the available sludge, generate 1.293 MW with a simplified plant layout without a pre-heat exchanger and without the shell and tube heat exchangers on the exhausts of the combined heat and power units.

From the hydraulic modelling and development of a mixing system it can be concluded that the proposed design is a better option to use for digester mixing systems, as it has no mechanical moving parts inside the digester that can get clogged and require regular maintenance. The final proposed mixing system presented is able to achieve a DVTT range of 0.82 to 1.3 h, at an intensity of 70.58 to 35.88 s⁻¹ requiring a unit power per volume of 3.41 to 0.88 W/m³.

7. RECOMMENDATIONS AND FUTURE WORK

General Recommendations

When considering anaerobic digestion for stabilizing of raw municipal sludge careful consideration should be given to the nature of the feedstock as it is a toxic media to work with and can expose one to harmful environments.

Anaerobic digestion is a complex degradation process and is affected by several environmental and process operating factors and the plant designer should be well aware of the different reaction inside a digester as well as the speed of the degradation process.

Studying the hydraulic side of anaerobic digestion plants it is recommended that when selecting the mixing system of a digester, the internal biological digester requirements has to be considered. Mixing of the digestate in a digester acts as the transportation mechanism of the micro bacteria to the organic substance and can either increase or decrease the biogas production rate of the digester.

It is also recommended when selecting a mixing system that the downtime, ease of maintenance and power requirement at increased total solid contents are considered as opening and exposing a digester to air inhibits the anaerobic digestion process.

Recommendations for decision makers

Using anaerobic digestion to treat wastewater sludge should not only be looked at as sludge treatment, but rather be considered as a more sustainable option to treat sludge and turn it into a carbon neutral power generation source. Organic fertilizer can be produced from the treated sludge along with the option whereby effluent of the plant can be further treated to obtain potable water.

It is recommended that bio-methane tests are done on the primary and secondary as well as combinations of mixing ratios of primary and secondary sludge to determine the possible methane yield from the feedstock for an input to a financial model.

It also recommended that a market for low grade steam or heated water from the shell tube heat exchanger on the CHPs exhausts should be investigated. In the proposed design of the anaerobic digestion plant a total of 683 kW of heat can be recovered.

It is also recommended that a market is sought for industrial or organic fertilizer and the market value of the industrial or organic fertilizer is compared against investment cost.

From studying the thermal side of anaerobic digestion plant, it is recommended that feedstock of an anaerobic plant should be increased to 6 % and above preferably to 8 % TS as the overall electrical generation, energy production and processing capacity can be increased. Careful consideration should be taken when selecting the plant layout at low total solid contents (less than 4 %), as the heat demand of the anaerobic plant can exceed the available supply.

Future work

A number of recommendations for future work can be made based on the results of the present study:

- To conduct a case study on a Gammams digester and measure the digester temperature, volume and temperature of sludge entering and exiting digester as well as the atmospheric conditions to verify the energy model
- Investigate the use of feedstock pre-treatment using electrolysis or ultrasonic pulses to improve biogas yield
- The CHPs can be turbo charged to improve thermal efficiency and power output which will relate to less CHP unit required and lower investment capital.
- To find the optimum feeding frequency for a continuous stirred reactor fed by sewage sludge by keeping the hydraulic and solid retention time constant throughout the work
- To conduct an experimental case study to resolve the dispute of the effect of shear forces on the micro-bacteria inside the anaerobic digester when mixed
- Conduct an experimental study on a scale size proposed concept design on the primary sludge, secondary sludge as well as the in mixing ratio to verify methane production rate as well as the methane yields
- To determine the optimum mixing interval and intensity of an anaerobic digester fed by sewage sludge, as this currently is the subject of much debate
- To taper the draft tube geometry to improve its effectiveness
- To conduct a hydraulic modelling comparison study using a non-Newtonian fluid model at increased total solid contents of up to 10 % between the mechanical and gas recirculation mixing method in the plug-flow regime at the same digester volume turnover time comparing the power consumption
- To determine a set of correlations that can predict the film thickness of the liquid film around a plug in a vertical tube, as well as the slip velocity as a function of the volume of the plug

REFERENCES

- Augusto de Lemos Chernicharo C., 2007, Anaerobic reactors: Biological Wastewater Treatment Volume 4. Federal University of Minas Gerais, Brazi, IWA Publishing.
- Azbar N. & Speece R. E., 2001, Two-phase, two-stage and single-stage anaerobic process comparison. *Journal of Environmental Engineering*, 127, 240-248.
- Batstone D.J., Keller J., Angelidaki I., Kalyuzhnyi S.V., Pavlostathis S.G., Rozzi A., Sanders W.T.M., Siegrist H. & Vavilin V.A., 2002, The IWA anaerobic digestion model No 1 (ADM1). *Water Science & Technology*, 45, 65-73.
- Binix W., 2010, CFD simulation of mixing in egg-shaped anaerobic digesters. *Water Research* 44, 1507-1519.
- Boe K., 2006, Online monitoring and control of the biogas process. PhD dissertation, Institute of Environment & Resources, Technical University of Denmark.
- Bombardiére J., Espinosa-Solares T., Domaschko M. & Chatfield M., 2007, Thermophilic anaerobic digester performance under different feed-loading frequency. *Applied Biochemistry and Biotechnology*, 137-140, 765-775.
- CAE., 2012, Photo library, Cape Advanced Engineering Ltd. Tel, +27 21 577 3413.
- CAE., 2014, Experimental performance test work on CHP unit conducted by Cape Advanced Engineering Ltd., Tel, +27 21 577 3413.
- Çalli B., 2010, Anaerobic treatment. ENVE 424 Conference: Turkey, Marmara University, 12 to 18 December.
- Çengle Y.A., 2007, Heat and mass transfer: A practical approach, third edition. New York, McGraw-Hill publications.
- Da Hlaing N., Sirivat A., Siemanond K. & Wilkes J.O., 2014, Identifying opportunities to reduce water pollution and encourage voluntary compliance in Windhoek, Namibia. Bachelor of Science, Worcester Polytechnic Institute.
- Da Hlaing N., Sirivat A., Siemanond K. & Wilkes J.O., 2007, Vertical two-phase flow regimes and pressure gradients: Effect of viscosity. *Experimental Thermal and Fluid Science*, 31, 567-577.
- De Henau V. & Raithby D.G., 1994, A transient two-phase model for the simulation of slug flow in pipelines. *International Journal Multiphase Flow*, 21, 335-349.
- Demirer G.N. & Chen S., 2005, Two-phase anaerobic digestion of unscreened dairy manure. *Process Biochemistry*, 40, 3542-3549.
- Dennis A. & Burke P.E., 2001, Dairy waste anaerobic digestion handbook, first edition. Olympia, Environmental Energy Company.
- Donoso-Bravo A., Retamal C., Carballa M., Ruiz-Filippi G. & Chamy R.C., 2009, Influence of temperature on the hydrolysis, acidogenesis and methanogenesis in mesophilic anaerobic digestion: Parameter identification and modelling application. *Water Science and Technology*, 60, 9-17.
- Du Pisani P.L., 2006, Direct reclamation of potable water at Windhoek's Goreangab reclamation plant. *Desalination*, 188, 79-88.
- Duffie J.A., & Beckman W.A., 2006, Solar engineering of thermal processes, third edition. New Jersey, University of Wisconsin-Madison, Willey Publications.
- DWAF, 2009, Guidelines for the utilization and disposal of wastewater sludge, Volume 3 of 5, first edition. South Africa, Water Research Commission.

- Eliyan C., 2007, Anaerobic digestion of municipal solid waste in thermophilic continuous operation. MSc thesis, Thailand, Asian Institute of Technology.
- El-Mashad H. M., Zeeman G., van Loon W.K.P., Bot G.P.A. & Lettinga G., 2004, Effect of temperature and temperature fluctuation on thermophilic anaerobic digestion of cattle manure. *Bioresource Technology*, 95, 191-201.
- Google Earth 6.8, 2015, Gammams water care works -22°32'2.8"N, 17°01'50.51"W, elevation 1703 m. Available through: <http://www.google.com/earth/index.html> (Accessed, 31 August 2013).
- Halalsheh M., Koppes J., den Elzen J., Zeeman G., Fayyad M. & Lettinga G., 2005, Effect of SRT and temperature on biological conversions and the related scum-forming potential. *Water Research*, 39, 2475-2482.
- Hanafizadeh P., Saidi M.H., Karimi A. & Zamiri A., 2010, Effect of bubble size and angle of tapering riser pipe on the performance of airlift pumps. *Particulate Science and Technology*, 28, 332-347.
- Hasheela R., 2009, Municipal Waste Management in Namibia: The Windhoek Case Study. PhD dissertation, Mexico, Universidad Azteca.
- Il-Su L., Parameswaran P. & Rittmann B.E., 2011, Effects of solids retention time on methanogenesis in anaerobic digestion of thickened mixed sludge. *Bioresource Technology*, 102, 10266-10272.
- Kaparaju P., Buendia I., Ellegaard L. & Angelidakia I., 2008, Effects of mixing on methane production during thermophilic anaerobic digestion of manure: Lab-scale and pilot-scale studies. *Bioresource Technology*, 99, 4919-4928.
- Karim A., Hanafizadeh P., Ghanbarzadeh S. & Saidi M.H., 2010, Augmentation of airlift pump performance in step geometry. 7th International Conference on Multiphase flow, Tampa, 30 May to 4 June .
- Karim K., Hoffmann R., Klasson T. & Al-Dahhan M.H., 2005a, Anaerobic digestion of animal waste: Waste strength versus impact of mixing. *Bioresource Technology*, 96, 1771-1781.
- Karim K., Hoffmann R., Thomas K. & Al-Dahhan M.H., 2005b, Anaerobic digestion of animal waste: Effect of mode of mixing. *Water Research*, 39, 3597-3606.
- Kassab S.Z., Kandil H.A., Warda H.A. & Ahmed W.H., 2009, Air-lift pumps characteristics under two-phase flow conditions. *International Journal of Heat and Fluid Flow*, 30, 88-98.
- Kjeldby T.K., Henkes R.A.W.M. & Nydal O.J., 2013, Lagrangian slug flow modelling and sensitivity on hydrodynamic slug initiation methods in severe slugging case. *International Journal of Multiphase Flow*, 53, 29-39.
- Lahnsteiner J. & Lempert G., 2007, Water management in Windhoek, Namibia. *Water Science and Technology*, 55, 441-448.
- Lui H. & Kakac S., 2002, Heat Exchangers Selection, Rating and Thermal Design. Florida, University of Miami, Department of Mechanical Engineering, CRC Press.
- Mahrous A.F., 2012, Numerical study of solid particles-based airlift pump performance. *WSEAS Transaction on Applied and Theoretical Mechanics*, 7, 2224-3429.
- Mema V., 2009, Impact of poorly maintained wastewater and sewage treatment plants. CSIR, Email: vmema@csir.co.za, Tel. +27 12 841 3406.
- Moo-Young M., 2011, Comprehensive Biotechnology, second edition. Waterloo, University of Waterloo, Elsevier.

- Nasr N., Elbeshbishy E., Hafez H., Nakhla G. & Hesham El Naggar M., 2012, Comparative assessment of single-stage and two-stage anaerobic digestion for the treatment of thin stillage. *Bioresource Technology*, 111, 122-126.
- Nges I.A. & Liu J., 2010, Effects of solid retention time on anaerobic digestion of dewatered-sewage sludge in mesophilic and thermophilic conditions. *Renewable Energy*, 35, 2200-2206.
- NWN, 2010, Namibia weather network, <http://www.namibiaweather.info/> (Accessed , 13 May 2013)
- Panichnumsin P., Ahring B.K., Nopharatana A. & Chaipresert P., 2010, Comparative performance and microbial community of single and two-phase anaerobic co-digesting cassava pulp and pig manure. *World Academy of Science*, 62, 721-726.
- Piao Z.H., Kimand C.H. & Kim J.Y, 2013, Effect of Feeding Frequency on Performance of Laboratory-Scale Anaerobic Digestion Reactor. Hokkaido University, Japan: Department of Civil and Environmental Engineering.
- Popiel C.O., Wojtkowaik J. & Biernacka B., 2001, Measurements of temperature distribution in the ground. *Experimental Thermal and Fluid Science*, 25, 301-309.
- Schafer P.L., Farrell J.B., Newman G. & Vandeburgh S., 2002, Advanced anaerobic digestion performance comparisons. *Water Environment Federation*, 50, 468-484.
- Schön M., 2009, Numerical modelling of anaerobic digestion processes in agricultural biogas plants. PhD dissertation, Austria, Innsbruck University.
- Stroot P.G., McMahon K.D., Mackie R.I. & Raskin L., 2001, Anaerobic codigestion of municipal solid waste and biosolids under various mixing conditions: Digester performance. *Water Research*, 35, 1804-1816.
- Taha T. & Cui .F., 2005, CFD modelling of slug flow in vertical tubes. *Chemical Engineering Science*, 61, 676-687.
- Thornton I., Butler D. & Hession M., 2009, Pollutants in urban waste water and sewage sludge. IC Consultants Ltd, London.
- Turovskiy I.S. & Mathai P.K., 2006., *Wastewater sludge processing*, New Jersey, John Wiley & Sons.
- Vavilin V.A., Fernandez B., Palatsi J. & Flotats X., 2008, Hydrolysis kinetics in anaerobic degradation of particulate organic material: An overview. *Waste Management*, 28, 939-951.
- White F.M., 2007, *Fluid mechanics*, fourth edition. McGraw-Hill. New York, McGraw-Hill publications.
- Wu B., 2010a, CFD simulation of gas mixing in anaerobic digesters. *Computers and Electronics in Agriculture*, 109, 278-286.
- Wu B., 2010b, CFD simulation of gas and non-Newtonian fluid two-phase flow in anaerobic digesters. *Water Research*, 44, 3861-3874.
- Young-Chae S., Sang-Jo K. & Jung-Hui W., 2004, Mesophilic and thermophilic temperature co-phase compared with single-stage mesophilic- and thermophilic digestion of sewage sludge. *Water Research*, 38, 1653-1662.
- Zhang T.C. & Noike T., 1991, Comparison of one-phase and two-phase anaerobic digestion processes in characteristics of substrate degradation and bacterial population levels. *Water Science & Technology*, 23, 1157-1165.

APPENDIX A: VALIDATION AND VERIFICATION

A.1 Energy balance of plant

A.1.1 Selection of time step for feedstock model

The numerical model used to determine the energy requirement of the feedstock was a 1D transient model, using an explicit solving scheme. To determine the suitable time step for this numerical model the two-hour time duration of the feedstock in the sump was broken up into 30 to 706 time intervals.

After selecting a time step between the mentioned range, the numerical model was run, with a change in the residuals set to 1×10^{-6} . In each of these simulations the heat recovered and temperature after the two hours was captured, in order to see when the simulations converged. The summarised results of the simulations at the different time steps are illustrated in Figure A.1 below:

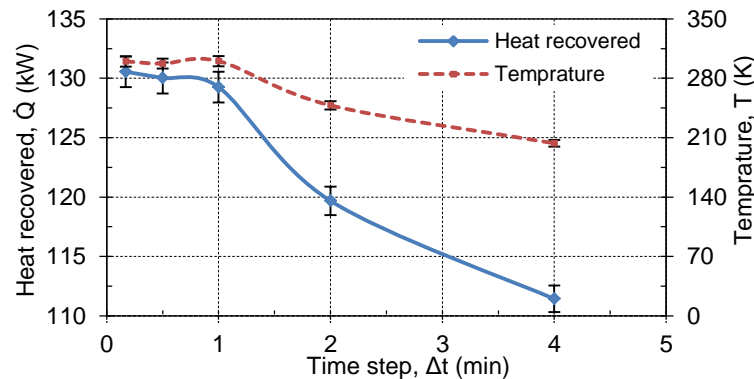


Figure A.1: Effect of time step on the numerical model of feedstock energy balance

The results plotted in the figure above indicate that a time step of smaller than one minute is suitable to use. To illustrate the increase in accuracy from decreasing the time step, a percentage error bar of $\pm 1\%$ was added to the heat recovered and $\pm 2\%$ to the temperature. From these percentage error bars, the figure indicates that the simulation converges at a time step of one minute and this time interval was used for the simulations of the incoming feedstock in the thesis.

A.1.2 Selection of time step for digester energy model

To calculate the digester environmental losses and heat requirement for each of the concepts presented in the thesis, a numerical model was constructed using equations 3.5 to 3.9 and A-1 to A-26 following the time step selection. In order to determine the suitable time step for this model in a day (24 hours), the time duration of 24 hours were broken up into 96 to 12 intervals, with time steps ranging from 15 min to 2 hour.

The weather data for Windhoek was supplied in an hour interval, and had to be averaged for the smaller time steps. The data was inserted into the numerical model of concept 1 post-digesters, with a change in the residuals set to 1×10^{-6} . After each simulation was run at the selected time steps, the average heat loss per day and temperature of the digesters at the end of the day was captured. The results of the simulations at the selected time steps are illustrated in Figure A.2.

A percentage error bar of $\pm 6\%$ was added to the heat losses of the post-digesters and $\pm 0.3\%$ to the temperature of the digesters to illustrate the increase in accuracy from decreasing the time step of the model.

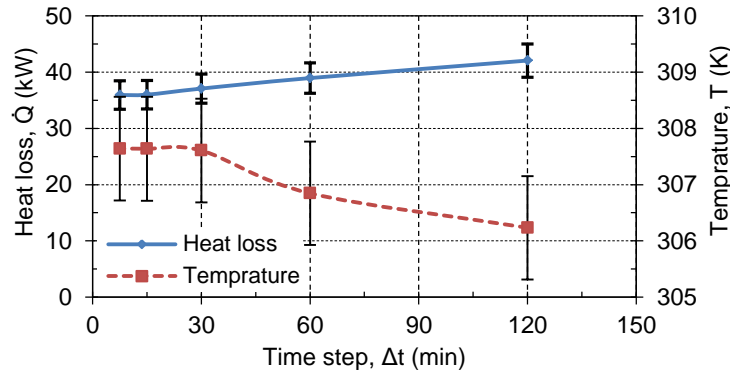


Figure A.2: Effect of time step on the numerical model of concept 1 post-digesters energy balance on 23 September

The results in the figure illustrates that, the solution converges at a 15 minute time step interval, however the percentage error bars shows that when selecting a time step of one hour there is only a percentage error of 7 % on the average heat losses and 0.25 % on the digester temperature at the end of the day.

Based on these results, a time step of one hour was selected to simulate the environmental losses and heat requirement for each of the concepts presented in this study to reduce the computing time.

To determine the environmental loss the following equations were used;

The irradiation heat, Q_i (W), in equation 3.9 as

$$\dot{Q}_{I_i}^t = I_i^t A_{surf_out_i} \quad (A.1)$$

Heat reflection, Q_{ref} (W), in equation 3.10 as

$$\dot{Q}_{ref_i}^t = (1 - \alpha_D) \dot{Q}_{I_i}^t \quad (A.2)$$

The heat radiated, Q_{rad} (W), in equation 3.10 as

$$\dot{Q}_{rad_i}^t = \varepsilon_{out} \sigma A_{surf_out_i} (T_{surf_out_i}^4 - T_{amb}^4) \quad (A.3)$$

Heat convected, Q_h (W), in equation 3.10 as

$$\dot{Q}_{h_i}^t = h_{out_i}^t A_{surf_out_i} (T_{surf_out_i}^t - T_{amb}^t) \quad (A.4)$$

Heat conducted, Q_k (W), in equation 3.10 as

$$\dot{Q}_{k_i}^t = \sum_{n=1}^{k=8} \left(\frac{T_w^t - T_{gr_i}^t}{\Sigma R} \right) \quad (A.5)$$

and where

Global aperture radiation, I_i (W/m²), in equation A.1 was taken as

$$I_i^t = I_{DNI}^t \cos \theta_i^t + \left[I_{DNI}^t \left(\frac{1 + \cos \beta^t}{2} \right) + \rho_{gr} I_{GHI}^t \left(\frac{1 - \cos \beta^t}{2} \right) \right] \quad (A.6)$$

Angle of inclination, θ_i (rad), in equation A.6 was calculated with

$$\cos \theta_i^t = \cos \beta (\sin \delta \sin \varphi + \cos \delta \cos \varphi \cos \omega) - \cos \delta \sin \omega \sin \beta \sin \gamma + \sin \beta \cos \gamma (\sin \delta \cos \varphi - \cos \delta \cos \omega \sin \varphi) \quad (A.7)$$

Solar azimuth angle, γ^t (rad), in equation A.7

$$\gamma^t = \sin \omega \left| \cos^{-1} \frac{(\cos \theta_z \sin \varphi - \sin \delta)}{\sin \theta_z \cos \varphi} \right| \quad (\text{A.8})$$

Zenith angle, θ_z (rad), in equation A.8

$$\cos \theta_z^t = \cos \varphi \cos \delta \cos \omega + \sin \varphi \sin \delta \quad (\text{A.9})$$

Hour angle, ω (rad), in equations A.7 to A.9

$$\omega = 15(t_s - 12) \quad (\text{A.10})$$

Declination angle, δ (rad), in equations A.7 to A.9

$$\begin{aligned} \delta^t = & 0.006918 - 0.399912 \cos B + 0.070257 \sin B - 0.006758 \cos 2B \\ & + 0.000907 \sin 2B - 0.002679 \cos 3B + 0.00148 \sin 3B \end{aligned} \quad (\text{A.11})$$

Solar time, t_s^t (h), in equation A.10

$$t_s^t = \frac{(4(L_{st} - L_{loc}) + \Xi)}{60} + t_{Std} \quad (\text{A.12})$$

Equation of time, Ξ^t (min), in equation A.12

$$\begin{aligned} \Xi^t = & 229.2(0.000075 + 0.001868 \cos B - 0.032077 \sin B - 0.014615 \cos 2B \\ & - 0.04089 \sin 2B) \end{aligned} \quad (\text{A.13})$$

Where B , in equation A.13 is

$$B^t = (n - 1) \left(\frac{360}{365} \right) \quad (\text{A.14})$$

the other parameters in the numerical model were taken as follows

Sky temperature, T_{sky} (K), in equation A.3

$$T_{sky} = (0.777 T_{amb}^4)^{0.25} \quad (\text{A.15})$$

Convection heat transfer coefficient, h_{out} (W/m²K), as

$$h_{out} = \frac{kNu_{out}}{D} \quad (\text{A.16})$$

Nusselt number outside digester, Nu_{out} , in equation A.16

- Laminar flow

$$Nu_{out} = 0.664 Re^{0.5} Pr^{\frac{1}{3}} \quad \text{where } Re < 5E^5 \quad (\text{A.17})$$

- Turbulent flow

$$Nu_{out} = 0.037 Re^{0.8} Pr^{\frac{1}{3}} \quad \text{where } 5E^5 \leq Re \leq 10E^7 \quad (\text{A.18})$$

where

Reynolds number, Re

$$Re = \frac{\rho V D}{\mu} \quad (\text{A.19})$$

The fluid properties were taken at the film temperature, and the film temperature outside digester, $T_{film,out}$ (K) as

$$T_{film,out} = \frac{T_{sutf out} + T_{amb}}{2} \quad (\text{A.20})$$

Convection heat transfer coefficient inside digester, h_{in} (W/m²K)

$$h_{in} = \frac{kNu_{in}}{L_c} \quad (A.21)$$

Nusselt number inside digester, Nu_{in} in equation A.21

- Hot surface at top

$$Nu_{in} = 1 \quad (A.22)$$

- Hot surface at bottom

Based on experiments with air, Çengle (2007) recommended this correlation for horizontal enclosures

$$Nu_{in} = 1 + 1.44 \left| 1 - \frac{1708}{Ra} \right| + \left| \frac{Ra^{\frac{1}{3}}}{18} - 1 \right| \text{ if } Ra < 1E^8 \quad (A.23)$$

Rayleigh number, Ra in equation A.23

$$Ra = \frac{g\beta(T_{sutf\ in} - T_w)L_c^3 Pr}{\nu^2} \quad (A.24)$$

where

$$\beta = \frac{1}{T_{film\ in}} \quad (A.25)$$

*Note all fluid properties are at film temperature
temperature of ground, $T_{gr_i}^t$ (K); in equation A.23

$$T_{gr_i}^t = (T_m \pm \Delta T_m) + \left[1.07k_v A_p E \left(-0.00031552 \left(\frac{1}{\alpha_{gr}} \right)^{-0.5} \right) \right] \\ * \cos \left[\frac{2\pi}{365} \left(t - PS - 0.018335 \left(\frac{1}{\alpha_{gr}} \right)^{-0.5} \right) \right] \quad (A.26)$$

Equations A.6 to A.15 were obtained from Duffie and Beckman (2006), and equation A.26, to calculate the ground temperature, was obtained from Popiel *et al.* (2001).

A.2 Digester Mixing System

A.2.1 Friction multiplier for two-phase numerical model

For the 1D numerical transient, mass momentum balance model, the friction coefficient (C_f) for the two-phase flow was needed. In the methodology in section 3.2.3, different 1D transient numerical models were reviewed and it was found that the friction coefficient at the interface between gas and liquid plug are still an uncertainty.

A decision was made to follow the same method as Kjeldbly *et al.* (2013) used for their interface friction coefficient. The method was to multiply the friction coefficient for the i 'th phase with an additional friction multiplier (FM) as presented in equation 3.65.

$$\lambda_i = FM_i C_{f_i} \quad (3.65)$$

The FM in Kjeldbly *et al.* (2013) was set at 100, but was not related to a parameter. In this thesis, the aim is to relate the FM to a parameter that will capture the effect as the plug size is increased from the experimental work to the full scale prototype. Different parameters were looked at to relate the FM to, in order to capture the effects

mentioned before. The experimental data of the liquid mass displaced by plug generator 1.1.1 with an orifice area of 201×10^{-6} and $415 \times 10^{-6} \text{ m}^2$ were plotted against the plug sizes and are illustrated in Figure A.3.

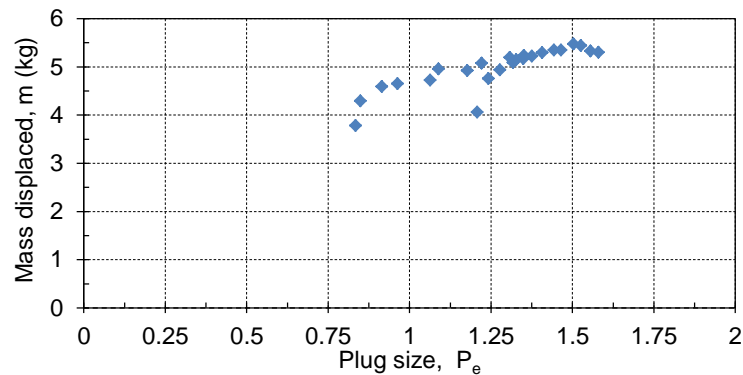


Figure A.3: Liquid mass displaced by draft tube as a function of plug size

Figure A.3 illustrated that as the plug size was increased the mass displaced by the draft tube also increased. This phenomenon has also been observed in Figures 4.4 to 4.6 where an increase in plug size led to an increase in mass displaced.

Based on this observation, a decision was made to relate the plug size with a function to the FM. To obtain this function the values of the FM were calculated with the numerical model using the experimental result of the draft tube and plug generator 1.1.1 with an orifice areas of 201×10^{-6} and $415 \times 10^{-6} \text{ m}^2$.

A multi-linear regression model was performed using MS Excel was used to determine the correlation between the plug size and the FM. The correlation obtained from the multi-linear regression model is presented in equation 3.40 and a R^2 value of 0.943 was obtained.

$$FM = e^{(-0.18393(\ln P_e)^8 + 4.93657)} \quad R^2 = 0.943 \quad (3.40)$$

The accuracy of the FM equation obtained was determined in Figure A.4, where the calculated FM was plotted against the predicted FM data points.

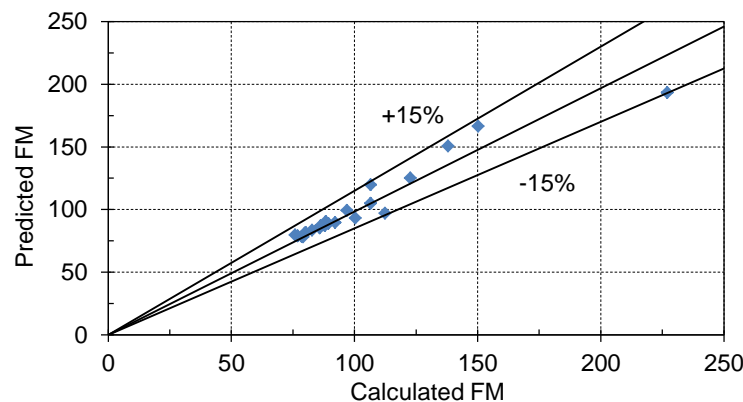


Figure A.4: Predicted friction multiplier as a function of calculated friction multiplier

In the figure above, the calculated FM using equation 3.67 was plotted against the predicted FM data points and a $\pm 15\%$ accuracy envelope was added. A linear curve fit was placed through the data point and forcing it to fit through the origin (0;0). The

incline of this linear curve fit indicates that the FM equation obtained tended to over predict by 1.03 %.

The FM equation was programmed into the 1D numerical model, to predict the experimental results obtained, at different hydrostatic pressures and at an increasing volumetric air supply flow rate, to see if the correlation of the FM was able to capture it. The results from the numerical model and the results measured in the experimental work were plotted on the same axis in Figure A.5.

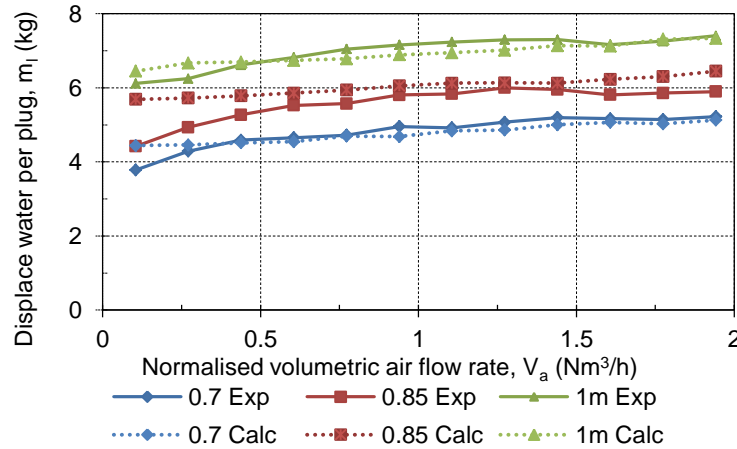


Figure A.5: Measured and calculated liquid displaced as a function of normalised volumetric flow rate at different liquid depths

In the figure above, the measured liquid displaced data were plotted as a solid line series and the calculated liquid displaced data were plotted as a hashed line series.

The figure illustrates that the numerical model is well capable to predicting the data points measured in the experimental work at a volumetric gas flow rate greater than $0.438 \text{ Nm}^3/\text{h}$. The only points that the numerical model were not capable of capturing correctly were the initial points at a gas flow rate from 0.104 up to $0.438 \text{ Nm}^3/\text{h}$.

These measured and predicted data points in Figure A.4 were plotted against each other in Figure A.6, to determine the overall accuracy of the 1D numerical model for the mixing system.

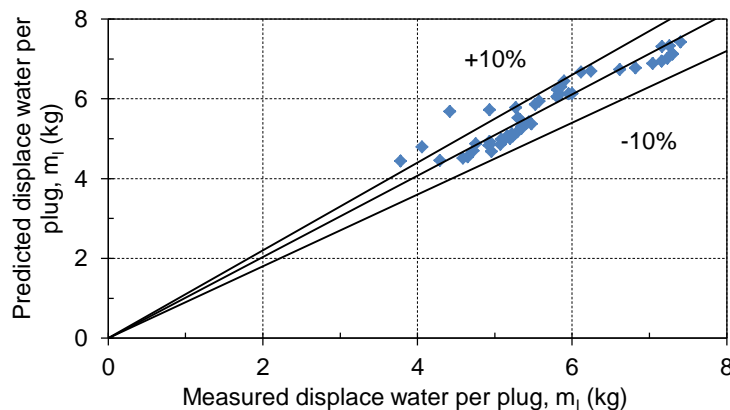


Figure A.6: Predicted liquid displaced as a function of calculated liquid displaced

From the figure above, it is illustrated that all the data points fall within the $\pm 10\%$ accuracy envelope except the four data points at initial volumetric air flow rate from 0.104 up to $0.438 \text{ Nm}^3/\text{h}$.

A linear curve fit was again placed through the data points and origin and a R^2 value of 0.88 was obtained. The incline of this linear curve fit indicates that the numerical model slightly under predicts the liquid displaced by 2.16 %. Figure A.5 concludes that the correlation obtained for the FM falls within the ± 10 % accuracy envelope if the FM is smaller than 123.7.

A.2.2 Selection of time step for two-phase numerical model

For the 1D transient numerical model, an explicit solving scheme was used, as it is conditionally stable and only needs the source term from the previous time step to determine that of the new time step. Although the accuracy of an explicit solving scheme is only of a first order, the accuracy of the solution can be increased by decreasing the value of the time step used to solve the solution.

In order to determine the suitable time step for the simulations of the scale model, the same numerical model was run with time steps ranging from 0.04 to 0.004 s divided the solution into 121 to 1210 time intervals. For all the simulations the maximum change in the parameters in the simulation were set to 1×10^{-6} before it stopped iterating. After each simulation, the amount of liquid displaced and the time interval of the cycle were recorded at the corresponding time step and plotted in Figure A.7.

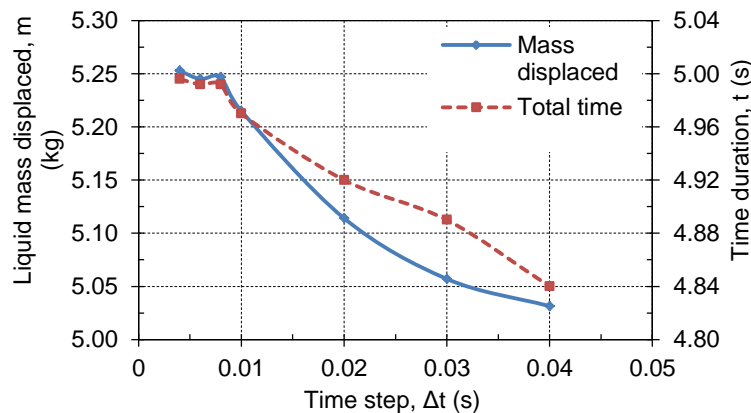


Figure A.7: Effect of time step on the explicit numerical model of the liquid mass displaced through the draft tube and the time duration of the cycle for scale model

Figure A.7 shows that times step of smaller than 0.008 s is where the numerical model converged. Based on these results, a time step of 0.006 s was selected to simulate the scale model of the draft tube.

The time step for the full-scale simulations also needed to be determined. To select the time step for the full scale simulation the same procedure was used as that of the scale model. The range of time steps selected for the full scale was from 0.1 to 0.03 s which divided the simulation in 396 to 1357 time intervals. For all the simulations the maximum change in the residuals in the simulation were again set to 1×10^{-6} before it stopped iterating. The liquid displaced and the time interval of the cycle was recorded again and plotted in Figure A.8.

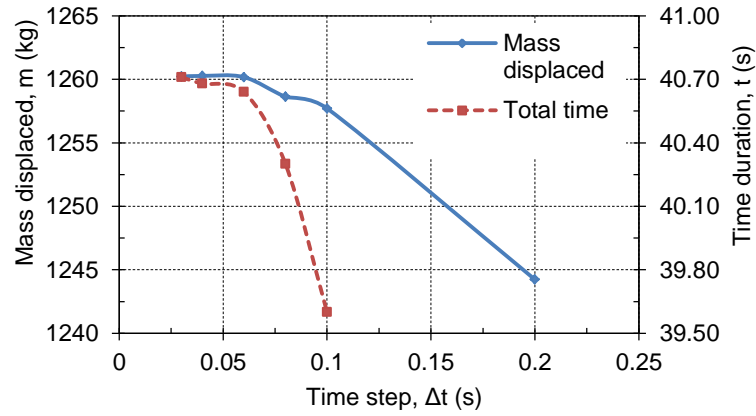


Figure A.8: Effect of time step on the explicit numerical model for the liquid mass displaced through the draft tube and time duration of cycle for the full-scale model

The results plotted in Figure A.8 above, indicate that a time step of smaller than 0.06 s can be used for the numerical model of the full-scale draft tube.

APPENDIX B: CALIBRATION AND ERROR ANALYSIS

B.1 Calibration of rotameter for experimental setup

The technique used to calibrate the rotameter flow rate, was the displacement of water of a known volume. To calibrate the rotameter the first objective was to determine the volume between the 5 mm line spacing between the top of chamber 2 and the bottom of chamber 1 of plug-flow generator 1.1.1 (refer back to Figure 4.1).

The volume between the lines was determined by placing the plug-flow generator upside down on an electric scale with an accuracy of ± 0.01 g. The plug-flow generator was filled on the scale to the top of chamber 2 and the scale was zeroed. Additional water was then added in increments up to each of the 5 mm spaced lines and a mass reading was recorded. The different mass readings recorded were averaged to determine the volume.

With the volume between the 5 mm lines known, the plug-flow generator was installed 0.7 m below the liquid level in the experimental setup presented in Figure 4.2. The video camera was installed with the centre of the lens on the same level as the fourth marked line from the top on the plug-flow generator to eliminate parallax error. The plug-flow generator was placed 200 mm away from the inspection window and the camera 200 mm away from the window outside the testing tank. The camera was set to a video setting of 100 frames per second at a pixel size of 1050 x 960.

The calibration procedure followed for the rotameter was;

1. Set the pressure regulator to 1 bar
2. Start recording the displacement of water inside the plug-flow generator by air with the rotameter set to a reading of 10 mm
3. Record five cycles of plug forming and then close the shutoff valve and stop the video recording
4. Increase the flow rate by 10 mm increments and repeat step 4 and 5 to the maximum flow reading of the rotameter
5. Correct the wide-angle lens effect and convert the video recording to picture frames using Adobe Photo Shop CS6
6. Capture the summation of frames to displace the liquid from the 3rd to 4th and 5th line of the plug-flow generator and calculate the time period

With the volume known and the time intervals, the volumetric flow rate could be calculated. The calculated volumetric flow rate at 0.7 m hydrostatic pressure was normalised to standard atmospheric conditions at a pressure of 101 325 Pa and a temperature of 25 °C. The normalised data is plotted in Figure B.1 and a linear curve fit was placed through the data points.

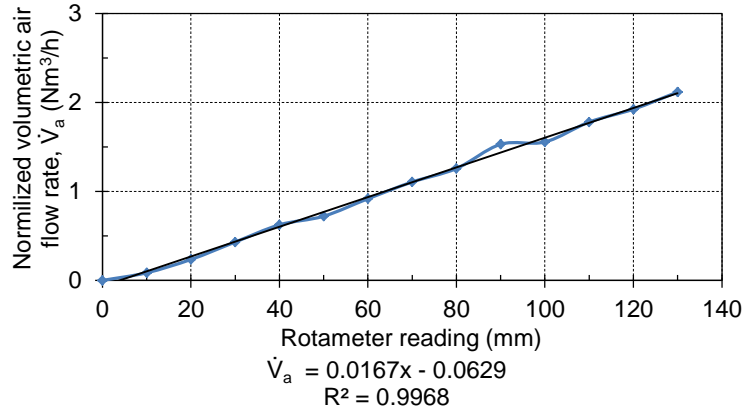


Figure B.1: Volumetric air flow rate calibration of the rotameter and curve fit

From the captured data in the figure above, it is shown that this displacement method used to calibrate the rotameter and the rotameter itself are quite accurate. In order to determine the accuracy of the curve fit, the measured data was plotted against the predicted data using the curve fit obtained in Figure B.1 and is plotted in Figure B.2 below.

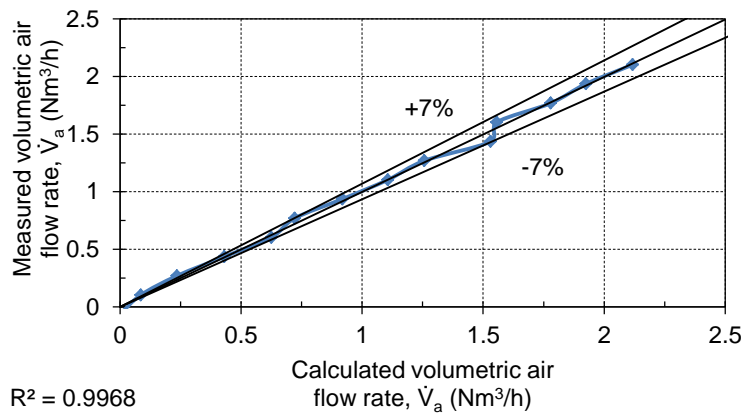


Figure B.2: Predicted volumetric air flow rate as a function of calculated volumetric air flow rate

From the data presented in the figure above, a linear curve fit was placed through forcing it to go through the origin, and a R^2 value of 0.9968 was obtained. A deviation envelope of $\pm 7\%$ was also included and it is shown that all the data points plotted lie within this deviation envelope. This means that the calibration curve fit obtained for the rotameter using the liquid displacement method has an accuracy of $\pm 7\%$.

B.2 Error analysis of experimental work

An error analysis was conducted on the data of the , plug size, the plug frequency and the liquid mass displaced obtained in the experimental work on the scale model to determine accuracy of the data presented in this thesis.

B.2.1 Error analysis of plug size

To determine the plug size generated by the plug-flow generator, the height difference at the third step of the plug generators cycle was recorded (refer back to section 4.1 and Figure 4.3). The mean values recorded for the plug-flow generator 1.1.1 with orifice area of $415 \times 10^{-6} \text{ m}^2$ were plotted against the normalised volumetric air flow rate in Figure B.3 below. The mean height difference was calculated from seven data points recorded at each air flow rate reading. The maximum and minimum data points at each air flow rate reading were included, as well as a $\pm 15 \%$ deviation error bars in the figure below, to define the percentage error of the plug size in the study.

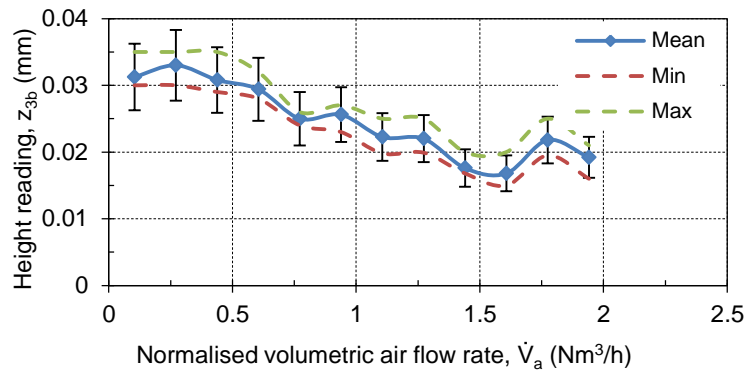


Figure B.3: Height reading of plug generator 1.1.1 with orifice area of $415 \times 10^{-6} \text{ m}^2$ as a function of normalised volumetric air flow rate

The figure above confirms that all the recorded height difference data points at the various air flow rates fell within the $\pm 15 \%$ percentage error band.

The standard deviations of the data points were calculated and it was found that the maximum standard deviation was at an air flow rate reading of $1.774 \text{ Nm}^3/\text{h}$ with 0.0019. The percentage deviation of the raw data points at the air flow rate reading of $1.774 \text{ Nm}^3/\text{h}$ from the mean were calculated and are presented in Figure B.4 below.

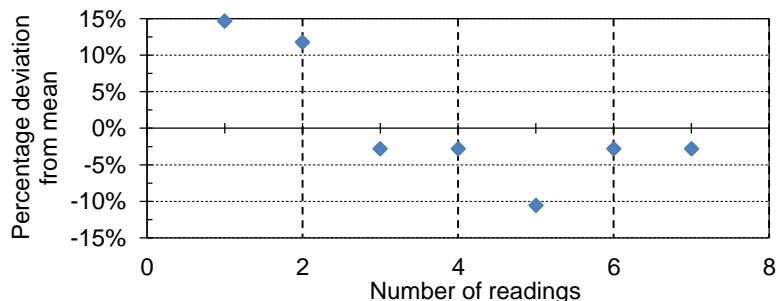


Figure B.4: Percentage deviation of recorded height reading from mean at $1.774 \text{ Nm}^3/\text{h}$ reading

The calculated percentage deviation of the height readings to determine the plug size illustrated in the figure above indicate that the recorded data points lay within a percentage deviation of $\pm 14.7 \%$.

B.2.2 Error analysis of plug frequency

To define the percentage error in the plug frequency data, the mean plug frequency data of plug generator 1.1.1 with orifice area of $415 \times 10^{-6} \text{ m}^2$ was plotted against the normalised volumetric air flow rate in Figure B.5 below. A percentage deviation of $\pm 15\%$ error band was added to the mean data point calculated from seven data points. The minimum and maximum data points at each of the corresponding air flow rates were also included in Figure B.5.

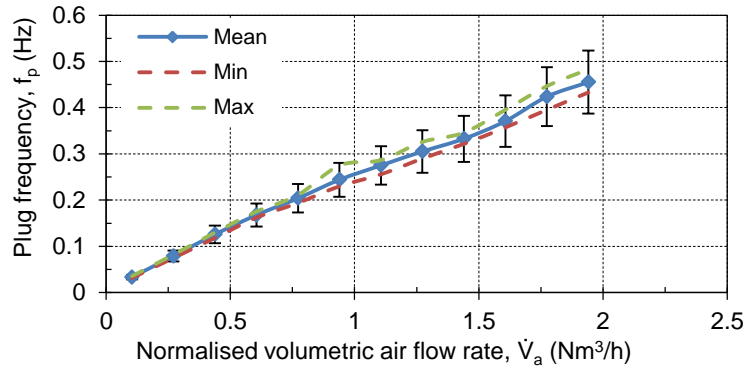


Figure B.5: Plug frequency of plug generator 1.1.1 with orifice area of $415 \times 10^{-6} \text{ m}^2$ as a function of normalised volumetric air flow rate

The figure above illustrates that all the raw data points obtained in the experimental work lay within a $\pm 15\%$ error band. The standard deviation in the plug frequency data points was calculated and it came out that the maximum standard deviation was at a flow rate of $0.9391 \text{ Nm}^3/\text{h}$ with 0.0121 .

The percentage deviation of the plug frequency data from the mean at the flow rate of $0.9391 \text{ Nm}^3/\text{h}$ was calculated and is presented in Figure B.6 below.

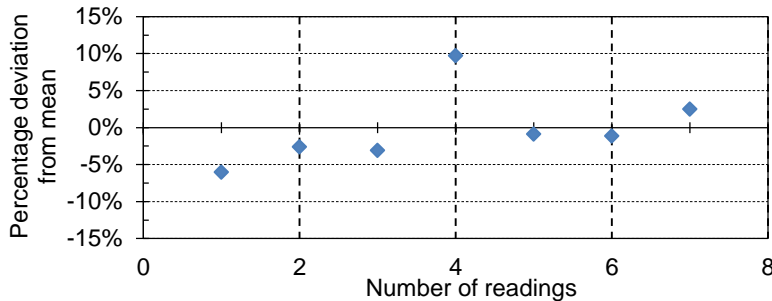


Figure B.6: Percentage deviation of recorded plug frequency from mean at $0.938 \text{ Nm}^3/\text{h}$ reading

The calculated percentage deviation of the plug frequency data presented in the figure above shows that there was a maximum deviation of 9.72% in the raw data obtained in the experimental work.

B.2.3 Error analysis of mass displaced

To determine the percentage deviation in the data obtained from the liquid mass displaced in the experimental work the mean of plug generator 1.1.1 with orifice area of $415 \times 10^{-6} \text{ m}^2$ was plotted against the normalised volumetric air flow rate in Figure B.7. A percentage deviation of $\pm 15\%$ was added to the calculated mean and the maximum and minimum data points at the corresponding flow rates was included in the figure.

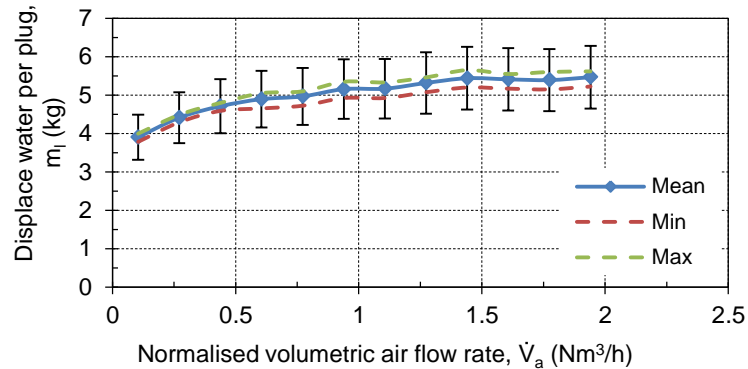


Figure B.7: Displaced water per plug of plug generator 1.1.1 with orifice area of $415 \times 10^{-6} \text{ m}^2$ as a function of normalised volumetric air flow rate

The figure above illustrates that all the data points obtained for the liquid mass displaced fell well within the $\pm 15\%$ deviation band. The standard deviations at all the air flow rates were calculated and the maximum deviation was obtained at a flow rate of $0.938 \text{ Nm}^3/\text{h}$ with 0.1543 .

The percentage deviation of the displaced water per plug data from the mean at the flow rate of $0.938 \text{ Nm}^3/\text{h}$ was calculated and is presented in Figure B.8 below.

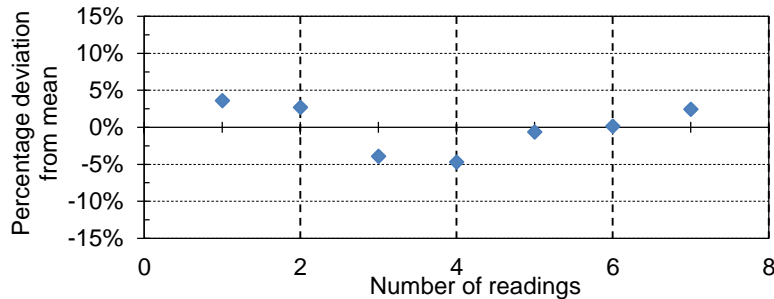


Figure B.8: Percentage deviation of recorded displaced water per plug from mean at $0.938 \text{ Nm}^3/\text{h}$ reading

The figure above shows that the maximum percentage deviation of the water mass displaced obtained in the experimental work was 4.47% .

B.3 Plug formation photo cycle

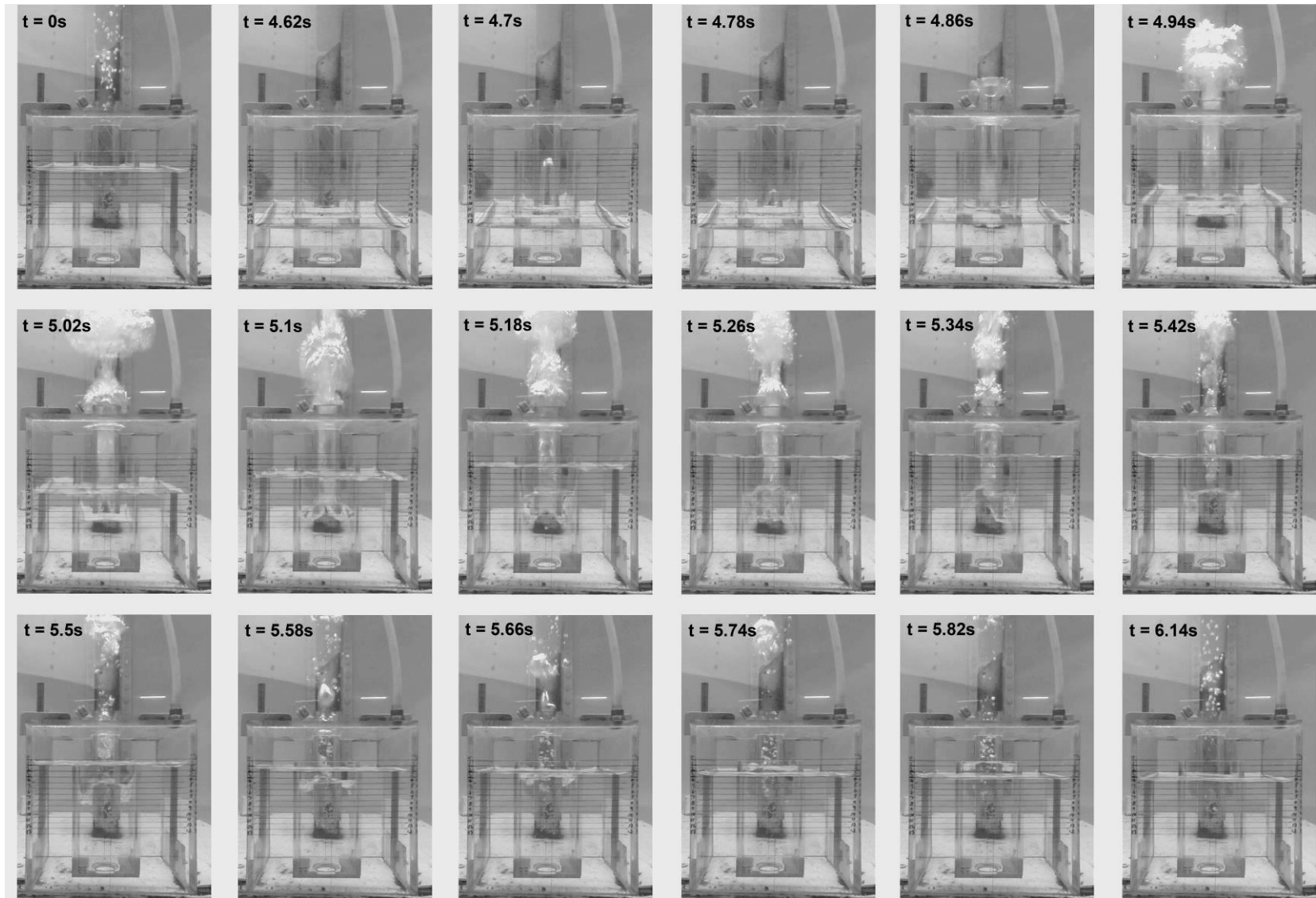


Figure B.9: Cycle of plug formation by plug generator 1.1.1

APPENDIX C: TECHNICAL DRAWING

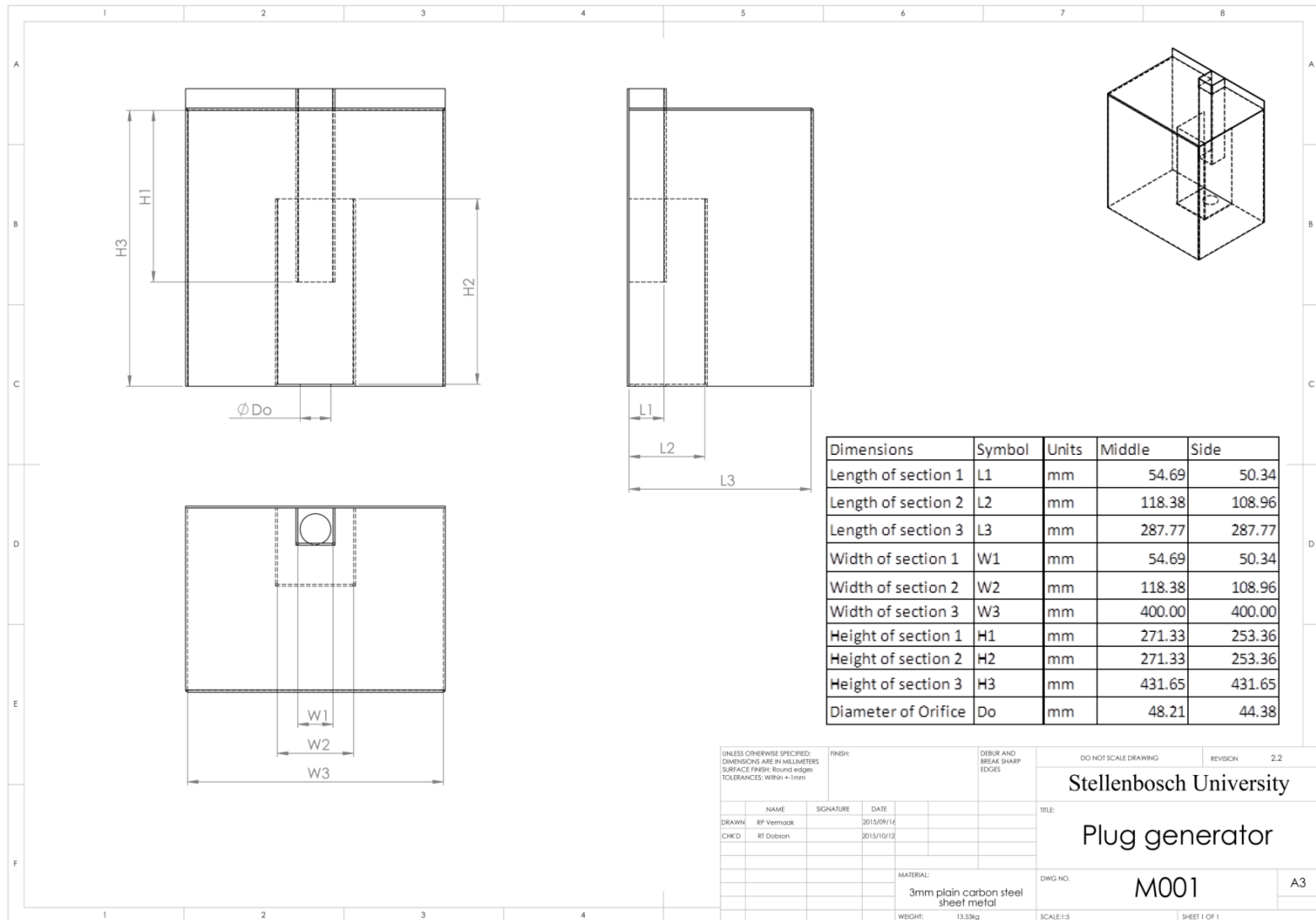


Figure C.1: Proposed design of plug generators for middle and side draft tubes

APPENDIX D: DATA SHEET

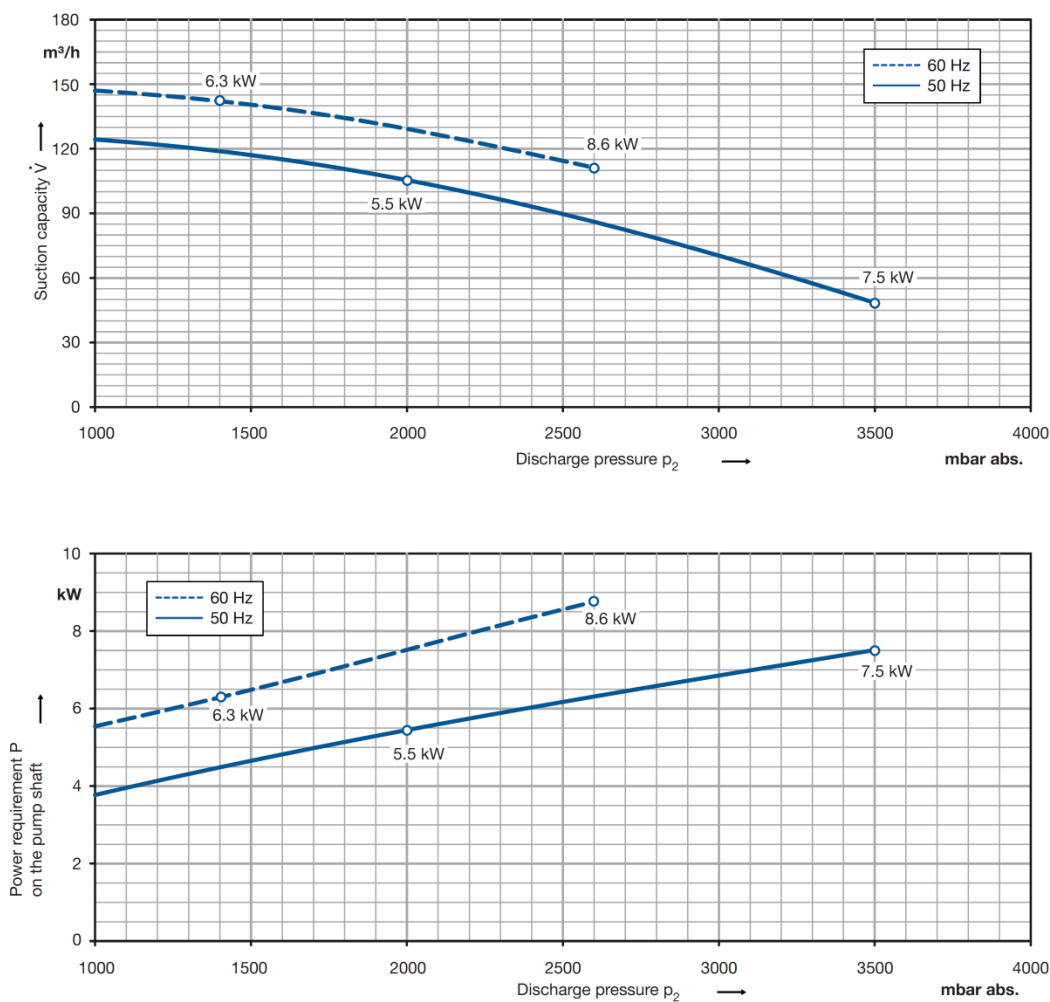
Data sheet liquidring pump



Series L-BV2 | L_200
Range 2BV2 071 Compressor



Performance curves for compressor operation



The characteristics are valid for the inlet of air with a relative humidity of 50 % and a temperature of 20 °C at a atmospheric pressure of 1013 mbar abs. and water at 15 °C as operating liquid. The tolerance is ± 10 %.

The motors are supplied as standard for the input voltage ranges of 50 and 60 Hz and for the protection category IP55 as well as approbated for UL and CSA. Compressors with ATEX 94/9 EG for category 2G are available, too.

Figure D.1: Data sheet of selected liquid ring compressor

APPENDIX E: EXPERIMENTAL DATA

E.1 Effect of geometry change on plug-flow generator

Table E.1: Mean experimental results of the effect of geometry change

Plug Flow Generator	Volumetric air flow rate (Nm ³ /h)	Orifice 201.1E ⁻⁶ m ²			Orifice 415.5E ⁻⁶ m ²			Orifice 804.3E ⁻⁶ m ²		
		Vp (m ³)	Vp (m ³ /h)	f (Hz)	Vp (m ³)	Vp (m ³ /h)	f (Hz)	Vp (m ³)	Vp (m ³ /h)	f (Hz)
1.1.1	0.104	9.34E-04	1.28E-03	0.020	6.45E-04	9.30E-04	0.033	2.74E-04	4.01E-04	0.070
	0.271	9.60E-04	1.38E-03	0.054	6.57E-04	9.74E-04	0.079	2.98E-04	4.80E-04	0.154
	0.438	9.88E-04	1.43E-03	0.088	7.08E-04	1.05E-03	0.126	3.41E-04	5.82E-04	0.242
	0.605	1.02E-03	1.48E-03	0.117	7.45E-04	1.17E-03	0.167	3.84E-04	6.29E-04	0.327
	0.772	1.05E-03	1.53E-03	0.152	8.23E-04	1.22E-03	0.204	4.04E-04	6.87E-04	0.401
	0.939	1.09E-03	1.59E-03	0.181	8.42E-04	1.28E-03	0.243	4.49E-04	7.57E-04	0.439
	1.106	1.12E-03	1.65E-03	0.217	9.11E-04	1.37E-03	0.275	4.64E-04	7.44E-04	0.531
	1.273	1.13E-03	1.69E-03	0.248	9.45E-04	1.37E-03	0.305	5.13E-04	8.03E-04	0.556
	1.440	1.16E-03	1.78E-03	0.276	1.01E-03	1.51E-03	0.332	5.85E-04	8.97E-04	0.569
	1.607	1.18E-03	1.90E-03	0.309	1.04E-03	1.58E-03	0.370	6.03E-04	9.52E-04	0.605
	1.774	1.20E-03	1.98E-03	0.349	1.03E-03	1.54E-03	0.423	6.68E-04	1.12E-03	0.605
1.941	1.22E-03	2.06E-03	0.388	1.06E-03	1.68E-03	0.454	7.14E-04	1.17E-03	0.636	
1.1.2	0.104	7.64E-04	9.01E-04	0.023	3.84E-04	4.77E-04	0.040	1.74E-04	3.65E-04	0.081
	0.271	8.28E-04	1.03E-03	0.062	3.88E-04	5.31E-04	0.112	1.91E-04	3.54E-04	0.207
	0.438	8.99E-04	1.15E-03	0.100	4.55E-04	6.48E-04	0.181	2.18E-04	4.23E-04	0.334
	0.605	9.11E-04	1.19E-03	0.135	4.97E-04	6.96E-04	0.231	2.68E-04	5.14E-04	0.421
	0.772	9.72E-04	1.29E-03	0.174	5.61E-04	7.71E-04	0.281	3.34E-04	6.04E-04	0.450
	0.939	9.59E-04	1.35E-03	0.214	6.06E-04	8.60E-04	0.339	3.13E-04	6.85E-04	0.590
	1.106	1.02E-03	1.41E-03	0.244	6.09E-04	8.78E-04	0.356	3.86E-04	7.67E-04	0.601
	1.273	1.04E-03	1.48E-03	0.281	6.57E-04	9.74E-04	0.407	4.12E-04	8.18E-04	0.626
	1.440	1.11E-03	1.59E-03	0.300	7.28E-04	1.07E-03	0.455	3.74E-04	7.00E-04	0.778
	1.607	1.11E-03	1.63E-03	0.337	7.56E-04	1.07E-03	0.486	3.41E-04	6.76E-04	0.896
	1.774	1.15E-03	1.67E-03	0.373	7.81E-04	1.11E-03	0.534	4.30E-04	8.04E-04	0.980
1.941	1.20E-03	1.70E-03	0.435	8.17E-04	1.13E-03	0.592	4.62E-04	8.99E-04	1.020	
1.1.3	0.104	7.81E-04	9.36E-04	0.023	6.56E-04	7.18E-04	0.025	3.23E-04	4.29E-04	0.060
	0.271	8.10E-04	1.03E-03	0.062	7.00E-04	9.31E-04	0.076	3.64E-04	5.00E-04	0.134
	0.438	8.66E-04	1.13E-03	0.100	8.41E-04	1.18E-03	0.114	4.19E-04	6.35E-04	0.195
	0.605	9.25E-04	1.21E-03	0.135	8.99E-04	1.27E-03	0.151	4.86E-04	7.60E-04	0.254
	0.772	9.45E-04	1.30E-03	0.174	9.37E-04	1.44E-03	0.184	5.28E-04	7.70E-04	0.325
	0.939	9.49E-04	1.32E-03	0.215	1.01E-03	1.47E-03	0.216	5.93E-04	9.42E-04	0.352
	1.106	1.04E-03	1.41E-03	0.244	1.03E-03	1.59E-03	0.251	6.03E-04	9.22E-04	0.419
	1.273	1.05E-03	1.39E-03	0.282	1.11E-03	1.66E-03	0.277	6.56E-04	1.03E-03	0.419
	1.440	1.12E-03	1.56E-03	0.299	1.06E-03	1.71E-03	0.317	6.68E-04	1.01E-03	0.517
	1.607	1.14E-03	1.57E-03	0.337	1.14E-03	1.73E-03	0.354	7.06E-04	1.05E-03	0.562
	1.774	1.16E-03	1.59E-03	0.373	1.19E-03	1.82E-03	0.377	7.61E-04	1.16E-03	0.577
1.941	1.20E-03	1.65E-03	0.407	1.22E-03	1.93E-03	0.427	7.65E-04	1.18E-03	0.607	

1.2.1	0.104	7.43E-04	9.84E-04	0.024	5.37E-04	7.26E-04	0.034	2.76E-04	3.90E-04	0.053
	0.271	8.20E-04	1.13E-03	0.064	5.98E-04	8.30E-04	0.084	3.01E-04	4.72E-04	0.145
	0.438	8.47E-04	1.24E-03	0.104	6.29E-04	8.74E-04	0.116	3.48E-04	5.66E-04	0.217
	0.605	8.75E-04	1.30E-03	0.138	7.06E-04	1.03E-03	0.161	3.62E-04	5.84E-04	0.296
	0.772	9.00E-04	1.38E-03	0.180	7.26E-04	1.07E-03	0.228	4.09E-04	6.47E-04	0.368
	0.939	9.22E-04	1.47E-03	0.216	7.48E-04	1.15E-03	0.269	4.59E-04	7.83E-04	0.396
	1.106	9.49E-04	1.52E-03	0.252	7.75E-04	1.20E-03	0.310	4.77E-04	7.71E-04	0.474
	1.273	9.82E-04	1.53E-03	0.290	8.18E-04	1.28E-03	0.338	5.03E-04	8.89E-04	0.502
	1.440	1.00E-03	1.61E-03	0.321	8.67E-04	1.33E-03	0.371	5.87E-04	1.00E-03	0.509
	1.607	1.02E-03	1.71E-03	0.357	9.15E-04	1.49E-03	0.393	6.48E-04	1.06E-03	0.531
	1.774	1.04E-03	1.75E-03	0.380	9.52E-04	1.54E-03	0.430	7.09E-04	1.19E-03	0.550
1.941	1.09E-03	1.79E-03	0.428	9.66E-04	1.58E-03	0.487	6.83E-04	1.15E-03	0.617	
1.2.2	0.104	5.59E-04	7.81E-04	0.034	4.34E-04	5.98E-04	0.036	2.50E-04	3.65E-04	0.058
	0.271	5.93E-04	9.32E-04	0.092	4.87E-04	7.30E-04	0.102	2.77E-04	4.95E-04	0.157
	0.438	6.21E-04	9.73E-04	0.140	5.23E-04	7.34E-04	0.161	3.25E-04	5.52E-04	0.233
	0.605	6.56E-04	1.05E-03	0.189	5.58E-04	8.80E-04	0.208	3.62E-04	6.31E-04	0.299
	0.772	6.78E-04	1.12E-03	0.231	5.65E-04	9.77E-04	0.257	3.91E-04	7.43E-04	0.359
	0.939	7.02E-04	1.13E-03	0.278	5.75E-04	1.09E-03	0.313	4.61E-04	9.26E-04	0.379
	1.106	7.28E-04	1.23E-03	0.319	6.58E-04	1.17E-03	0.346	4.57E-04	9.56E-04	0.435
	1.273	7.81E-04	1.34E-03	0.345	6.65E-04	1.28E-03	0.391	4.93E-04	1.02E-03	0.472
	1.440	8.25E-04	1.35E-03	0.375	7.30E-04	1.36E-03	0.415	5.73E-04	1.07E-03	0.511
	1.607	8.76E-04	1.34E-03	0.397	7.73E-04	1.43E-03	0.452	5.90E-04	1.10E-03	0.556
	1.774	8.92E-04	1.46E-03	0.447	8.36E-04	1.32E-03	0.489	5.84E-04	1.07E-03	0.646
1.941	9.28E-04	1.48E-03	0.494	8.61E-04	1.40E-03	0.543	6.26E-04	1.22E-03	0.686	
1.3.1	0.104	4.62E-04	6.83E-04	0.036	3.60E-04	5.20E-04	0.046	1.49E-04	3.17E-04	0.090
	0.271	5.29E-04	8.11E-04	0.097	4.11E-04	6.57E-04	0.116	1.88E-04	3.75E-04	0.232
	0.438	5.62E-04	9.04E-04	0.141	4.55E-04	7.21E-04	0.184	2.48E-04	4.71E-04	0.322
	0.605	5.89E-04	9.69E-04	0.198	5.58E-04	9.03E-04	0.229	2.45E-04	4.16E-04	0.473
	0.772	6.13E-04	1.02E-03	0.251	5.62E-04	8.78E-04	0.290	3.11E-04	5.19E-04	0.495
	0.939	6.37E-04	1.09E-03	0.308	5.88E-04	9.77E-04	0.319	3.33E-04	5.93E-04	0.581
	1.106	6.56E-04	1.12E-03	0.344	6.32E-04	1.07E-03	0.366	3.68E-04	6.55E-04	0.622
	1.273	6.74E-04	1.26E-03	0.381	6.35E-04	1.03E-03	0.451	4.19E-04	7.73E-04	0.635
	1.440	7.03E-04	1.25E-03	0.446	6.46E-04	1.13E-03	0.485	3.80E-04	6.81E-04	0.820
	1.607	7.24E-04	1.32E-03	0.480	6.83E-04	1.20E-03	0.528	4.33E-04	7.40E-04	0.839
	1.774	7.45E-04	1.35E-03	0.532	7.03E-04	1.35E-03	0.550	4.76E-04	8.68E-04	0.867
1.941	7.70E-04	1.40E-03	0.581	7.18E-04	1.19E-03	0.656	4.85E-04	9.15E-04	0.938	
1.3.2	0.104	1.26E-03	1.57E-03	0.015	8.64E-04	1.06E-03	0.019	3.41E-04	5.10E-04	0.045
	0.271	1.27E-03	1.59E-03	0.041	9.11E-04	1.11E-03	0.057	3.76E-04	5.74E-04	0.121
	0.438	1.35E-03	1.67E-03	0.064	9.46E-04	1.16E-03	0.096	4.23E-04	6.65E-04	0.187
	0.605	1.38E-03	1.70E-03	0.091	9.91E-04	1.28E-03	0.124	4.62E-04	6.94E-04	0.239
	0.772	1.43E-03	1.91E-03	0.118	1.05E-03	1.41E-03	0.152	5.09E-04	7.65E-04	0.281
	0.939	1.47E-03	2.03E-03	0.141	1.14E-03	1.51E-03	0.175	5.59E-04	8.55E-04	0.337
	1.106	1.48E-03	2.07E-03	0.167	1.13E-03	1.48E-03	0.219	5.62E-04	8.47E-04	0.397
	1.273	1.51E-03	2.19E-03	0.191	1.18E-03	1.51E-03	0.241	6.53E-04	1.00E-03	0.422
	1.440	1.55E-03	2.21E-03	0.213	1.21E-03	1.61E-03	0.278	7.08E-04	1.08E-03	0.464
	1.607	1.57E-03	2.30E-03	0.247	1.28E-03	1.73E-03	0.292	6.68E-04	1.01E-03	0.557
	1.774	1.57E-03	2.24E-03	0.268	1.32E-03	1.75E-03	0.327	7.23E-04	1.16E-03	0.579
1.941	1.61E-03	2.23E-03	0.301	1.34E-03	1.77E-03	0.360	7.51E-04	1.20E-03	0.586	

E.2 Effect of hydrostatic pressure change on plug-flow generator

Table E.2: Mean experimental results of the effect of hydrostatic pressure

Plug Flow Generator	Volumetric air flow rate (Nm ³ /h)	0.7 m			0.85 m			1 m		
		Vp (m ³)	Vp (m ³ /h)	f (Hz)	Vp (m ³)	Vp (m ³ /h)	f (Hz)	Vp (m ³)	Vp (m ³ /h)	f (Hz)
1.1.1	0.104	6.45E-04	9.30E-04	0.033	7.71E-04	1.10E-03	0.024	6.25E-04	8.06E-04	0.030
	0.271	6.57E-04	9.74E-04	0.079	8.07E-04	1.10E-03	0.073	6.52E-04	9.67E-04	0.082
	0.438	7.08E-04	1.05E-03	0.126	8.44E-04	1.23E-03	0.118	6.97E-04	1.00E-03	0.130
	0.605	7.45E-04	1.17E-03	0.167	8.80E-04	1.26E-03	0.157	7.37E-04	1.08E-03	0.166
	0.772	8.23E-04	1.22E-03	0.204	9.39E-04	1.25E-03	0.190	8.33E-04	1.18E-03	0.204
	0.939	8.42E-04	1.28E-03	0.243	9.85E-04	1.40E-03	0.218	8.47E-04	1.27E-03	0.244
	1.106	9.11E-04	1.37E-03	0.275	1.03E-03	1.53E-03	0.259	9.21E-04	1.48E-03	0.274
	1.273	9.45E-04	1.37E-03	0.305	1.03E-03	1.55E-03	0.295	9.82E-04	1.56E-03	0.297
	1.440	1.01E-03	1.51E-03	0.332	1.03E-03	1.65E-03	0.327	9.98E-04	1.49E-03	0.359
	1.607	1.04E-03	1.58E-03	0.370	1.08E-03	1.57E-03	0.361	1.11E-03	1.56E-03	0.367
	1.774	1.03E-03	1.54E-03	0.423	1.12E-03	1.74E-03	0.387	1.10E-03	1.63E-03	0.415
1.941	1.06E-03	1.68E-03	0.454	1.19E-03	1.71E-03	0.429	1.16E-03	1.78E-03	0.457	

E.3 Effect of volume of plug on liquid mass displaced

Table E.3: Mean experimental results of volume of plug on the mass displaced

Orifice area	Volumetric air flow rate (Nm ³ /h)	V _p (m ³)	V _p (m ³ /h)	f (Hz)	m _i (kg)	m _i (kg/s)
201.1E ⁻⁶ m ²	0.104	9.34E-04	1.28E-03	0.020	4.061	0.080
	0.271	9.60E-04	1.38E-03	0.054	4.755	0.258
	0.438	9.88E-04	1.43E-03	0.088	4.934	0.432
	0.605	1.02E-03	1.48E-03	0.117	5.085	0.594
	0.772	1.05E-03	1.53E-03	0.152	5.236	0.794
	0.939	1.09E-03	1.59E-03	0.181	5.291	0.958
	1.106	1.12E-03	1.65E-03	0.217	5.347	1.158
	1.273	1.13E-03	1.69E-03	0.248	5.346	1.323
	1.440	1.16E-03	1.78E-03	0.276	5.473	1.511
	1.607	1.18E-03	1.90E-03	0.309	5.441	1.682
	1.774	1.20E-03	1.98E-03	0.349	5.325	1.857
	1.941	1.22E-03	2.06E-03	0.388	5.301	2.056
415.5E ⁻⁶ m ²	0.104	6.45E-04	9.30E-04	0.033	3.781	0.126
	0.271	6.57E-04	9.74E-04	0.079	4.290	0.338
	0.438	7.08E-04	1.05E-03	0.126	4.587	0.576
	0.605	7.45E-04	1.17E-03	0.167	4.651	0.779
	0.772	8.23E-04	1.22E-03	0.204	4.722	0.962
	0.939	8.42E-04	1.28E-03	0.243	4.957	1.205
	1.106	9.11E-04	1.37E-03	0.275	4.923	1.352
	1.273	9.45E-04	1.37E-03	0.305	5.072	1.545
	1.440	1.01E-03	1.51E-03	0.332	5.196	1.727
	1.607	1.04E-03	1.58E-03	0.370	5.166	1.913
	1.774	1.03E-03	1.54E-03	0.423	5.147	2.177
	1.941	1.06E-03	1.68E-03	0.454	5.222	2.371
804.3E ⁻⁶ m ²	0.104	2.74E-04	4.01E-04	0.070	1.705	0.119
	0.271	2.98E-04	4.80E-04	0.154	2.147	0.331
	0.438	3.41E-04	5.82E-04	0.242	2.578	0.624
	0.605	3.84E-04	6.29E-04	0.327	2.741	0.898
	0.772	4.04E-04	6.87E-04	0.401	2.814	1.129
	0.939	4.49E-04	7.57E-04	0.439	3.142	1.379
	1.106	4.64E-04	7.44E-04	0.531	2.942	1.562
	1.273	5.13E-04	8.03E-04	0.556	3.090	1.719
	1.440	5.85E-04	8.97E-04	0.569	3.222	1.835
	1.607	6.03E-04	9.52E-04	0.605	3.279	1.982
	1.774	6.68E-04	1.12E-03	0.605	3.697	2.235
	1.941	7.14E-04	1.17E-03	0.636	3.738	2.377

E.4 Effect of hydrostatic pressure change on plug-flow generator

Table E.4: Mean experimental results of the effect of hydrostatic pressure on mass flow

Liquid depth (m)	Volumetric air flow rate (Nm ³ /h)	Vp (m ³)	Vp (m ³ /h)	f (Hz)	m _i (kg)	m _i (kg/s)
0.7 m	0.104	6.45E-04	9.30E-04	0.033	3.781	0.126
	0.271	6.57E-04	9.74E-04	0.079	4.290	0.338
	0.438	7.08E-04	1.05E-03	0.126	4.587	0.576
	0.605	7.45E-04	1.17E-03	0.167	4.651	0.779
	0.772	8.23E-04	1.22E-03	0.204	4.722	0.962
	0.939	8.42E-04	1.28E-03	0.243	4.957	1.205
	1.106	9.11E-04	1.37E-03	0.275	4.923	1.352
	1.273	9.45E-04	1.37E-03	0.305	5.072	1.545
	1.440	1.01E-03	1.51E-03	0.332	5.196	1.727
	1.607	1.04E-03	1.58E-03	0.370	5.166	1.913
	1.774	1.03E-03	1.54E-03	0.423	5.147	2.177
1.941	1.06E-03	1.68E-03	0.454	5.222	2.371	
0.85 m	0.104	7.71E-04	1.10E-03	0.024	4.419	0.105
	0.271	8.07E-04	1.10E-03	0.073	4.933	0.359
	0.438	8.44E-04	1.23E-03	0.118	5.272	0.623
	0.605	8.80E-04	1.26E-03	0.157	5.526	0.868
	0.772	9.39E-04	1.25E-03	0.190	5.573	1.061
	0.939	9.85E-04	1.40E-03	0.218	5.805	1.266
	1.106	1.03E-03	1.53E-03	0.259	5.835	1.514
	1.273	1.03E-03	1.55E-03	0.295	5.999	1.767
	1.440	1.03E-03	1.65E-03	0.327	5.953	1.949
	1.607	1.08E-03	1.57E-03	0.361	5.812	2.100
	1.774	1.12E-03	1.74E-03	0.387	5.857	2.267
1.941	1.19E-03	1.71E-03	0.429	5.897	2.529	
1 m	0.104	6.25E-04	8.06E-04	0.030	6.117	0.184
	0.271	6.52E-04	9.67E-04	0.082	6.245	0.513
	0.438	6.97E-04	1.00E-03	0.130	6.618	0.857
	0.605	7.37E-04	1.08E-03	0.166	6.821	1.129
	0.772	8.33E-04	1.18E-03	0.204	7.045	1.439
	0.939	8.47E-04	1.27E-03	0.244	7.158	1.743
	1.106	9.21E-04	1.48E-03	0.274	7.236	1.981
	1.273	9.82E-04	1.56E-03	0.297	7.297	2.169
	1.440	9.98E-04	1.49E-03	0.359	7.301	2.624
	1.607	1.11E-03	1.56E-03	0.367	7.165	2.630
	1.774	1.10E-03	1.63E-03	0.415	7.259	3.014
1.941	1.16E-03	1.78E-03	0.457	7.404	3.381	